TAMPEREEN TEKNILLINEN YLIOPISTO
TAMPERE UNIVERSITY OF TECHNOLOGY

Anssi Mäki

Effects of Partial Shading Conditions on Maximum Power Points and Mismatch Losses in Silicon-Based Photovoltaic Power Generators

Julkaisu 1157 • Publication 1157

Tampere 2013

Tampereen teknillinen yliopisto. Julkaisu 1157
Tampere University of Technology. Publication 1157

Anssi Mäki

Effects of Partial Shading Conditions on Maximum Power Points and Mismatch Losses in Silicon-Based Photovoltaic Power Generators

Thesis for the degree of Doctor of Science in Technology to be presented with due permission for public examination and criticism in Sähkötalo Building, Auditorium S2, at Tampere University of Technology, on the 1st of November 2013, at 12 noon.

Tampereen teknillinen yliopisto - Tampere University of Technology
Tampere 2013

ISBN 978-952-15-3137-8 (printed)
ISBN 978-952-15-3142-2 (PDF)
ISSN 1459-2045

ABSTRACT

Photovoltaic (PV) power generators can be used for converting the energy of solar radiation directly into electrical energy without any moving parts. The operation of the generators is highly affected by operating conditions, most importantly irradiances and temperatures of PV cells. PV power generators are prone to electrical losses if the operating conditions are non-uniform such as in a case where part of the modules of a generator are shaded while the rest are receiving the global solar radiation. These conditions are called partial shading conditions and they have been recognized as a major cause of energy losses in PV power generators.

In this thesis, the operation of silicon-based PV power generators under partial shading conditions is studied using Matlab Simulink simulation model. The operation of the model has been verified by measurements of electrical characteristics of a PV module under several different operating conditions and also under partial shading conditions. A systematic approach to study the effects of partial shading conditions has been developed and used. In addition to the systematic approach, a vast amount of data measured from the Tampere University of Technology (TUT) Solar Photovoltaic Power Station Research Plant are analyzed and used as input for the simulation model to study operation of PV power generators under actual operating conditions.

Partial shading conditions have severe effects on the electrical characteristics of PV power generators and can cause multiple maximum power points (MPPs) to the power-voltage curve of the generators. In most cases, partial shading conditions lead to the occurrence of multiple MPPs, but also only one MPP can be present despite of partial shading. Reasons for this phenomenon are presented and analyzed in this thesis. Because of multiple MPPs, a considerable amount of available electrical energy may be lost when the generator is operating at a local MPP with low power instead of the global MPP. In order to optimize the operation of PV power generators under partial shading conditions it is crucial to be familiar with the operation of the generators under these conditions. Results of a systematic study of the effects partial shading conditions on MPP characteristics are shown and a method to differentiate between local and global MPPs will be presented in this thesis.

Partial shading conditions cause also mismatch losses when the individual PV cells are not operating at their own MPPs although the generator would operate at its own MPP. The amount of mismatch losses depends on the partial shading conditions but also on the electrical configuration of the PV power generator. In this thesis, different configurations are based on different inverter concepts such as central inverter, string inverter and multi-string inverter. The mismatch losses under partial shading conditions of these different PV power generator configurations are studied. It is shown that long series connections of PV modules are most severely affected by partial shading conditions.

PREFACE

This work was carried out at the Department of Electrical Engineering at Tampere University of Technology (TUT) during the years 2010–2013. The research was funded by TUT, Tekes and ABB Ltd. Financial support in the form of personal grants from the Fortum and Ulla Tuominen Foundations are greatly appreciated.

I want to thank Professor Seppo Valkealahti for supervising my thesis and encouraging me throughout my efforts towards the doctoral degree. Also many discussions with Professor Teuvo Suntio are highly valued. I also want to thank my colleagues, PhD's Jari Leppäaho, Joonas Puukko, Juha Huusari and Lari Nousiainen and Masters of Science (M.Sc.'s) Diego Torres Lobera, Tuomas Messo, Juha Jokipii, Jukka Viinamäki and Kari Lappalainen, and also the rest of the personnel in the Department of Electrical Engineering who provided a productive and inspiring working environment. Special thanks goes to PhD Juha Huusari for providing me the latex template for this thesis. It made my writing task a lot easier. I am thankful to Professors Franz Baumgartner and Giovanni Spagnuolo for examining my thesis and their constructive comments that improved the quality of the manuscript. I would also like to thank Merja Teimonen for providing valuable assistance regarding practical everyday matters. Pentti Kivinen, Pekka Nousiainen and Mikko Kunnari, in turn, deserve a special distinction for their craftsmanship in building the TUT Solar Photovoltaic Power Station Research Plant and M.Sc. Jussi Ahola for designing the measurement and data acquisition system for the test plant. These systems weren't just useful but vital in the research work.

I also want to thank my parents Sisko and Hannu, my brother Jani and his family for encouraging me during my work and studies. Finally, I want to thank my beloved wife Meiju and our firstborn daughter Vilja for all the support they have given me. Vilja, especially, for the smiles after a hard day's work and Meiju for being there for me through thick and thin.

Seinäjoki, August 2013

Anssi Mäki

TABLE OF CONTENTS

LIST OF ABBREVIATIONS

AC	Alternating current
AM0	Air mass zero
AM1.5	Air mass 1.5
AM1.5G	Air mass 1.5 global
ASTM	American Society for Testing and Materials
DC	Direct current
DIRECT	Dividing rectangles
EU	European Union
IC	Incremental conductance
IEA	International Energy Agency
MPP	Maximum power point
MPPT	Maximum power point tracking
NOCT	Nominal operating cell temperature
NREL	National Renewable Energy Laboratory
OC	Open-circuit
P&O	Perturb and observe
PV	Photovoltaic
SC	Short-circuit
STC	Standard test conditions
TUT	Tampere University of Technology

LIST OF SYMBOLS

ΔT	Temperature difference
A	Ideality factor
A_{bypass}	Ideality factor of bypass diode
a-Si	Amorphous silicon
CdTe	Cadmium telluride
CIGS	Copper indium gallium selenide
CO_2	Carbon dioxide
$\mathrm{d}P/\mathrm{d}I\|_{\text{MPP}}$	Notation for differentiation (derivative of power with respect to current at maximum power point)
E_{g}	Band gap energy
G	Irradiance
G_{STC}	Irradiance in standard test conditions
GaAs	Gallium arsenide
GaInNAs	Gallium indium nitride arsenide
GaInP	Gallium indium phosphide
H_2O	Water
I	Current
I_{d}	Current through the diode in one-diode model
$I_{\text{MPP,STC}}$	Current at maximum power point in standard test conditions
$I_{\text{MPP,high}}$	Current at the maximum power point at high values of current (low values of voltage)
InGaAs	Indium gallium arsenide
InGaP	Indium gallium phosphide
I_{o}	Dark saturation current
$I_{\text{o,bypass}}$	Dark saturation current of bypass diode
$I_{\text{o,ns}}$	Dark saturation current of non-shaded PV cells
$I_{\text{o,s}}$	Dark saturation current of shaded PV cells
$I_{\text{o,STC}}$	Dark saturation current in standard test conditions
I_{o1}	Dark saturation current in quasi-neutral regions
I_{o2}	Dark saturation current in depletion region
I_{ph}	Light-generated current
$I_{\text{ph,STC}}$	Light-generated current in standard test conditions
I_{SC}	Short-circuit current
$I_{\text{SC,STC}}$	Short-circuit current in standard test conditions
k	Boltzmann constant
K_{i}	Temperature coefficient of short-circuit current
K_{t}	Temperature-rise coefficient

K_{u}	Temperature coefficient of open-circuit voltage
L1, L2, L3	Phases 1, 2 and 3 of electrical grid
N	Neutral of electrical grid
N_{c}	Number of series-connected cells in a PV module
N_{s}	Number of series-connected blocks of series-connected PV cells with an anti-parallel-connected bypass diode
P	Power
P_{MPP}	Power at maximum power point
q	Elementary charge
R_{s}	Series resistance
$R_{\mathrm{s,bypass}}$	Series resistance of bypass diode
R_{sh}	Shunt resistance
S1, S2, S3, ...	Photodiode sensors 1, 2, 3 and so on of Tampere University of Technology Solar Photovoltaic Power Station Research Plant
T	Temperature of a PV cell/module
T_{amb}	Ambient temperature
T_{STC}	PV module temperature in standard test conditions
U	Voltage
U_{bd}	Bypass diode voltage
U_{d}	Voltage of the diode in one-diode model
$U_{\mathrm{lim,high}}$	Relative voltage difference limit to differentiate between local and global MPPs in case of an MPP at high voltages
$U_{\mathrm{lim,low}}$	Relative voltage difference limit to differentiate between local and global MPPs in case of an MPP at low voltages
$U_{\mathrm{MPP,ns}}$	Maximum power point voltage of a block of series-connected non-shaded PV cells with an anti-parallel-connected bypass diode
$U_{\mathrm{MPP,STC}}$	Maximum power point voltage in standard test conditions
U_{ns}	Voltage of a block of series-connected non-shaded PV cells with an anti-parallel-connected bypass diode
$U_{\mathrm{OC,STC}}$	Open-circuit voltage in standard test conditions
U_{s}	Voltage of a shaded block of series-connected PV cells with an anti-parallel-connected bypass diode
U_{t}	Thermal voltage
$U_{\mathrm{t,ns}}$	Thermal voltage of a block of series-connected non-shaded PV cells with an anti-parallel-connected bypass diode
$U_{\mathrm{t,s}}$	Thermal voltage of a block of series-connected shaded PV cells with an anti-parallel-connected bypass diode
x	System shading
x_{lim}	Limit of system shading for which only one maximum power point exists due to power losses in bypass diodes

y	Shading strength
y_{lim}	Limit of shading strength for which only one maximum power point exist due to low shunt resistance
y_{max}	Maximum shading strength for which only one maximum power point exists due to low shading strength

LIST OF RELATED PUBLICATIONS

The content of this thesis is based on the contents of the following scientific publications.

P1. Mäki, A., Valkealahti, S. and Suntio, T. (2010). Dynamic terminal characteristics of a photovoltaic generator, *14th International Power Electronics and Motion Control Conference*, Ohrid, Macedonia, pp. T12-76–T12-80, DOI: 10.1109/EPEPEMC.2010.5606786.

P2. Mäki, A. and Valkealahti, S. (2011). Operation of long series-connected silicon-based photovoltaic module string and parallel-connected short strings under partial shading conditions, *26th European Photovoltaic Solar Energy Conference and Exhibition*, Hamburg, Germany, pp. 4227–4232, DOI: 10.4229/26thEUPVSEC-2011-5BV.2.10.

P3. Mäki, A., Valkealahti, S. and Leppäaho, J. (2012). Operation of series-connected silicon-based photovoltaic modules under partial shading conditions, *Progress in Photovoltaics: Research and Applications* **20**(3): 298–309. DOI: 10.1002/pip.1138.

P4. Mäki, A. and Valkealahti, S. (2012). Power losses in long string and parallel-connected short strings of series-connected silicon-based photovoltaic modules due to partial shading conditions, *IEEE Transactions on Energy Conversion* **27**(1): 173–183. DOI: 10.1109/TEC.2011.2175928.

P5. Mäki, A. and Valkealahti, S. (2012). Mismatch losses in photovoltaic power generators due to partial shading caused by moving clouds, *27th European Photovoltaic Solar Energy Conference and Exhibition*, Frankfurt, Germany, pp. 3911–3915, DOI: 10.4229/27thEUPVSEC2012-5AV.1.6.

P6. Mäki, A. and Valkealahti, S. (2013). Effect of photovoltaic generator components on the number of MPPs under partial shading conditions, *IEEE Transactions on Energy Conversion*, to be published, DOI: 10.1109/TEC.2013.2274280.

P7. Mäki, A. and Valkealahti, S. (2013). Differentiation of multiple maximum power points of partially shaded photovoltaic power generators, *Renewable Energy*, in review.

P8. Nousiainen, L., Puukko, J., Mäki, A., Messo, T., Huusari, J., Jokipii, J., Viinamäki, J., Torres Lobera, D., Valkealahti, S. and Suntio, T. (2013). Photovoltaic generator as an input source for power electronic converters, *IEEE Transactions on Power Electronics* **28**(6): 3028–3038, DOI: 10.1109/TPEL.2012.2209899.

The author of this thesis carried out the research work presented in publications P1–P7, analysed the results and wrote the publications themselves. Only the experimental measurements in P3 were carried out together with PhD Jari Leppäaho. In P8, the measurements and analyses related to the properties of the PV module were done by the author of the thesis in co-operation with the other authors of the paper.

1 INTRODUCTION

> ”We are like tenant farmers, chopping down the fence around our house for fuel, when we should be using nature’s inexhaustible sources of energy – sun, wind and tide.
> ...
> I’d put my money on the sun and solar energy. What a source of power!
> I hope we don’t have to wait till oil and coal run out before we tackle that.”[1]
>
> – Thomas A. Edison

Thomas Edison said the quoted words above in 1931. About 80 years later in 2010, the world’s total primary energy supply was over ten times the amount it was in 1931 (International Energy Agency, 2012; Rogner, 2012). Taking this into account with the fact that there are only limited fossil fuel reserves on our planet, it can be said that we are ”chopping down the fence around our house” at an ever-increasing rate. As these reserves begin to deplete, the prices of fossil fuels are getting higher. The price increase along with the recognized problems related to the utilization of fossil fuels, such as environmental pollution and the global warming (Bose, 2010), has raised a concern about the future of our current lifestyle which is more energy intensive than ever before. Fortunately, this concern has lead to some positive developments. In 2007, for example, the European Union (EU) leaders agreed on new energy policies which included a goal to reduce the effects of energy production on the environment and atmosphere. The policies included a target according to which 20% share of the energy consumed in EU in 2020 should come from renewable sources (European Commission, 2012). These ”nature’s inexhaustible sources of energy” can be regarded as clean and abundant and the potential of these sources is enormous (Abbott, 2010; Bull, 2001).

Although there are several different renewable energy sources available, the first one on Edison’s list is the most promising, i.e., the energy coming from the Sun, the solar radiation. The energy of solar radiation is vital to all living species on our planet and

[1] Said in a conversation with Henry Ford and Harvey Firestone in 1931. Quoted as it appears in (Newton, 1987).

the amount of energy is substantial. Kroposki et al. (2009) estimated in 2009 that the amount of energy coming from the Sun to Earth in one hour is more than the mankind consumes in a year. As Edison stated, "What a source of power!"

The two main ways of utilizing the energy of solar radiation are as heat or by converting it to electrical energy using photovoltaic (PV) cells. The radiation can be utilized as such or by concentrating the Sun's rays from a larger area to a smaller one using lenses (Abbott, 2010).

The operation of PV cells is based on the photovoltaic effect, first observed by Alexandre-Edmond Becquerel in 1839. The phenomenon was not fully understood until 1905 when Albert Eistein suggested that energy is exchanged only in discrete amounts, i.e., photons. Eistein was later awarded the Nobel Prize in Physics 1921 "for his services to Theoretical Physics, and especially for his discovery of the law of the photoelectric effect" (Nobelprize.org, 2013a).

The first functional PV cell, which had an efficiency of about 1%, was made in 1883 by Charles Fritts (Luque and Hegedus, 2003). The first practical silicon PV cell for energy production purposes was developed in Bell Laboratories by Chapin et al. (1954) with an efficiency of 6%. This was a major improvement in efficiency compared to earlier cells with efficiencies of about 1%. PV cell research experienced rapid development during the 1950s owing to space programs and utilization of PV cells in satellites. The energy crisis during the 1970s gave another boost to the research and development of PV cells (Razykov et al., 2011). In 1993, the confirmed maximum efficiency of a terrestrial silicon-based PV module, which is typically an interconnection of several tens of cells, had reached 18.2% (Green and Emery, 1993). Twenty years later in 2013 the efficiency was already 22.9% (Green et al., 2013). At the same time, efficiency of the best research silicon PV cell under non-concentrated irradiance conditions had already reached 25.0%. According to Tiedje et al. (1984), the maximum theoretical efficiency of a silicon PV cell under non-concentrated irradiance conditions is 29.8%, which means that in 2013 the efficiency of the best research silicon cell was less than 5% away from the theoretical maximum.

Despite of the progress during almost 130 years since the development of the first functional PV cell, in 2011 a share of the energy produced using PV systems was less than 1% of the world total primary energy supply (International Energy Agency, 2012). Fortunately, the utilization of renewable energy sources has become more and more popular since the beginning of this millenium thanks to support mechanisms such as tax incentives, feed-in-tariffs and subsidies which have made PV power systems economically more attractive (Barroso et al., 2010; Jäger-Waldau, 2007). According to Valkealahti (2011) renewables have already started to impact global energy production and will have a major impact during the next 30 years. The installed total capacity of PV power sys-

tems has increased with a remarkable pace (Renewable Energy Policy Network for the 21st Century, 2008; Wiese et al., 2009, 2010). Most of the installed systems are composed of silicon PV cells, which were the most commonly used PV cells with a market share of over 90% in year 2009 (Kroposki et al., 2009). Thus, PV power generators composed of silicon PV cells were also chosen as the focus in this thesis. Although the characteristics of PV modules used as an example and in measurements in this thesis are composed of polycrystalline silicon, similar behavior would also be found with thin film and amorphous silicon PV cells. Most important differences are related to temperature coefficients and to the values of certain parameters but the basic operation is still the same.

Electrical characteristics of a silicon PV cell are non-linear and have only one point at which the maximum power can be obtained, the maximum power point (MPP). Voltage and power at the MPP of a single cell are relatively low (of the order of 0.6 V and 4 W, respectively). Due to low voltage and power ratings, a certain amount of PV cells are typically connected in series to form PV modules, which are the basic building blocks of any PV power generator. PV modules can further be connected in series and in parallel to increase the voltage and power levels of the whole PV power generator (Häberlin, 2012).

The series connection of PV cells is, however, prone to losses if the electrical characteristics of the PV cells are not similar (Bucciarelli, 1979; Chamberlin et al., 1995) or the cells do not operate under uniform conditions (Alonso-García, Ruiz and Chenlo, 2006). In series connection, the PV cell with the lowest short-circuit (SC) current limits the current of the whole series connection (Wenham et al., 2007). Under non-uniform irradiance conditions, such as in partial shading conditions when some of the cells of the generator are shaded, the shaded PV cells have lower SC current than the non-shaded cells. If then the current of the PV power generator is higher than the SC current of the shaded cells, the cells will be reverse biased due to the other cells in the series connection. In this case, the reverse biased cells act as a load in the series connection dissipating part of the power generated by the other cells leading to power losses. These losses can lead to hot-spots in the shaded cells and the cells can be irreversibly damaged (Lashway, 1988).

The effects of partial shading conditions on PV power generators has been noticed to be a major cause of power losses and lower-than-expected system efficiencies. Therefore, the effects of partial shading has been extensively investigated. Several papers have been published about the modeling of partially shaded PV power generators such as (Alonso-García, Ruiz and Chenlo, 2006; Karatepe et al., 2007; Patel and Agarwal, 2008; Quaschning and Hanitsch, 1996; Ramabadran and Mathur, 2009b; Silvestre and Chouder, 2008; Spertino and Akilimali, 2009; Villalva et al., 2009a). The losses due to partial shading conditions have been studied previously, for example, in (Gao et al., 2009; García et al., 2008; Kovach and Schmid, 1996; Martínez-Moreno et al., 2010; Paraskevadaki and

Papathanassiou, 2011; Uchida et al., 2001; Wang and Hsu, 2011b; Xiao et al., 2007a). Experimental studies of the operation of PV power generators are reported in (Alonso-García, Ruiz and Herrmann, 2006; Woyte et al., 2003) and losses due to mutual shading of PV module rows is studied in (Drif et al., 2008). The effect of different PV module array schemes on the sensitivity to partial shading conditions has also been studied in (Karatepe et al., 2007; Kaushika and Gautam, 2003). The effects of partial shading specifically due to clouds are studied in (Giraud and Salameh, 1999; Jewell and Ramakumar, 1987; Jewell and Unruh, 1990; Kern et al., 1989) in which the main objective has been to study the effects of clouds on energy production of PV power generators from the electrical grid perspective or on the design of energy storage for a PV system. Although the electrical characteristics of PV power generators have been studied in several publications, typically only few current-voltage (I-U) and power-voltage (P-U) curves are given under certain specific operating conditions and, therefore, we are still missing a systematic and comprehensive study of the effects of partial shading conditions on PV power generators.

The operation of different PV power generator configurations, such as the ones based on central, string and multi-string inverter and AC module concepts (Kjaer et al., 2005), has also been studied under partial shading conditions. In (Reinoso et al., 2010, 2013) the operation of different configurations were studied under shading conditions by clouds. Different generator configurations were also studied experimentally in (García et al., 2008; Woyte et al., 2003). It was noticed in these papers that although PV power generators with modular structure should have less losses under partial shading conditions, the results indicate otherwise. It is, however, not clear what was causing the losses. It is likely that the generator configuration is not the cause of these losses but rather a failure in maximum power point tracking (MPPT) to reach the MPP with highest power, the global MPP (García et al., 2008). These losses are not characteristics for the configuration but to the MPPT technique.

The performance of MPPT is one of the most important concerns in any PV power system. In order to obtain maximum amount of energy from PV power generators, the operating point must be forced to be at the global MPP. This is a relatively simple task under uniform conditions, because there is only one MPP. There are popular techniques such as perturb and observe (P&O) and incremental conductance (IC) algorithms for finding a local MPP which under uniform conditions is also the global one (Esram and Chapman, 2007; Salas et al., 2006). Under partial shading conditions, however, there are typically multiple MPPs on the electrical characteristics of the PV power generator. Conventional MPPT algorithms are unable to recognize if they are operating at a local MPP with less power than could be obtained at the global MPP (García et al., 2008).

There has been a lot of research related to the development of global MPPT algorithms. The typical idea in these algorithms is to search the global MPP by scanning the

whole *P-U* curve (Kazmi et al., 2009; Noguchi et al., 2002). The advantage of these algorithms is that they are relatively simple and can be used in any system without specific information about the system or without the knowledge about the operating conditions. The major disadvantage is that energy is lost every time the search is performed.

P-U curves can also be scanned more efficiently by using the knowledge about the system and operating conditions which has ben used, for example, in (Alonso et al., 2009) by noticing that the minimum distance between two local MPPs is the MPP voltage of the shaded series-connected PV cells connected in anti-parallel with a bypass diode. Other techniques to improve the performance of the scanning are utilized, for example, in Fibonacci Search (Ahmed and Miyatake, 2008), DIRECT Search (Nguyen and Low, 2010) and Particle Swarm Optimization (Miyatake et al., 2011). Two-stage MPPT algorithm has been developed by combining a conventional MPPT, such as IC, and some other scanning method (Kobayashi et al., 2006). In the first stage, the operating point is moved into the vicinity of the global MPP. In the second stage, the conventional MPPT algorithm is used to reach the global MPP. It has been shown, however, that under certain partial shading conditions, the first stage of the algorithm is unable to move the operating point into the vicinity of the global MPP (Alonso et al., 2009). Also some other techniques which are not, strictly speaking, MPPT techniques, have been developed to minimize the effects of partial shading on the operation of PV power generators (Karatepe et al., 2008; Nguyen and Lehman, 2008). Despite of the great amount of work done in the field of MPPT techniques we are still missing techniques that are able to track to the global MPP under all conditions without the disadvantages such as the need to scan the *P-U* curve and thus losing some part of the energy. There is still work to be done in order to develop an optimal MPPT method.

1.1 Objectives and Scientific Contribution of the Thesis

The first objective of this thesis is to develop a systematic approach to study the effects of partial shading conditions on silicon-based PV power generators. Second objective is to show the effects of partial shading conditions on the *P-U* curves and the MPPs of silicon-based PV power generators. These include the number of MPPs and the behavior of MPP current and voltages under partial shading conditions. It will be shown that there are three different phenomena that can lead to only one MPP despite of the partial shading conditions. Also a method to differentiate between local and global MPPs will be presented. In this thesis the effect of partial shading conditions on mismatch losses in case of several different PV power generator configurations operating under partial shading conditions are studied. Mismatch losses in cases of shading caused by static objects such as buildings and by dynamic objects such as clouds are studied. The objective is to show which PV power generator configuration is the least sensitive to partial shading

conditions.

This thesis attempts to reach the above-mentioned objectives by using an experimentally verified Matlab Simulink simulation model of the operation of PV power generators. The model is based on the well-known one-diode model of the operation of PV cells. The model takes into account the most important parameters affecting the operation of PV cells and generators such as irradiance and temperature of the cells. Also the effects of bypass diodes are modeled. In addition to systematic approach, a vast amount of irradiance and PV module temperature data recorded with the data acquisition system of Tampere University of Technology (TUT) Solar Photovoltaic Power Station Research Plant will be analyzed and used as input data for the simulation model when studying the effect of partial shading conditions caused by clouds.

The main scientific contributions of this thesis can be summarized as follows:

- A systematical method to analyze the effects of partial shading conditions on PV power generators.
- Comprehension on the number of MPPs and the explanation of the one-MPP phenomenon under partial shading conditions.
- Comprehension on current and voltage characteristics of the MPPs under partial shading conditions.
- Method to differentiation between the local and global MPP.
- Comprehension on mismatch losses in different PV power generator configurations due to partial shading conditions caused by both buildings and clouds.

1.2 Organization of the Thesis

The rest of the thesis is organized as follows. Chapter 2 guides the reader through the backgrounds of electrical energy production using PV power generators. Characteristics of solar radiation and the fundamentals of the operation of PV cells will be shortly presented as well as the effects of the most important operating conditions on PV cells, the irradiance and PV cell temperature. The effects of bypass diodes on the operation of PV modules and generators will be presented and the effect on MPPT during partial shading conditions will be discussed. In the end of the chapter, different electrical configurations of PV power generators will be presented and discussed.

Chapter 3 presents the simulation model which was used in the research work. The experimental verification of the model is also presented. It is shown that the model is sufficiently accurate for the phenomema studied in this thesis and that it takes into account the most important parameters related to the operation of PV power generators. In the end of the chapter, a systematic approach to study the effects of partial shading

conditions and the approach to study the effects of clouds on mismatch losses during actual operating conditions by using the data from the TUT Solar Photovoltaic Power Station Research Plant has been described and discussed. The systematic method has been used to obtain results presented in Chapter 4 and part of the results in Chapter 5. The results of using actual data are presented and discussed in the end of Chapter 5.

Chapter 4 presents the effects of partial shading conditions on the number of MPPs and on MPP currents and voltages. Typically *P-U* characteristics have multiple MPPs under partial shading conditions. It will be shown that under certain environmental conditions there can be just one MPP on the *P-U* curve of the PV power generator despite of the partial shading conditions. In the end of the chapter, it is shown that it is possible to differentiate between local and global MPPs based on the knowledge of the system, of the operating conditions and of the MPP (whether it is a local or the global MPP) at which the generator is operating.

Chapther 5 presents the effect of partial shading conditions on mismatch losses occurring in PV power generators with different configurations. The effects are studied by using both systematic approach and practical partial shading scenarios due to static objects. The chapter also discusses the effect of PV power generator configuration on the mismatch losses under partial shading conditions due to clouds by using the simulation results having actual measured data recorded with the data acquisition system of the TUT Solar Photovoltaic Power Station Research Plant as input for the simulation models.

Finally in Chapter 6, the conclusions of the thesis are presented. In the end of the chapter some recommendations for further research work are presented.

2 BACKGROUND OF THE THESIS

This chapter guides the reader through the backgrounds of the utilization of the energy of solar radiation by using PV power generators. First a brief introduction of the characteristics of solar radiation is given. After that the photovoltaic effect and fundamentals of the operation of PV cells is given without going too deep into semiconductor physics. Then the most commonly used modeling methods for modeling the operation of PV cells are presented as well as alternative methods found in the literature. The effects of the most important operating conditions on the operation of PV cells are explained. The effect of non-uniform conditions will be presented and the role and effect of bypass diodes in PV modules to prevent the damaging of PV cells is shown. In the end of the chapter maximum power point tracking and different electrical configurations of PV power generators are discussed.

2.1 The Sun as an Energy Source

The energy from the Sun comes to the Earth in the form of electromagnetic radiation traveling over a distance of approximately 150 million kilometers. The energy is originated from the fusion reactions in the core of the Sun (Messenger and Ventre, 2010). The energy released from the fusion reactions heats up the Sun resulting in a surface temperature of some 5800 K from which the energy is radiated into space (Luque and Hegedus, 2003). A certain part of that energy, vital to all living things on Earth, comes in our direction.

Characteristics of solar radiation can be studied in more detail by investigating its spectrum. The spectrum just outside the Earth's atmosphere, also known as the air mass zero AM0 spectrum, according to Guyemard (2004) is shown in Fig. 2.1 with respect to spectral irradiance with spectrum of air mass 1.5 global (AM1.5G) according to American Society for Testing and Materials (ASTM) (ASTM International, 2008). AM1.5G corresponds to the spectrum of global irradiance of which the direct part has traveled through the atmosphere along a path which is 1.5 times the thickness of the atmosphere in length. By integrating the spectral irradiance AM0 over all wavelengths we get the generally accepted value of solar constant of 1366.1 W/m^2 (Guyemard, 2004). Integration of AM1.5G over all wavelengths gives basically the maximum value of irradiance reaching the surface of the Earth on a clear sky day, approximately 1000 W/m^2.

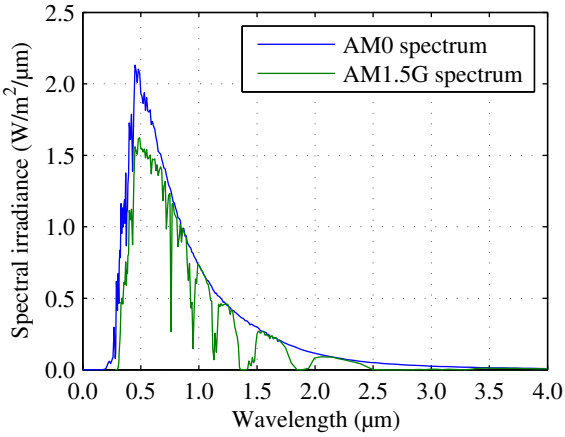

Fig. 2.1: Spectrum of solar radiation outside the Earth's atmosphere (AM0) and on the sea level when irradiance has traveled a distance of 1.5 times the thickness of the atmosphere (AM1.5G).

After reaching the outer part of the Earth's atmosphere, the solar radiation must still travel through the atmosphere before we can utilize it (excluding satellites). The effect of atmosphere on the spectrum of incoming solar radiation can clearly be seen in Fig. 2.1. At the short wavelengths the most important absorber of irradiance is ozone. The absorption caused by ozone is very important for life on Earth because short wavelength radiation (in the ultraviolet region of the spectrum) can damage the living. The narrow absorption band just below 0.8 μm is due to dioxygen. Two absorption bands just below 1.0 μm and the one in the range from 1.1 to 1.2 μm are caused by water vapour (H_2O) in the atmosphere. The rest of the absorption bands are caused by H_2O and carbon dioxide (CO_2) (Wenham et al., 2007). CO_2 is one of the greenhouse gases which are released to the atmosphere when utilizing fossil fuels such as coal in energy production. This is claimed to be at least partly responsible for the increase in the average temperature of Earth's atmosphere also known as the global warming (Bose, 2010).

2.2 The Photovoltaic Effect and Photovoltaic Cells

Without going too deep into semiconductor physics, the operation of the PV cells can be explained by using the energy band structure according to which the most weakly bonded electrons have energies in the energy band called the valence band. The next band with higher values of energy is called the conduction band. The energy separating the valence and conduction bands is called the band gap energy (E_g). When a sufficient amount of energy ($\geq E_g$) is applied to an electron in the valence band, the atomic bonds of the electron are broken and the electron is excited into conduction band and it is then

free to conduct current through the material. When electron is excited into conduction band, an empty vacancy opens to the valence band where the electron used to be located creating a positive charge, a hole.

In case of a pure semiconductor material, after certain time the free electron will recombine, which means the elimination of the electron-hole pair. Due to recombination, the free electron becomes trapped again in the atomic bonds of the material. This is why typical PV cells are composed of two different types of semiconductors, p- and n-type semiconductors. Different types of materials are created by introducing a small amount of impurity atoms (such as boron and phosphorus in case of silicon PV cells). When the two different materials are joined together, an electric field is created in the junction between the materials (called pn-junction) which separates the created electron-hole pairs and enables utilization of the free charges in electrical energy production. The theory of semiconductor pn-junctions and transistors was developed by Shockley (1949); Shockley et al. (1951). Shockley was awarded Nobel Prize in Physics 1956 jointly with John Bardeen and Walter Houser Brattain "for their researches on semiconductors and their discovery of the transistor effect" (Nobelprize.org, 2013b).

In 2009, the most widely used PV cells were based on crystalline silicon (Kroposki et al., 2009). The production technology of silicon cells is mature and the cost of cells is becoming lower as the production of cells and the amount of installed PV power systems increases. It should also be noticed that other types of cells have also been developed and a lot of research has been done to improve their performance and decrease costs. These are, for example, thin-film amorphous silicon (a-Si), cadmium telluride (CdTe), copper indium gallium diselenide (CIGS), gallium arsenide (GaAs) and gallium indium phosphide (GaInP). There are also emerging technologies such as dye-sensitized and organic cells for which the best confirmed cell efficiencies in 2013 were already 11.9% and 10.7%, respectively (Green et al., 2013; Razykov et al., 2011). So called multi-junction cells have also been developed which are able to utilize a bigger part of the spectrum of solar radiation compared to conventional single-junction cells. These cells can theoretically have efficiencies of up to 67% and 86% for non-concentrated and highly concentrated irradiance, respectively. These cells are, however, more expensive to manufacture compared to conventional silicon PV cells.

The efficiencies of currently the best research cells according to U.S. National Renewable Energy Laboratory (NREL) (NREL, 2013) are shown in Fig. 2.2. As can be seen, the highest reported efficiencies of 37.8% and 44% had been obtained in 2013 with three-junction PV cells under non-concentrated (InGaP/GaAs/InGaAs) and concentrated (GaInP/GaAs/GaInNAs) irradiances, respectively. According to Green et al. (2013), the best confirmed (under standard test conditions (STC) with an irradiance of 1000 W/m^2 with AM1.5 spectrum and at a cell temperature of 25 °C) efficiency of a

terrestrial PV module was 24.1% and it was obtained with a thin film PV module based on GaAs.

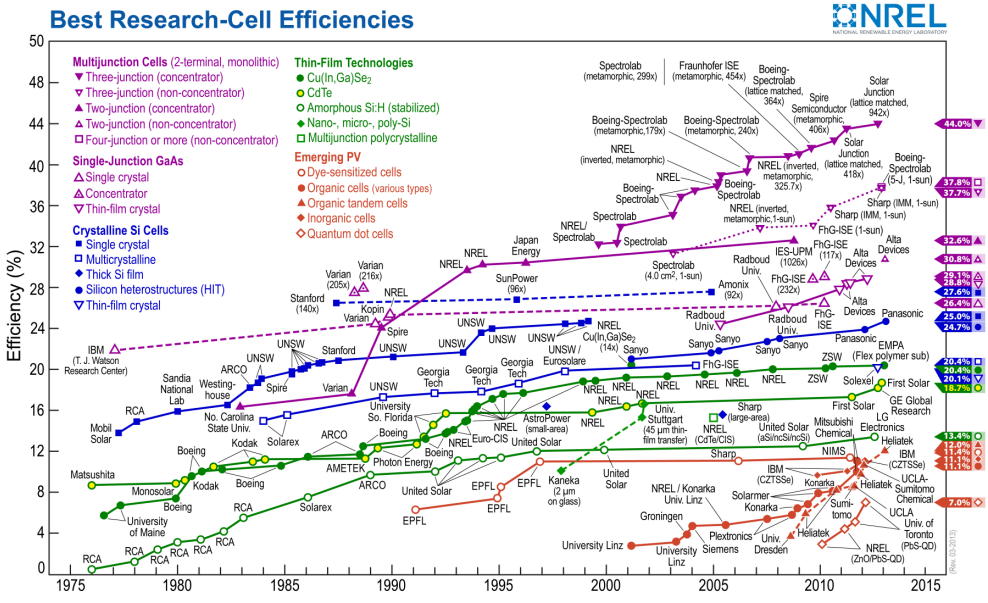

Fig. 2.2: Development of efficiencies of different PV cells according to NREL (2013).

2.3 Mathematical Modeling of the Operation of Photovoltaic Cells

In order to optimize the operation of PV power systems it is important to be able to model the electrical behavior of PV cells. Mathematical presentation for the I-U characteristic of a PV cell can be derived based on extensive knowledge of semiconductor physics (Luque and Hegedus, 2003). The general expression for the current of a PV cell I is

$$I = I_{\mathrm{SC}} - I_{\mathrm{o1}} \left[\exp\left(\frac{\mathrm{q}U}{\mathrm{k}T} \right) - 1 \right] - I_{\mathrm{o2}} \left[\exp\left(\frac{\mathrm{q}U}{2\mathrm{k}T} \right) - 1 \right], \tag{2.1}$$

where I_{SC} is the SC current, U the voltage, k the Boltzmann constant, q the elementary charge, T the temperature, I_{o1} and I_{o2} the dark saturation currents in the quasi-neutral and depletion regions of the cell, respectively. Eq. (2.1) neglects the effects of parasitic series resistance R_{s} and shunt resistance R_{sh}. These resistances are typically associated with real PV cells and they represent losses due to several reasons (Messenger and Ventre,

2010). Incorporating the resistances into Eq. (2.1) yields

$$I = I_{\mathrm{ph}} - I_{\mathrm{o1}}\left[\exp\left(\frac{U + R_{\mathrm{s}}I)}{U_{\mathrm{t}}}\right) - 1\right] - I_{\mathrm{o2}}\left[\exp\left(\frac{U + R_{\mathrm{s}}I}{2U_{\mathrm{t}}}\right) - 1\right] - \frac{U + R_{\mathrm{s}}I}{R_{\mathrm{sh}}}, \quad (2.2)$$

where $U_{\mathrm{t}} = \mathrm{k}T/\mathrm{q}$ is the thermal voltage of the cell. An electrical equivalent circuit diagram shown in Fig. 2.3 can be drawn based on Eq. (2.2). This model is widely used in the literature, for example, in (Chamberlin et al., 1995; Galiana et al., 2008; Gow and Manning, 1999; Sandrolini et al., 2010; Silvestre et al., 2009; Vorster and van Dyk, 2005).

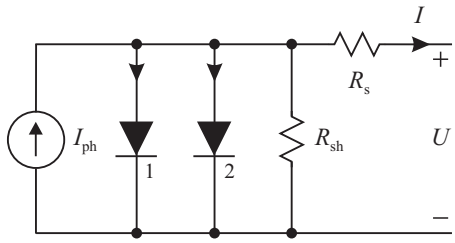

Fig. 2.3: The electrical equivalent circuit diagram of a PV cell based on the two-diode model.

It is, however, often assumed for the sake of simplicity that the effect of dark saturation current in the depletion region (diode 2 in Fig. 2.3) is relatively small. This is a reasonable assumption in case of high quality PV cells (Luque and Hegedus, 2003). The effects of both diodes are then taken into account by using ideality factor A. Combining the effects of the diodes by using A yields the well-known one-diode model in which the current of the PV cell

$$I = I_{\mathrm{ph}} - I_{\mathrm{o}}\left[\exp\left(\frac{U + R_{\mathrm{s}}I}{AU_{\mathrm{t}}}\right) - 1\right] - \frac{U + R_{\mathrm{s}}I}{R_{\mathrm{sh}}}, \quad (2.3)$$

where I_{o} is the dark saturation current of the cell.

The electrical equivalent circuit diagram based on the one-diode model is shown in Fig. 2.4. The one-diode model is widely used in the literature (Brano et al., 2010; Liu and Dougal, 2002; Nema et al., 2009; Nousiainen et al., 2013; Shockley and Queisser, 1961; Villalva et al., 2009a), because it is easier to use than the two-diode model to mathematically model the operation of PV cells and modules. In Fig. 2.4, I_{d} is the current and $U_{\mathrm{d}} = U + R_{\mathrm{s}}I$ the voltage of the diode. I_{d} is the product of the dark saturation current I_{o} and the exponential term subtracted by one in Eq. (2.3).

The circuit diagram in Fig. 2.4 consists of a current source representing the light-generated current which is directly proportional to the amount of irradiance reaching

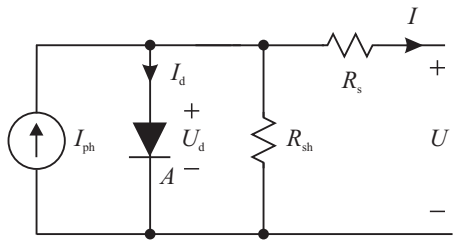

Fig. 2.4: The electrical equivalent circuit diagram of a PV cell based on the one-diode model.

the surface of a PV cell. It is connected in parallel with a diode which represents the recombination in the PV cell. In addition to irradiance, the light-generated current of a PV cell is also dependent on the operating temperature of the cell. This simplified model is well-known and widely used in the literature and has, therefore, been also used in this thesis to model the operation of PV power generators. Although the shunt resistance of two and one-diode models also decribes the operation of PV cells at negative voltages (in this thesis also) (Alonso-García and Ruiz, 2006), it is quite common to add an additional term into the two and one-diode models in order to model the effect of the Avalanche breakdown phenomenon (Bishop, 1988; Kawamura et al., 2003; Quaschning and Hanitsch, 1996; Silvestre and Chouder, 2008). Adding an additional term into the model would only increase the complexity of the simulation model, therefore, requiring more computational effort to run it. Moreover, adding an additional term would not give much more information because of the way the partial shading conditions are studied in this thesis by using the developed systematic method presented in Section 3.3.

The electrical characteristics of a PV cell modeled by using the one-diode model can also be solved using the Lambert W-function (Ding and Radhakrishnan, 2008; Ghani et al., 2013; Petrone et al., 2007). Although the one-diode model is a non-linear and implicit function of PV cell voltage, use of the Lambert W-function allows apparently explicit calculation of PV cell current as a non-linear function of PV cell voltage. Lambert W-function cannot be expressed in terms of elementary functions, but can be efficiently solved by using software such as Matlab and Mathematica.

Although two and one-diode models are the most widely used modeling methods, other methods can also be found in literature such as the model based on using piecewise linear parallel branches which use linear models to model different parts of the I-U curve of a PV cell (Wang and Hsu, 2011b). According to Saetre et al. (2011), the I-U characteristics can also be modeled using equations for current and voltage based on SC current, open-circuit (OC) voltage and two different shape parameters.

2.4 Effect of Environmental Conditions

The *I-U* and *P-U* curves of a PV cell obtained by using the one-diode model of a PV cell are shown in Fig. 2.5 relatively to the values of current and voltage at MPP. As can be seen, the electrical characteristics are non-linear and have only one point at which the maximum amount of power can be obtained, i.e. MPP at the point (1.0, 1.0). The other important points on the curve are the value of SC current (at zero voltage) and value of OC voltage (at zero current).

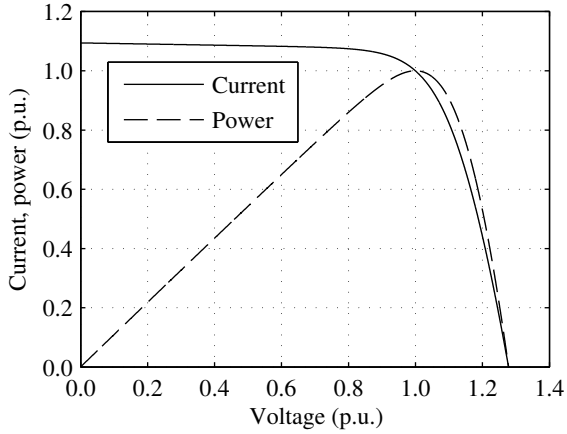

Fig. 2.5: Non-linear electrical characteristics of a PV cell shown relatively to the values at the MPP.

The most important conditions affecting the operation of silicon PV cells are the irradiance absorbed by the cells and the temperature of the cells, which is affected by ambient temperature, wind speed, humidity and, most importantly, the irradiance heating up the cells. The effect of irradiance on silicon PV cells is shown in Fig. 2.6. The SC current of the cell is directly proportional to irradiance, which can be seen when comparing the SC currents under irradiance conditions of 500 W/m^2 and 1000 W/m^2. When irradiance doubles, the SC current also doubles. The irradiance also affects the value of OC voltage, but the effect is smaller than on the SC current. This is due to the fact that OC voltage is logarithmically dependent on the irradiance. At high values of irradiance ($>$ 100 W/m^2), the change of OC voltage with respect to temperature is relatively small.

Temperature is the other important factor affecting the operation of silicon PV cells. The effect of temperature on *I-U* curve is shown in Fig. 2.7. For a silicon PV cell, the effect of temperature on OC voltage is approximately –2.3 mV/°C (Wenham et al., 2007). The temperature also affects the SC current, but the effect is much smaller than on the

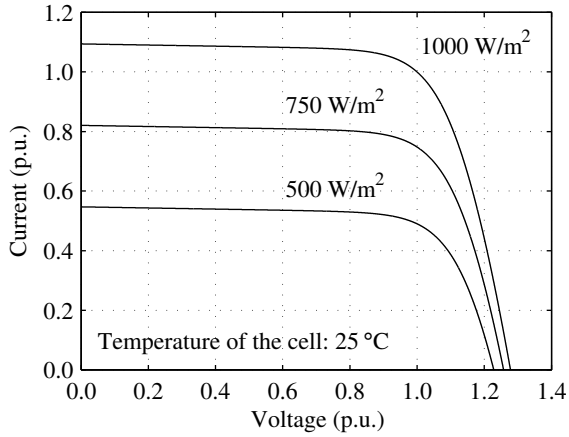

Fig. 2.6: The effect of irradiance on electrical characteristics of a silicon PV cell relative to the values at MPP for an irradiance of 1000 W/m^2.

OC voltage.

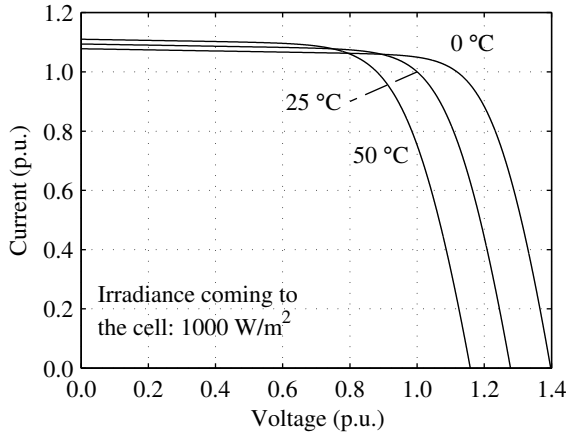

Fig. 2.7: The effect of temperature on electrical characteristics of a silicon PV cell relative to the values at MPP for a cell temperature of 25 °C.

2.5 The Operation of PV Modules Under Partial Shading Conditions

PV cells are typically connected in series and/or parallel in order to be used in electrical energy production (Häberlin, 2012). This is due to the fact that the voltage and power levels of a single PV cell are quite low. Series connection of PV cells increases the maximum voltage of the system and parallel connection the maximum current. By using

both series and parallel connections, the PV system can be designed to have the desired nominal voltage and power levels. Typically the cells are connected in series to form PV modules, which are the basic building blocks of PV power generators. The amount of PV modules in a generator depends on such things as the area in which the generator is installed, voltage and power ratings or limitations of other components of the system or just basically the cost of the system (Häberlin, 2012).

The series connection of PV cells is, however, prone to mismatch losses if the electrical characteristics of the PV cells are not similar (Chamberlin et al., 1995) or the cells do not operate under uniform conditions due to, for example, partial shading conditions (Alonso-García, Ruiz and Chenlo, 2006). Mismatch losses are losses which occur when all the PV cells are not operating at their own MPPs despite the fact that the whole system would operate at its own MPP. In this thesis, partial shading conditions mean all conditions during which the operating conditions of all of the PV cells are not identical but the main focus is on conditions with non-uniform irradiance conditions. In series connection the PV cell with the lowest SC current limits the current of the whole series connection (Wenham et al., 2007). Under partial shading conditions, shaded PV cells have lower SC current than the non-shaded cells. If then the current of the PV power generator is higher than the SC current of the shaded cell, the cell will be reverse biased due to the other cells in the series connection. In this case, the reverse biased cell acts as a load in the series connection dissipating part of the power generated by the other cells leading to power losses. These losses can lead to a phenomenon called hot-spot heating in the shaded cell and the cell can be irreversibly damaged (Lashway, 1988).

The mismatch losses due to differences in electrical characteristics of PV cells are studied in (Bishop, 1988; Bucciarelli, 1979; Chamberlin et al., 1995; Iannone et al., 1998; Kaushika and Rai, 2007; Saha et al., 1988). It has been found that as long as the deviation in the MPP currents of the PV cells under uniform conditions is small enough, the mismatch losses remain quite low (Bucciarelli, 1979). Manufacturers of PV modules select the cells to be used in a certain module from a set of cells with similar characteristics thus making sure that the mismatch losses do not become too high. Bishop (1989) studied the different phenomena such as thermal, avalanche or Zener breakdown leading to the damaging of PV cells due to hot-spots when the cells operate at negative voltages.

In order to prevent PV cells from damaging due to hot-spots (Muñoz et al., 2008), bypass diodes are connected in anti-parallel with certain amount of PV cells (Silvestre et al., 2009). There are 54 series-connected PV cells and three bypass diodes, each of them connected in anti-parallel with 18 PV cells in the studied PV modules in this thesis. The optimal amount of bypass diodes in a PV module have been studied earlier in (Al-Rawi et al., 1994; Silvestre et al., 2009; Ubisse and Sebitosi, 2009). The amount of cells per bypass diode ultimately depend on the breakdown voltage of the cells so that the

cell should not be able to operate at reverse bias with negative voltage close to or less than the breakdown voltage. According to Al-Rawi et al. (1994) the reliability of the PV module improved as the number of PV cells protected by a bypass diode was decreased. Losses due to partial shading can be minimized if there is one bypass diode for every cell (Quaschning and Hanitsch, 1996; Roche et al., 1995). This, on the other hand, increases the cost of PV modules. Typically bypass diodes are Schottky diodes, but they can also be controllable switches, which have lower losses than the diodes (Acciari et al., 2011).

Partial shading conditions can occur due to multiple of reasons such as buildings, trees or clouds. Shading due to static objects typically moves slowly as the Earth spins around its axis. Shading due to clouds is dynamic in a way that the shading conditions come suddenly and also leave the area of the generator quickly. The differences between these different causes of shading are studied and discussed more in Chapter 5 of this thesis.

The operation of bypass diodes is further illustrated in Fig. 2.8. When the series connection is operating at a current higher than the SC current of the block of shaded cells, the bypass diode of that block bypasses the amount of current exceeding the value of SC currents. If, on the other hand, the operating point is at currents less than the SC current of the block of shaded cells, none of the bypass diodes conduct.

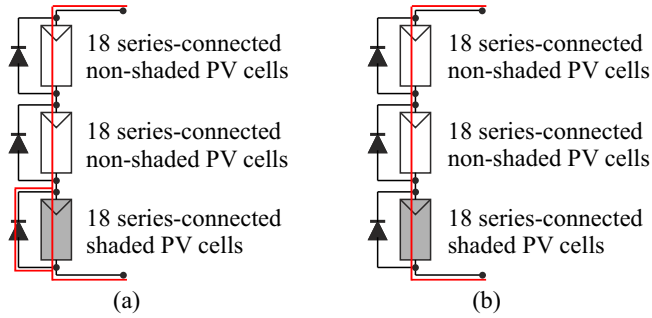

Fig. 2.8: The operation of bypass diodes when the current of the PV module is (a) higher or (b) lower than the SC current of the shaded cells.

In addition to preventing hot-spots occurring in PV cells, bypass diodes alter the electrical characteristics of the modules as can be seen in Fig. 2.9. *I-U* curve of the module has now multiple steps due to which the *P-U* curve in Fig. 2.10 has two MPPs, one at 16.7 V and the other at 28.7 V.

2.6 Maximum Power Point Tracking

In order to extract maximum amount of energy from PV power generators, they must be made to operate at their MPP as was shown in Fig. 2.5. There has been a great amount of

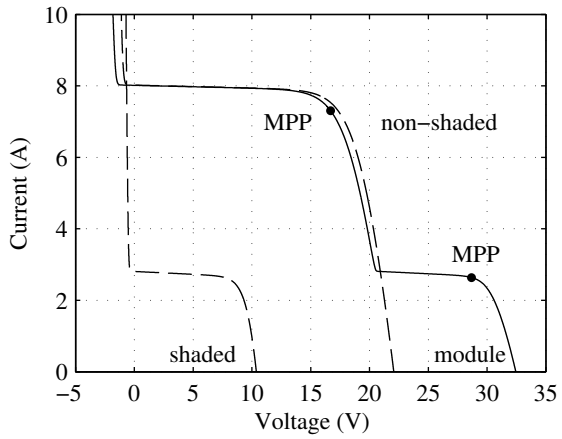

Fig. 2.9: Effect of partial shading conditions on *I-U* curve of a PV module. One block of 18 series-connected cells with anti-parallel-connected bypass diodes is shaded and two are non-shaded.

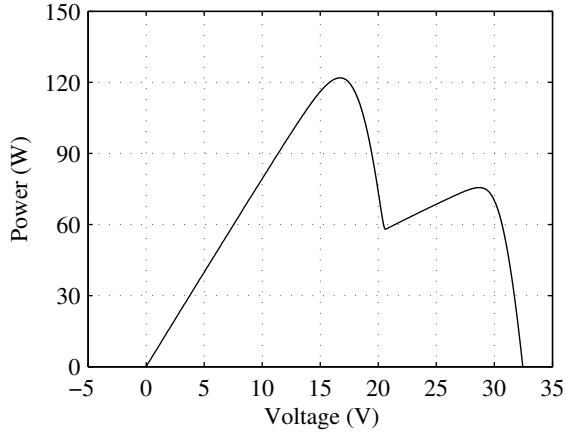

Fig. 2.10: Effect of partial shading conditions on *P-U* curve of a PV module. One block of 18 series-connected cells with anti-parallel-connected bypass diodes is shaded and two are non-shaded.

research and development in the field of MPPT techniques (Esram and Chapman, 2007; Salas et al., 2006). The operation of different MPPT techniques differ, for example, in convergence speed, range of effectiveness, complexity, required amount of sensors for measurements and implementation hardware.

Salas et al. (2006) divides different techniques into indirect and direct techniques. An example of an indirect technique is the fractional OC method, which makes use of

the information that the MPP voltage of silicon cells is approximately 80% of the OC voltage. OC voltage can then be measured in certain time intervals and the operating point can be adjusted based on the measurement. This technique does not quarantee operation at the MPP, but is suitable for small generators and is also easy to implement and cost-effective (Lopez-Lapeña and Penella, 2012). Direct methods ensure that the operating point is really at least at some of the MPPs. A conventional and popular direct method is the P&O algorithm. The basic idea is to perturb the operating point of the PV power generator and observe the change in power. If the power increases, the operating point is varied in the same direction also in the next step. If power decreases, the direction of the perturbation is changed. The algorithm does not recognize when it is at the MPP but keeps on oscillating around the MPP. It has been shown that the most basic version can fail to stay at the MPP during changing irradiance conditions (Hussein et al., 1995). Optimization of P&O algorithm in rapidly changing operating conditions has been discussed, for example, by Femia et al. (2005).

In case of partial shading conditions with multiple MPPs on the *P-U* curve of the generator such as in Fig. 2.10, the MPPT becomes more complicated. There has also been extensive research related to the development of these global MPPT algorithms. The typical idea in these algorithms is to search the global MPP by scanning the whole *P-U* curve or part of it. The scan can be realized with an additional circuit, which scans the *P-U* curve between SC and OC operating points (Noguchi et al., 2002), or with an interfacing converter connected to the input terminals of the PV power generator (Kazmi et al., 2009). The advantage of these algorithms is that they are relatively simple and can be used in any system without specific information about the system or without knowledge about the operating conditions. The major disadvantage is that energy is lost every time the scan is performed.

P-U curves can also be scanned more efficiently by using knowledge about the system and operating conditions. Then it is not necessary to scan the whole *P-U* curve of the generator. For example in (Alonso et al., 2009) this is done by noticing that the minimum distance between two local MPPs is the MPP voltage of the shaded series-connected PV cells connected in anti-parallel with a bypass diode. Several techniques to improve the performance of the scanning have been developed, such as Fibonacci Search (Ahmed and Miyatake, 2008), DIRECT Search (Nguyen and Low, 2010) and Particle Swarm Optimization (Miyatake et al., 2011). However, these algorithms also perform a scan for the global MPP either within certain time intervals or when certain predetermined conditions take place. Unfortunately, these predetermined conditions can be satisfied also due to other changes in operating conditions than partial shading leading to unnecessary scanning of the power curve. Also some other techniques which are not, strictly speaking, MPPT algorithms, have been developed to minimize the effects of partial shading on the

operation of PV power generators (Karatepe et al., 2008; Nguyen and Lehman, 2008).

A two-stage MPPT algorithm (Kobayashi et al., 2006) has been developed by combining a scanning method and a conventional MPPT, such as IC. In the first stage, the OC voltage and SC current are measured online, which means that power delivery is interrupted during the measurement and some energy is lost. Measurements are then used to move the operating point into the vicinity of the global MPP. In the second stage, the conventional MPPT algorithm is used to reach the global MPP. It has been shown, however, that under certain partial shading conditions the first stage of the algorithm is unable to move the operating point into the vicinity of the global MPP (Alonso et al., 2009).

2.7 PV Power Systems and Generator Configurations

PV power generators can basically be classified into stand-alone and grid-connected generators (Gow and Manning, 2000). In stand-alone systems, the energy storage has a big influence on the design of the systems. In grid-connected systems, the grid acts as an energy storage into which the PV power generator can inject power whenever power is available. According to Eltawil and Zhao (2010) most of the new installed systems are grid-connected PV systems.

Due to the fact that the output of PV power generators is direct current (DC) and the electricity in electrical grids is alternating current (AC), there is a need for an additional component, an inverter. The main function of the inverter is to convert DC into AC. In PV power systems, the inverter can also have other important functions such as MPPT, islanding detection, safety and monitoring functions (Teodorescu et al., 2011). In case of grid-connected systems, several different inverter concepts have been developed (Abella and Chenlo, 2004; Araújo et al., 2010; Kjaer et al., 2005). In this thesis, the configurations of PV power generators have been named based on the names of the inverter concepts, because the PV power generator has certain characteristics when it is used as an input source for a certain type of inverter. Different inverter concepts are shown in Fig. 2.11.

Most of the systems in the past have been based on the central inverter concept in which a certain amount of PV modules are connected in series (to form strings) in order to obtain a high enough voltage level. These strings are then connected in parallel to increase the power level of the generator. According to Kjaer et al. (2005) the drawbacks of this configuration are power losses due to centralized MPPT, mismatch losses occuring due to non-uniform conditions between the PV modules (due to a high amount of modules distributed on a large area), losses in string diodes (connected in series with strings to prevent reverse current flow) and non-flexible design.

In the string inverter concept, only one string (or few strings) is connected to an inverter. There are no losses associated with string diodes and separate MPPTs can be

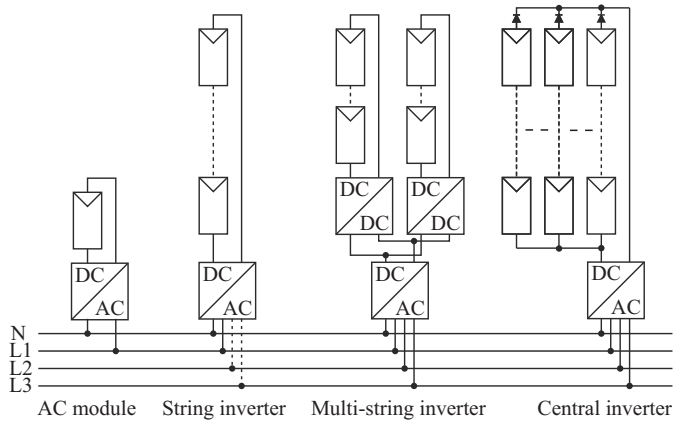

Fig. 2.11: Different inverter concepts used in PV power systems.

applied to each string, which can further reduce losses. The string inverter concept is also more modular compared to the central inverter and thus the system is more flexible if upgraded to higher power levels (Kjaer et al., 2005).

AC modules are results of integrating one inverter and a PV module into one device. They remove mismatch losses completely if it is assumed that individual PV modules operate under uniform conditions. Only minor losses due to differences in electrical characteristics of the cells in PV modules remain. The AC module concept is also the most modular solution. However, the efficiency of the AC module inverters are typically not as high as the efficiency of the inverters with higher power ratings (Kjaer et al., 2005).

The multi-string inverter concept is a product of further developing the string inverter concept. Every string of the generator has its own interfacing DC-DC converter, which is able to perform MPPT function. The power rating of the inverter in this concept is of the same order as in a central inverter concept so the efficiency of the inverter is high. More flexibility is also achieved because new strings can be plugged into the existing system (Kjaer et al., 2005).

All of the above-mentioned inverter concepts can also be realized using a single or two cascaded power processing stages (Carrasco et al., 2006). A single-stage inverter must handle all the tasks such as MPPT and grid current control. The number of PV modules in the strings must also be high to have high enough of a voltage level in order for the inverter to produce pure sinusoidal grid current (or currents in case of three-phase systems). Another solution is the dual-stage inverter which has a separate DC-DC converter on the generator side and an inverter on the grid side. Basically, a multi-string inverter is already an example of the dual-stage scheme, because it has a DC-DC converter performing MPPT and an inverter which converts DC into AC and injects the power to the electrical grid.

3 MODELING AND SIMULATION OF THE OPERATION OF PHOTOVOLTAIC POWER GENERATORS

This chapter presents the simulation model used to obtain results presented in Chapters 4 and 5 and a method to obtain the parameters of the model. The experimental verification of the model is also presented and the validity of the model for the purposes of the thesis is discussed.

A systematic method to analyze the effect of partial shading conditions on the operation of PV power generators is also presented and discussed. This systematic method has been utilized to obtain results presented in Chapter 4 and part of the results in Chapter 5. In the end of the chapter, an approach to study the mismatch losses in PV power power generators under partial shading conditions caused by clouds is presented. The approach is based on using actual measured data from TUT Solar Photovoltaic Power Station Research Plant as input for the simulation model.

3.1 Simulation Model of PV Power Generator

The well-known one-diode model in Eq. (2.3) is used in this thesis to model the operation of PV power generators. The model for the operation of a PV module composed of 54 series-connected PV cells can be obtained by scaling the parameter values used in the one-diode model for one cell by the number of PV cells in the module. Thermal voltage of the PV module is then $U_\mathrm{t} = N_\mathrm{c}\mathrm{k}T/\mathrm{q}$, where N_c is the number of cells in the module.

The method presented by Villalva et al. (2009a) to obtain the values of parameters used in modeling the operation of PV power generators has been used in this thesis. It is based on three points in the electrical characteristics of the PV module: the OC voltage, the SC current and the current and voltage at the MPP. These three points are measured in STC and presented by the manufacturer of the PV module. The ideality factor $A = 1.3$ is used as a typical value found in literature for silicon-based PV modules (Villalva et al., 2009a; Wenham et al., 2007).

Light-generated current in any environmental conditions can be obtained as a function of SC current by current division from the one-diode model. The current of the diode I_d is neglected assuming that in SC condition it is very small and almost all of the

light-generated current flows to the terminals of the module. Accordingly,

$$I_{\mathrm{ph}} = (I_{\mathrm{SC,STC}} + K_{\mathrm{i}}\Delta T)\frac{G}{G_{\mathrm{STC}}}\frac{R_{\mathrm{sh}} + R_{\mathrm{s}}}{R_{\mathrm{sh}}}, \tag{3.1}$$

where $I_{\mathrm{SC,STC}}$ is the SC current in STC, K_{i} the temperature coefficient of the SC current, G the irradiance reaching the surface of the module and the temperature difference ΔT=T–T_{STC}, where T is the temperature of the PV module. In STC, the module temperature T_{STC} and the irradiance G_{STC} are 25 °C and 1000 W/m^2, respectively. The spectral conditions are AM1.5.

The dark saturation current I_{o} depends on the structure and material of the PV cell. It is obtained in OC operating point by adding the effect of temperature on the OC voltage in STC. Dark saturation current then becomes

$$I_{\mathrm{o}} = \frac{I_{\mathrm{ph}} - (U_{\mathrm{OC,STC}} + K_{\mathrm{u}}\Delta T)/R_{\mathrm{sh}}}{\exp[(U_{\mathrm{OC,STC}} + K_{\mathrm{u}}\Delta T)/(AU_{\mathrm{t}})] - 1}, \tag{3.2}$$

where $U_{\mathrm{OC,STC}}$ is the OC voltage in STC and K_{u} the temperature coefficient of the OC voltage. The operation of PV modules and PV power generators have been modeled in this thesis by using Eqs. (2.3), (3.1) and (3.2).

A method to obtain the series and shunt resistances is also presented by Villalva et al. (2009a). It has been pointed out that there is only one pair of values for R_{s} and R_{sh} for which the MPP of the model coincides with the one given by the manufacturer for a specific PV module in STC. This is due to the fact that the power must match at MPP as shown in Eq. (3.3) and the derivative of power must also be zero at MPP. This pair of values can be obtained from

$$P_{\mathrm{MPP,STC}} = U_{\mathrm{MPP,STC}}\left\{I_{\mathrm{ph,STC}} - I_{\mathrm{o,STC}}\left[\exp\left(\frac{U_{\mathrm{MPP,STC}} + R_{\mathrm{s}}I_{\mathrm{MPP,STC}}}{AU_{\mathrm{t,STC}}}\right) - 1\right] - \frac{U_{\mathrm{MPP,STC}} + R_{\mathrm{s}}I_{\mathrm{MPP,STC}}}{R_{\mathrm{sh}}}\right\}, \tag{3.3}$$

where $P_{\mathrm{MPP,STC}}$ is the power, $U_{\mathrm{MPP,STC}}$ the voltage and $I_{\mathrm{MPP,STC}}$ the current of the module at MPP in STC. The light-generated current in STC $I_{\mathrm{ph,STC}}$ can be obtained from Eq. (3.1) by inserting $\Delta T = 0$ K and $G = G_{\mathrm{STC}}$. The shunt resistance R_{sh} can be obtained from Eq. (3.3) as a function of series resistance R_{s} as follows:

$$R_{\mathrm{sh}} = \frac{U_{\mathrm{MPP,STC}} + R_{\mathrm{s}}I_{\mathrm{MPP,STC}}}{I_{\mathrm{ph,STC}} - I_{\mathrm{o,STC}}\left\{\exp\left[(U_{\mathrm{MPP,STC}} + R_{\mathrm{s}}I_{\mathrm{MPP,STC}})/(AU_{\mathrm{t,STC}})\right] - 1\right\} - I_{\mathrm{MPP,STC}}}. \tag{3.4}$$

Although the equation of the light-generated current $I_{\mathrm{ph,STC}}$ includes both the series

and the shunt resistance as shown in Eq. (3.1), it is still possible to solve R_{sh} explicitly as a function of series resistance R_{s}. The pair of resistances is solved iteratively by using a typical series resistance of the PV module as a starting point and finding the pair for which the maximum power in STC is exactly the same as given by the manufacturer. By using this method the electrical characteristics of the modeled PV module can be made to match the three known points of the *I-U* characteristic in STC. In other conditions than STC, the operating conditions are taken into account as shown in Eqs. (3.1) and (3.2). In this thesis, the resistances has been solved by using the Matlab script presented in Appendix A.

Characteristics of the bypass diodes used in the PV module to protect the cells against hot-spots are modeled with Eq. (2.3) by assuming the shunt resistance R_{sh} of the diode to be infinite and the light-generated current I_{ph} to be zero. The rest of the parameters in Eq. (2.3), such as the diode ideality factor (A_{bypass}), series resistance ($R_{\mathrm{s,bypass}}$) and diode dark saturation current ($I_{\mathrm{o,bypass}}$), are obtained by means of curve fitting to a measured *I-U* characteristic of a Schottky diode. Parameters used in the model of a bypass diode are shown in Table 3.1.

Table 3.1: Parameters used to model the operation of a bypass diode.

Parameter	Value
$R_{\mathrm{s,bypass}}$	0.02 Ω
A_{bypass}	1.50
$I_{\mathrm{o,bypass}}$	3.20 μA

The method to obtain parameters for the PV module considers only the characteristics of the PV module. The bypass diode and the PV cell are separate and independent components of the PV module and, therefore, they have also been modeled separately. Then, in the Simulink simulation model, a block of series-connected PV cells and a bypass diode connected in anti-parallel are modeled as an integrated system as presented in Appendix B.

Electrical characteristics of a NAPS NP190GKg PV module, particularly designed to be used in grid-connected PV power generators, have been used in the simulations. The technical specifications of a NAPS NP190GKg PV module have been shown in Appendix C. NAPS NP190GKg PV module is composed of 54 series-connected polycrystalline silicon cells. The PV module consists of three similar parts, each having 18 series-connected cells with an anti-parallel-connected bypass diode to protect them against hot-spots. The nominal operating cell temperature (NOCT) is 46 °C. NOCT is measured in nominal operating conditions in which the irradiance is 800 W/m^2, ambient temperature is 20 °C and wind speed is 1 m/s with free air access to the rear of the module. Based on

these parameter values, the temperature-rise coefficient K_t of the module can be calculated (Dunlop, 2005). K_t represents the increase of cell temperature due to irradiance. Then by knowing the temperature-rise coefficient, the ambient temperature T_amb and the irradiance G, the module temperature can be calculated as follows:

$$T = T_\mathrm{amb} + K_\mathrm{t} G. \tag{3.5}$$

The effect of the PV module temperature-rise due to irradiance on the operation of the PV power generator has been demonstrated by applying the realistic temperature-rise coefficient $K_\mathrm{t} = 0.033$ Km^2/W and by ignoring it ($K_\mathrm{t} = 0$ Km^2/W) in the simulation model. Irradiance on the studied PV power generator in Chapter 4 (composed of 18 series-connected PV modules) was varied from 0 to 1000 W/m^2 and it operated under uniform conditions at $T_\mathrm{amb} = 20$ °C. The MPP currents of the simulated cases are shown as a function of MPP voltage in Fig. 3.1. Both the MPP current and voltage increase continuously with increasing irradiance, if the module temperature is kept constant at ambient temperature ($K_\mathrm{t} = 0$ Km^2/W). For the realistic value of $K_\mathrm{t} = 0.033$ Km^2/W, the MPP current increases more or less similarly with increasing irradiance as for $K_\mathrm{t} = 0$ Km^2/W. However, the MPP voltage first increases rapidly, but then starts to decrease with increasing irradiance. At high irradiance levels the MPP voltage difference between the two curves is considerable demonstrating the importance of the module temperature-rise effect due to irradiance on the operation of PV power generators. The effect of K_t is also visible in the results in (Giesler et al., 2012) in which the measured MPP voltages of two systems during several years have been shown.

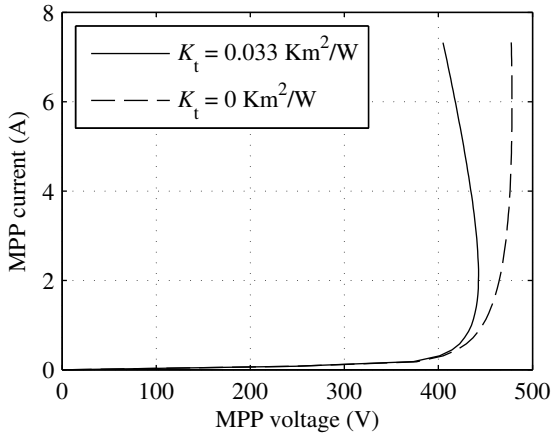

Fig. 3.1: MPP current of the PV power generator as a function of MPP voltage under uniform operating conditions for irradiances from 0 to 1000 W/m^2 for two values of the temperature-rise coefficient K_t.

The electrical characteristics of a single NAPS NP190GKg PV module and the parameters used in simulations are shown in Table 3.2. Temperature coefficients of SC current and OC voltage K_i and K_u, respectively, and the ideality factor A are based on well-known properties of silicon (Wenham et al., 2007).

Table 3.2: Electrical characteristics and parameters used in simulations for a NAPS NP190GKg PV module.

Parameter	Value	Parameter	Value
$U_{\mathrm{OC,STC}}$	33.1 V	K_u	–0.124 V/K
$I_{\mathrm{SC,STC}}$	8.02 A	K_i	0.0047 A/K
$U_{\mathrm{MPP,STC}}$	25.9 V	K_t	0.033 Km^2/W
$I_{\mathrm{MPP,STC}}$	7.33 A	R_s	0.33 Ω
$P_{\mathrm{MPP,STC}}$	190 W	R_sh	188 Ω
		A	1.30

The used simulation models of the PV module and the generator are, naturally, simplifications of the operation of real modules and generators. For example, the light-generated current is dependent on the energy of the band gap of the PV cell material and on the spectrum of the irradiance, and not just on the value of irradiance as assumed in the model. Also the PV modules are not identical in practice. However, the used model is accurate enough for analyzing the phenomena studied in this thesis.

3.2 Experimental Verification of the Operation of the Simulation Model

The operation of the simulation model can be seen in Fig. 3.2 with measured *I-U* curves in three different irradiance and temperature conditions. The irradiance of the module was measured using Kipp & Zonen SP Lite2 pyranometer, which was attached to the module frame and had the same tilt angle as the module. The temperature of the PV module was deduced from the measured irradiance, ambient temperature and back plate temperature of the module (Rubio et al., 2010). Cell temperature was estimated to be 3 °C higher than the backplate temperature under an irradiance of 1000 W/m^2. The ambient and back plate temperatures were measured by using Vaisala HMP155 temperature probe and a PT100 sensor, respectively. *I-U* curves in different operating conditions were measured by using a large capacitor. Once the capacitor was connected in parallel with the PV module via a switch, the operating point of the PV module changed from SC to OC. The current and voltage were measured using data acquisition device from National Instruments (NI DAQPad-6015). The measurement setup is shown in Appendix D.

The accuracy of the simulation model is sufficiently high, especially under high irradiance conditions. This can be seen in Fig. 3.2 by comparing the simulated and measured

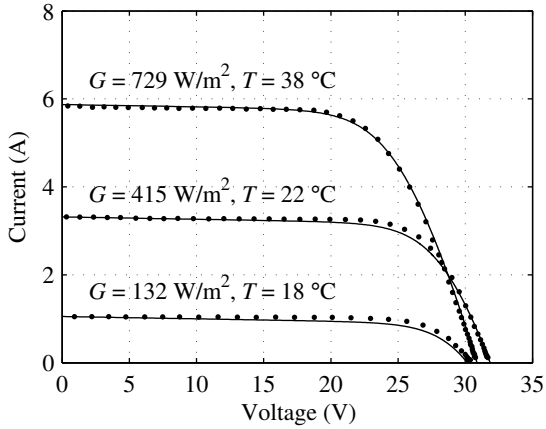

Fig. 3.2: Simulated and measured *I-U* characteristics under three different operating conditions.

I-U curves of the module in the case when irradiance is 729 W/m^2. The accuracy of the simulation model slightly decreases around the MPPs (the knees in the curves) with decreasing irradiance as can be seen for 415 and 132 W/m^2 irradiances. The differences between the simulated and measured currents at the MPPs are 0.04 A, 0.11 A and 0.12 A for irradiances of 729, 415 and 132 W/m^2, respectively, and are in line with the results presented in (Villalva et al., 2009a). The operation of the simulation model under partial shading conditions has been previously verified in (Mäki et al., 2012) for Raloss SR30-36 PV modules manufactured using monocrystalline silicon PV cells. Furthermore, the simulation model is in accordance with the results presented in (Villalva et al., 2009a) for two different PV modules under several operating conditions.

By experimentally verifying the accuracy of the simulation model for a single PV module under several uniform conditions and by modeling the operation of bypass diodes based on the measured characteristics of a Schottky diode, it is reasonable to state that the simulation model gives reliable results of the general effects of partial shading conditions for any PV power generator modelled by using these verified components.

3.3 Systematic Approach to Study the Effects of Partial Shading Conditions

In this section, a systematic approach has been developed and used to study the effects of partial shading conditions on the number of MPPs, characteristics of voltages and current at MPPs. This approach has also been used in this thesis to study mismatch losses of PV power generators with different configurations.

In the approach, the shading of the generators is done by shading one block of series-connected PV cells protected by an anti-parallel-connected bypass diode at a time. This is shown in Fig. 3.3 for the first five cases. In the first case, the PV power generator operates under uniform conditions without shading. In the second case, one third of the first PV module is shaded. After that the shading is increased one third of a module at a time until the whole PV power generator is shaded.

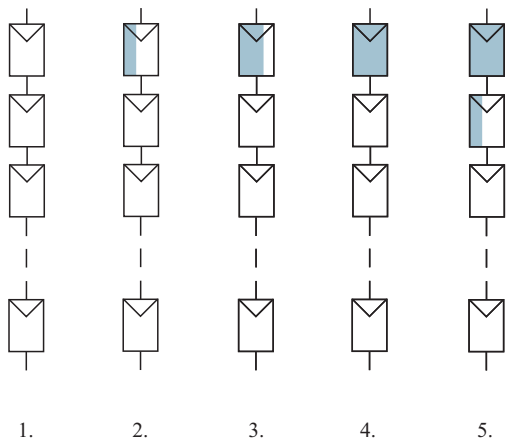

Fig. 3.3: Systematic partial shading of PV power generators.

In Chapter 4, the simulation model of the operation of a PV power generator composed of 18 series-connected NAPS NP190GKg PV modules has been used. This generator corresponds to a single-phase grid-connected generator. However, the studied phenomena are similar for all PV power generators composed of series-connected PV modules. According to the systematic approach, the shading of the PV power generator in Chapter 4 has been done one block of 18 series-connected PV cells with an anti-parallel-connected bypass diode at a time. This yields a total amount of 55 different shading conditions (shading of 0 to shading of 54 blocks) for a certain value of irradiance for the shaded cells. In this thesis, these different shading conditions are described with a term system shading. System shading represents relative amount of shaded blocks of PV cells with an anti-parallel-connected bypass diode compared to the total amount of blocks in the generator (54). A system shading of 0% means that there are no shaded cells and 100% that all the cells are shaded. For the generator studied in Chapter 4, the values of system shading in the first five cases shown in Fig. 3.3 are 0.00, 1.85, 3.70, 5.56 and 7.41%, respectively.

In the systematic approach, the irradiance of the shaded cells was also varied in addition to system shading. This was done by systematically decreasing the value of

irradiance of the shaded cells starting from the value of irradiance of the non-shaded cells. In the results in Chapter 4, the irradiance of non-shaded cells was 1000 W/m^2 and in the first section of Chapter 5 in was 800 W/m^2 representing NOCT conditions. The ambient temperature in both cases was 20 °C. The ratio of the difference between the irradiances of the shaded and non-shaded cells to the irradiance of the non-shaded cells is described with a term shading strength. Therefore, shading strength represents the attenuation of the irradiance due to the shading. Shading strength of 0% means that the shaded cells receive the same irradiance as the non-shaded cells which means that the conditions are uniform. Shading strength of 100% means that the shaded cells are not receiving irradiance at all. In this thesis, the total amount of shading strength steps was also chosen to be same as for system shading, i.e., 55 steps yielding total amount of 3025 different operating conditions for the generator.

In this thesis, partial shading conditions are assumed to be caused by a single object, i.e., there are only two values of irradiances affecting the PV power generator. This means that there can be only two MPPs at maximum. In this way it is possible to have a systematic way to analyze the effects of partial shading by varying the values of system shading and shading strength. In practice, however, partial shading of PV power generators is caused by a variety of objects such as clouds, buildings, trees, animals, etc. Clouds cause shades which can move very rapidly over the PV power generator. Shading caused by surrounding structures is more stationary, moving slowly because of the rotation of the Earth around its axis. The shape of the shading object and the distance to the PV power generator also has an influence on the shading pattern and attenuation of the irradiance due to the shading and, accordingly, to the electrical characteristics and the energy yield of the generator (Martínez-Moreno et al., 2010). In order to understand the effects of particular shading objects on the operation of PV power generators comprehensively, different approaches are needed.

Shading of all the PV cells of one block of series-connected PV cells with an anti-parallel-connected bypass diode introduces a small error compared to results that would be obtained by using a cell-based modeling approach. This is because in practice there can be conditions in which only one or few cells of a block of series-connected PV cells with an anti-parallel-connected bypass diode are be shaded. The error caused by this simplification, which reduces the complexity of the simulation model significantly, is relatively small because by shading even a few of the PV cells in one block of cells affects the electrical characteristics so that they resemble the situation where all the of the block are shaded (Alonso-García, Ruiz and Herrmann, 2006; Karatepe et al., 2007). It becomes clear from the results in (Alonso-García, Ruiz and Herrmann, 2006; Karatepe et al., 2007) that by using the cell-based modeling would not affect the overall operation but only change the values of currents and voltage of MPPs slightly. It should also be

noted that if the cell-based modeling approach was to be used, more accurate model for the operation of PV cells under negative voltages including the effect of Avalanche breakdown phenomenon should also be taken into consideration. This would cause the simulation model to become very complex and computationally heavy. The developed systematic approach, however, is used in this thesis to study the behavior of PV power generators under static partial shading conditions to provide basic understanding on these effects. Despite of small errors, the approach and simulation model are sufficient for the purposes of this thesis.

In Chapter 5, the systematic approach has been used to study mismatch losses in PV power generators with different configurations. The different configurations are shown in Fig. 3.4. The Long string generator is composed of 18 series-connected PV modules and it is based on the string inverter concept. The Parallel strings generator has three parallel-connected strings of six series-connected PV modules and it is based on the central inverter concept. Finally, the Multi-string generator has three individually controlled strings of six series-connected PV modules and it is based on the multi-string inverter concept.

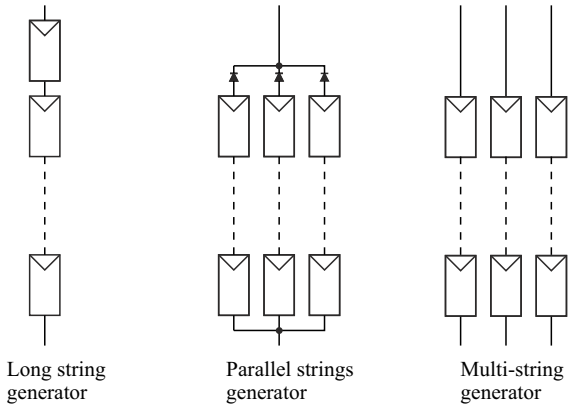

Fig. 3.4: Different PV power generator configurations. Long string generator is composed of 18 series-connected PV modules, Parallel string generator of three parallel-connected strings of six series-connected PV modules and Multi-string generator of three individually controlled strings of six series-connected PV modules.

The shading in cases of Parallel strings and Multi-string generators in Chapter 5 has been done so that one string is completely shaded before shading the next string. The strings are thought to be installed in adjacent rows and it is assumed that the shadow starts to cover the generator on one end and continues to shade the generator until all the modules are shaded. This way the basic behavior of different PV power generators configurations can be investigated systematically. The effects of partial shading conditions, for example, shading one-third of each PV string connected in parallel, can be deduced

based on the used shading pattern. In Section 5.1.1, three practical shading scenarios are studied in order to give more insight in addition to the results of the systematic approach.

3.4 Approach to Study Mismatch Losses Caused by Partial Shading due to Clouds

Partial shading conditions due to clouds are dynamic and affect the operation of PV power generators in different way than partial shading due to static objects. The edge of the shade caused by a static object such as a building is sharp. This means that when shading due to a building affects the generator, the non-shaded modules receive the global irradiance while the shaded modules receive the diffuse part of the irradiance which is typically around 20% of the global irradiance (Armstrong and Hurley, 2010; Oozeki et al., 2005). Shading due to clouds causes irradiance to change gradually when the shade of the cloud covers the generator. This means that all the PV modules of the generator can have different values of irradiance during the cloud shading event.

Mismatch losses due to clouds are analyzed in Chapter 5 by using actual measured environmental conditions. The irradiances were measured using Kipp & Zonen SP Lite2 photodiode sensors attached to the frames of the PV modules having, therefore, the same tilt angles as the modules. Temperatures of the PV modules were measured by using PT100 sensors attached to the back plate of the PV modules. The modules are located on the roof of the Department of Electrical Engineering (61°27'05"N, 23°51'28"E) and are part of the TUT Solar Photovoltaic Power Station Research Plant which layout is shown in Appendix E. The modules in question are part of String 2 and the photodiode sensors used in the study are S9-S14. The data from the irradiance and temperature sensors were recorded once per second. With such a high sampling frequency, it was possible to record even the fastest phenomena in the environmental conditions affecting the PV modules.

The basic weather conditions in Tampere region are such that the mean annual global irradiation on a horizontal plane is approximately 2.45 kWh/m^2/d (Häberlin, 2012; Pirinen et al., 2012). For the sake of comparison, the mean annual global irradiation on a horizontal plane in Berlin is 2.74 kWh/m^2/d and in Barcelona 3.96 kWh/m^2/d (Häberlin, 2012). This means that irradiation conditions are not much different in Tampere compared to Berlin. Mean annual air temperature in Tampere is 4.4°C and average wind speed is 3.1 m/s and the wind is blowing quite evenly from all directions, slightly more from the southwest than from the other directions (Pirinen et al., 2012).

The environmental data used in the simulations was measured during 180 days from 4 June to 7 September 2011 and from 14 April to 14 July 2012 excluding eight days during which the measurement system was halted due to maintenance work. The time period is chosen so that there was no snow covering the PV modules and the surrounding buildings

caused as little partial shading conditions as possible. Thus, mainly the rotation of the Earth around its axis and clouds affected the irradiance of the modules. The rotation of the Earth around its axis causes slow changes in irradiance (below 6.0 Ws/m^2). Changes in irradiance due to moving clouds, however, have been measured to be frequently higher than 10.0 Ws/m^2.

The whole 180-day data was classified into three separate groups of irradiance conditions: dark, uniform and non-uniform. The classification was made according to absolute values of irradiance and changes occurring between consecutive measurements. Small changes were assumed to be due to noise in the measurements or due to the rotation of the Earth around its axis. Higher changes were assumed to be due to moving clouds.

Dark irradiance conditions were present only when the measured absolute value of irradiance was zero. Uniform conditions were present when the change in irradiance for all six photodiode sensors was lower than the limit which was defined based on the changes occurring during a perfectly clear sky day without any objects causing shadows over the sensors. The rate of irradiance changes during a clear sky day was linearly dependent on the value of irradiance. For an irradiance of 0 W/m^2, changes were smaller than 1.2 Ws/m^2 and were due to noise in the measurements. For an irradiance of 1000 W/m^2, changes due to noise were higher, but still below 6.0 Ws/m^2.

Because the changes in irradiance due to noise depended linearly on the magnitude of irradiance, the limit to classify the data into separate data sets was also chosen to be dependent on the value of irradiance. In this way, the time intervals during which the changes in measured irradiances were caused by noise and rotation of the Earth around its axis were classified into the data set of uniform conditions. Non-uniform conditions were present when the irradiance of at least one photodiode sensor changed more than the limit of 1.2 to 6.0 Ws/m^2 for an irradiance of 0 to 1000 W/m^2. This means that non-uniform conditions constitute only of instances with clouds affecting the irradiances of the PV modules.

The three different sets of data are used in Chapter 5 to study the mismatch losses in five different configurations of PV power generators composed of six PV modules. The interest is on the physical length of the PV module strings in addition to the effect of PV power generator configuration on mismatch losses and, therefore, there are two versions of generators with multi-string and parallel strings configurations. Different versions have different amount of series-connected PV modules in the strings. Different generators are shown in Fig. 3.5 and they are the Short multi-strings generator composed of three individually operating strings of two series-connected PV modules, the Short parallel strings generator composed of three parallel-connected strings of two PV modules and a blocking diode connected in series, the Long multi-strings generator composed of two individually operating strings of three series-connected PV modules, the Long parallel

strings generator composed of two parallel-connected strings of three PV modules and a blocking diode connected in series, and the Long string generator composed of six series-connected PV modules. The studied generators are composed of only six PV modules due to the high computing power needed to analyze the extensive climatic data.

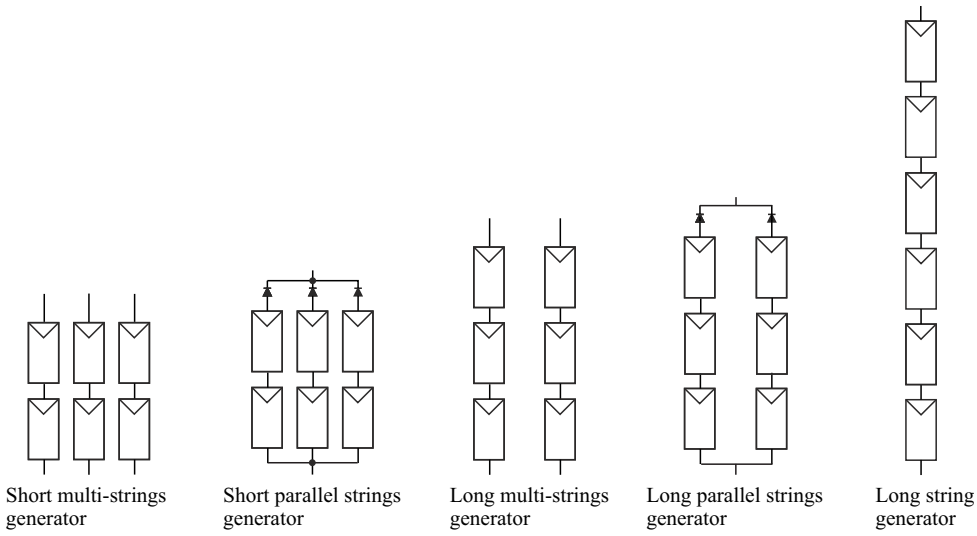

Fig. 3.5: Configurations of the studied PV power generators in case of partial shading due to clouds.

The physical layout of the studied PV power generator configurations can be seen in Fig. 3.6. Short multi-strings and Short parallel strings generators are composed of strings of two series-connected modules which are shown in Fig. 3.6 as short 1, 2 and 3. Long multi-strings and Long parallel strings generators are composed of strings of three series-connected modules which are shown in Fig. 3.6 as long 1 and 2. The Long string generator is the series connection of all six PV modules.

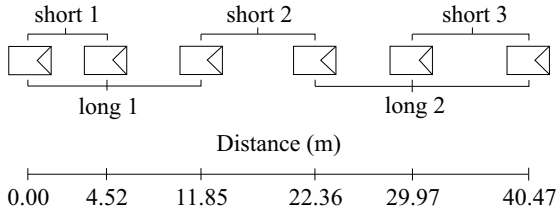

Fig. 3.6: Layout of the studied PV power generator configurations in case of partial shading due to clouds. Different configurations are composed of substrings which are marked as short 1 to 3 and long 1 and 2.

4 EFFECT OF PARTIAL SHADING CONDITIONS ON MAXIMUM POWER POINTS

The first section of this chapter presents the effect of partial shading conditions on the number of MPPs in a PV power generator composed of 18 series-connected PV modules. Different phenomena causing only one MPP despite of the partial shading conditions will be presented and analyzed. The contents of the first section are also presented in (Mäki and Valkealahti, 2013a).

The last section of this chapter studies the effect of partial shading conditions on the characteristics of MPP currents and voltages. The results of a thorough study of MPPs will be presented. First part of the contents of the last section has been published earlier in (Mäki et al., 2012) and the final part is presented in the manuscript (Mäki and Valkealahti, 2013b) which is currently in peer review process.

4.1 Number of Maximum Power Points

As a result of the systematic approach and use of the simulation model presented in Chapter 3, a contour graph of the number of MPPs is shown in Fig. 4.1 as a function of system shading (amount of shaded cells in the generator) and shading strength (attenuation of irradiance due to the shading). As can be seen, the central area of the figure contains two MPPs, which is the typical case when a PV power generator operates under partial shading conditions. There are also areas on the bottom, in the bottom right corner, on the right side as well as in the top left corner of the figure in which there is only one MPP despite of partial shading conditions. The P-I curve of the PV power generator operating under partial conditions with both system shading x and shading strength y of 50% is shown in Fig. 4.2 (the black dot in the center of Fig. 4.1) for a typical case with multiple MPPs. Most of the figures presenting electrical characteristics in this section are P-I curves instead of more conventional P-U curves. The reason for this is that for series-connected PV cells, the current is same for all the PV modules. It is, therefore, easier to show and explain the reasons for situation with only one MPP despite of the partial shading conditions using P-I curves because the operating points of interest are related to specific value of current rather than voltage.

In the systematic approach, only two values of irradiance at maximum affect the

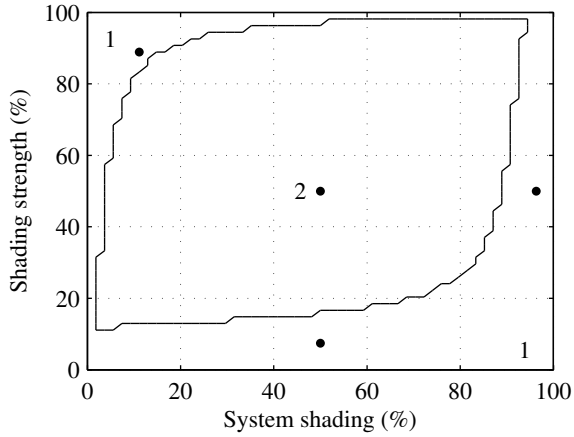

Fig. 4.1: Number of MPPs in the PV power generator as a function of system shading and shading strength. Irradiance of non-shaded PV cells was 1000 W/m^2.

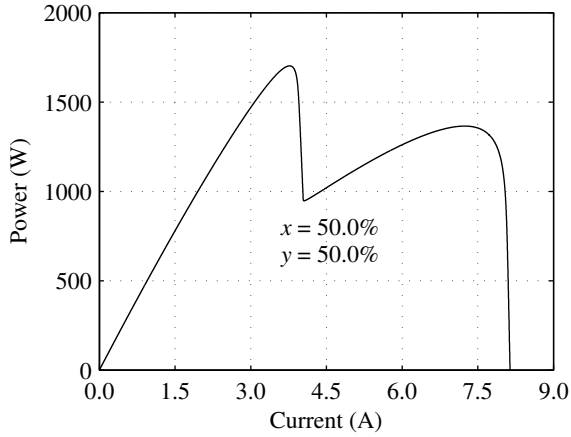

Fig. 4.2: *P-I* curve of the PV power generator operating under partial shading conditions with $x = 50.0\%$ and $y = 50.0\%$.

generator at once. This means that there can be only two MPPs at maximum as shown in Fig. 4.1. These two MPPs occurring under partial shading conditions are classified into MPPs at high and low currents. This is done based on the operating point of individual shaded and non-shaded PV cells. At an MPP at high currents, the current of the generator is higher than the SC current of the shaded cells. This current interval from SC current of shaded cells to SC current of the generator is called the high current region in this thesis. At the MPP at high currents, the non-shaded cells operate near to their MPPs while the bypass diodes protecting the shaded cells bypass the current

exceeding the SC current of the shaded cells. This means that the voltage of an MPP at high currents is a sum of the MPP voltages of blocks of non-shaded cells and the negative voltages of blocks of shaded cells with a forward biased anti-parallel-connected bypass diode.

At an MPP at low currents, the generator current is less than the SC current of the shaded cells. This current interval from zero to SC current of shaded cells is called the low current region in this thesis. At the MPP at low currents, the voltage is the sum of voltages of the blocks of shaded cells operating near to their MPPs and the voltage of blocks of non-shaded cells. Voltages of non-shaded cells are between their MPP and OC voltages defined by the MPP current at low currents. At this MPP, none of the bypass diodes conduct current.

P-I curves of the PV power generator operating under three different partial shading conditions with only one MPP are shown in Fig. 4.3. In case of system shading $x = 50.0\%$ and shading strength $y = 7.4\%$ (the black dot on the bottom of Fig. 4.1), the *P-I* curve has a turn when bypass diodes start to conduct approximately at 7.54 A and 1420 W, but it also has only one MPP on the curve around 6.95 A and 2850 W. The reason for only one MPP is that the value of shading strength is low and so the SC currents of the shaded cells are higher than the MPP current of the non-shaded cells. The value of shading strength, which causes only one MPP, depends on the ratio of MPP current to SC current of the PV cells. This ratio is closely related to the fill factor which is a commonly used parameter to evaluate the performance of PV cells. Low fill factor typically means low value of the ratio of MPP current to SC current. Accordingly, the one-MPP area increases with a decreasing value of the ratio of MPP current to SC current and, therefore, also with a decreasing value of fill factor.

In case of system shading $x = 96.3\%$ and shading strength $y = 50.0\%$ (the black dot on the right side of Fig. 4.1), the *P-I* curve has only one MPP at 3.63 A and 1590 W. The reason for only one MPP is that the power consumed by a high amount of conducting bypass diodes is higher than the MPP powers of the non-shaded cells. In case of system shading $x = 11.1\%$ and shading strength $y = 88.9\%$ (the black dot on the top left corner of Fig. 4.1), the *P-I* curve has a turn when bypass diodes start to conduct approximately at 0.89 A and 416 W, but it has only one MPP at 7.31 A and 2610 W. The reason for only one MPP is the low value of shunt resistance of the PV cells.

The above-mentioned three phenomena that cause only one MPP to the power curve of a PV power generator operating under partial shading conditions will be thoroughly explained in Sections 4.1.1–4.1.3. Different phenomena will be illustrated by using simulation results as well as a measured *I-U* curve in Section 4.1.3 related to the one MPP phenomenon in case of low value of shunt resistance. The reasons for having only one MPP in different operating conditions are also analysed.

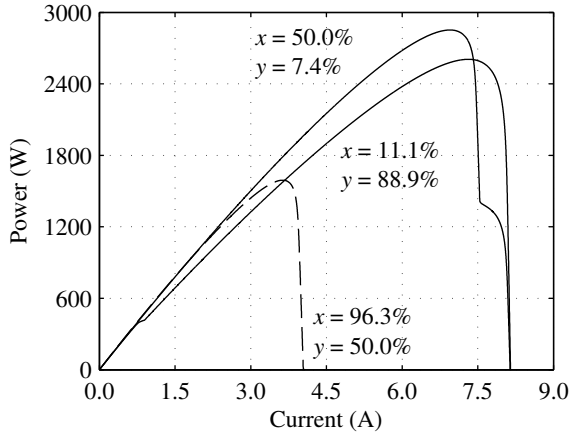

Fig. 4.3: *P-I* curves of the PV power generator operating under three different partial shading conditions with only one MPP (marked with dots in Fig. 4.1).

The analysis is started by assuming that the PV cells and modules are ideal in a way that the effects of parasitic series resistance ($R_\mathrm{s} = 0\ \Omega$) and shunt resistance ($R_\mathrm{sh} = \infty\ \Omega$) are neglected. Only the value of ideality factor A is used to adjust the model so that the ratio of MPP current to SC current in uniform conditions is the same as for the realistic model by which the results shown in Figs. 4.1–4.3 have been obtained. By neglecting the effects of parasitic resistances in Eq. (2.3) and noticing that for the ideal model $I_\mathrm{ph} = I_\mathrm{SC}$, the current I of an ideal PV cell becomes

$$I = I_\mathrm{SC} - I_\mathrm{o}\left[\exp\left(\frac{U}{AU_\mathrm{t}}\right) - 1\right], \tag{4.1}$$

which can be explicitly solved with respect to I and U. The PV power generator modelled by using Eq. (4.1) is referred to as ideal PV power generator later on in this chapter. For this ideal model, the voltage of a conducting bypass diode and the current of a reverse biased bypass diode are zero. It is important to be aware that the simulations are made using the realistic model unless otherwise noted.

4.1.1 Shading Strength

The one-MPP area on the bottom of Fig. 4.1 is due to the value of shading strength compared to the value of $I_\mathrm{MPP,high}/I_\mathrm{SC}$, where $I_\mathrm{MPP,high}$ is the current of the MPP at high currents (and low voltages) of the PV power generator and I_SC the SC current of the generator. In order to illustrate the reason for only one MPP due to low shading strength, *U-I* and *P-I* curves of the PV power generator are shown in Figs. 4.4–4.5 in

one and two-MPP conditions with a system shading of 50% and shading strengths of 7.4% and 18.5%, respectively. In Fig. 4.4, the *U-I* curves bend down abruptly (around 6.4 and 7.4 A) with increasing current. This is followed by a level of lower voltages and then the curves bend down again in the high current region (around 8.0 A). The point at which the bypass diodes start to bypass current around the shaded PV cells is at 7.54 A for a shading strength of 7.4% and 6.62 A for a shading strength of 18.5%. These are the values of the SC currents of the shaded cells. As can be seen, there is only one MPP on the *P-I* curve if the shading strength is so low (in this case 7.4%) that the SC currents of the shaded cells are higher than the MPP current at the MPP at high currents $I_{\mathrm{MPP,high}}$. In this case, the shaded cells generate power already at $I_{\mathrm{MPP,high}}$ and no MPP can take place in the high current region.

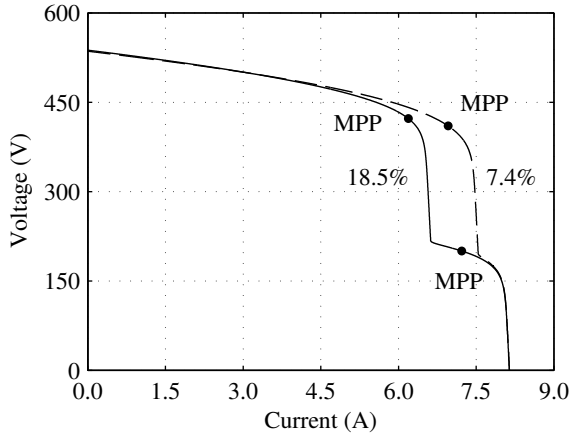

Fig. 4.4: *U-I* characteristics of the PV power generator under partial shading conditions with a system shading of 50% and shading strengths of 7.4% and 18.5%.

The phenomenon shown in Figs. 4.4–4.5 is also studied analytically by using the ideal one-diode model of a PV cell without the effects of parasitic series and shunt resistances given in Eq. (4.1). The voltage of the PV power generator U in the low current region (upper equation after the curly bracket) and in the high current region (lower equation after the curly bracket) can be written in the form

$$U = \begin{cases} (1-x)N_{\mathrm{s}}U_{\mathrm{ns}} + xN_{\mathrm{s}}U_{\mathrm{s}}, & 0 \le I \le (1-y)I_{\mathrm{SC}} \\ (1-x)N_{\mathrm{s}}U_{\mathrm{ns}}, & (1-y)I_{\mathrm{SC}} < I \le I_{\mathrm{SC}}, \end{cases} \tag{4.2}$$

where x is the system shading, N_{s} the number of blocks of 18 series-connected PV cells with an anti-parallel-connected bypass diode. Voltages U_{ns} and U_{s} are the voltages of one block of 18 non-shaded and shaded series-connected PV cells with an anti-parallel-

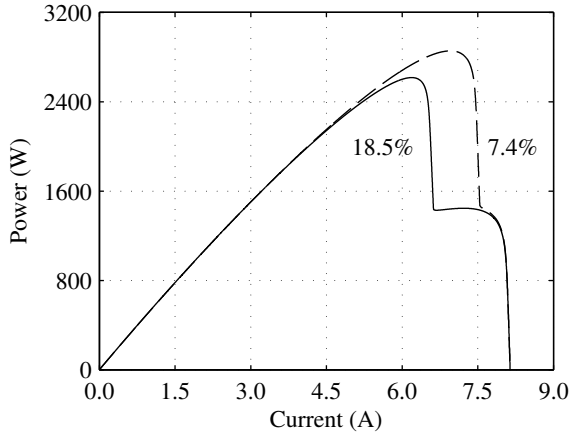

Fig. 4.5: *P-I* characteristics of the PV power generator under partial shading conditions with a system shading of 50% and shading strengths of 7.4% and 18.5%.

connected bypass diode, respectively.

Let us assume that $I_{\mathrm{SC}} >> I_{\mathrm{o}}$ (usually done in case of an irradiance > 0 W/m^2). Then by solving Eq. (4.1) with respect to U, we get the equations for U_{ns} and U_{s}. By substituting U_{ns} and U_{s} into Eq. (4.2), we get

$$U = \begin{cases} (1-x)N_{\mathrm{s}}AU_{\mathrm{t,ns}}\ln\left(\frac{I_{\mathrm{SC}}-I}{I_{\mathrm{o,ns}}}\right) \\ \qquad +xN_{\mathrm{s}}AU_{\mathrm{t,s}}\ln\left(\frac{(1-y)I_{\mathrm{SC}}-I}{I_{\mathrm{o,s}}}\right), & 0 \le I \le (1-y)I_{\mathrm{SC}} \\ (1-x)N_{\mathrm{s}}AU_{\mathrm{t,ns}}\ln\left(\frac{I_{\mathrm{SC}}-I}{I_{\mathrm{o,ns}}}\right), & (1-y)I_{\mathrm{SC}} < I \le I_{\mathrm{SC}}, \end{cases} \tag{4.3}$$

where y is the shading strength, A the ideality factor and $U_{\mathrm{t,ns}}$ and $U_{\mathrm{t,s}}$ the thermal voltages of the non-shaded and shaded PV cells, respectively. $I_{\mathrm{o,ns}}$ and $I_{\mathrm{o,s}}$ are the dark saturation currents of the non-shaded and shaded PV cells, respectively. The number of MPPs in the electrical characteristics of the PV power generator modeled by using Eq. (4.3) is shown in Fig. 4.6. As can be seen, the PV power generator has only one MPP when shading strength is small enough.

The power derivative $\mathrm{d}P/\mathrm{d}I$ at the MPP in the high current region $(1-y)I_{\mathrm{SC}} < I \le I_{\mathrm{SC}}$ for the ideal model of PV power generator can be solved from Eq. (4.3) as

$$\begin{aligned} \left.\frac{\mathrm{d}P}{\mathrm{d}I}\right|_{\mathrm{MPP,high}} &= (1-x)N_{\mathrm{s}}U_{\mathrm{MPP,ns}} + I_{\mathrm{MPP,high}}\left.\frac{\mathrm{d}U}{\mathrm{d}I}\right|_{\mathrm{MPP,high}} \\ &= (1-x)N_{\mathrm{s}}U_{\mathrm{MPP,ns}} - (1-x)N_{\mathrm{s}}AU_{\mathrm{t,ns}}\frac{I_{\mathrm{MPP,high}}}{I_{\mathrm{SC}}-I_{\mathrm{MPP,high}}} = 0, \end{aligned} \tag{4.4}$$

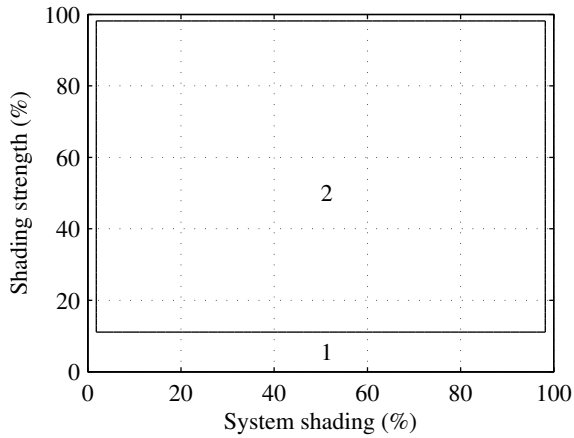

Fig. 4.6: Number of MPPs¨of the ideal PV power generator as a function of system shading and shading strength under partial shading conditions.

where $U_{\mathrm{MPP,ns}}$ is the MPP voltage of a block of 18 non-shaded PV cells protected by one bypass diode.

The ratio of MPP current to SC current at MPP at high currents can now be solved from Eq. (4.4) as

$$\frac{I_{\mathrm{MPP,high}}}{I_{\mathrm{SC}}} = \frac{U_{\mathrm{MPP,ns}}}{U_{\mathrm{MPP,ns}} + AU_{\mathrm{t,ns}}}. \tag{4.5}$$

As can be seen from Eq. (4.5), $I_{\mathrm{MPP,high}}/I_{\mathrm{SC}}$ is always smaller than one for practical cell temperatures and independent of both system shading x and shading strength y. This can also be seen in Fig. 4.6 where the bottom edge of the two-MPP area is a straight line. Although $U_{\mathrm{MPP,ns}}$ depends on the type of PV cells, operating conditions and aging, the order of magnitude of $U_{\mathrm{MPP,ns}}$ with respect to $AU_{\mathrm{t,ns}}$ is known and it depends mostly on the number of series-connected cells in anti-parallel with a bypass diode.

The derivatives of power with respect to the current of the ideal PV power generator modeled by Eq. (4.3) are shown in Fig. 4.7 under the same partial shading conditions as the P-I curves presented in Fig. 4.5. There are three points at which the derivative is zero in case of a shading strength of 18.5%. Two of these points at I = 6.20 A and I = 7.25 A are MPPs and one is a local minimum occurring at I = 6.62 A. At the local minimum, the shaded cells operate in SC conditions and the bypass diodes are not yet conducting current. For a shading strength of 7.4% the power derivate is zero only at I = 6.95 A. This is the MPP in the current interval $0 \leq I \leq (1-y)I_{\mathrm{SC}}$.

In order to have an MPP in the current interval $(1-y)I_{\mathrm{SC}} < I \leq I_{\mathrm{SC}}$ defined in Eq. (4.4), there must be a local minimum in the P-I characteristics. Otherwise the

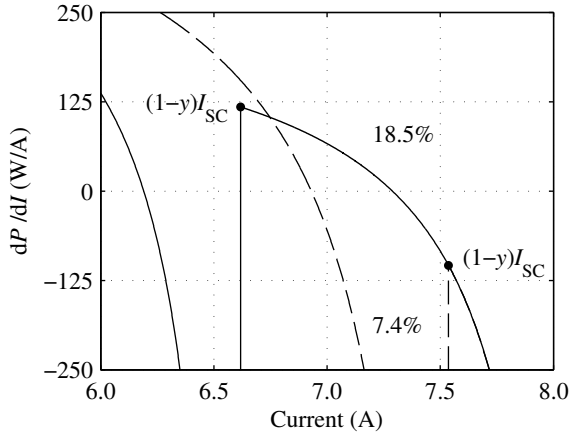

Fig. 4.7: $\mathrm{d}P/\mathrm{d}I$ curves of the ideal PV power generator for a system shading of 50% and shading strengths of 7.4% and 18.5%.

shaded cells generate power already at $I_{\mathrm{MPP,high}}$ and no MPP can exist at high currents. A local minimum exists, if the power derivative is positive when I approaches $(1-y)I_{\mathrm{SC}}$ from the right as is true for shading strength of 18.5% for which $(1-y)I_{\mathrm{SC}} = 6.62$ A in Fig. 4.7. For a shading strength of 7.4% for which $(1-y)I_{\mathrm{SC}} = 7.54$ A, the derivative is negative when $(1-y)I_{\mathrm{SC}} < I \leq I_{\mathrm{SC}}$. Maximum value of shading strength y_{max} for which only one MPP exists can be solved in case of the ideal model of PV power generator (Eq.(4.1)) by inserting $I_{\mathrm{MPP,high}} = (1-y)I_{\mathrm{SC}}$ into Eq. (4.5) as

$$y_{\mathrm{max}} = 1 - \frac{U_{\mathrm{MPP,ns}}}{U_{\mathrm{MPP,ns}} + AU_{\mathrm{t,ns}}} = 1 - \frac{I_{\mathrm{MPP,high}}}{I_{\mathrm{SC}}}. \tag{4.6}$$

If $I_{\mathrm{MPP,high}}/I_{\mathrm{SC}}$ is assumed to be 0.9, which is a typical value for silicon PV cells, two MPPs exist only if $y > y_{\mathrm{max}} = 0.1$. This means that for weak shading, the power curve of the PV power generator has only one MPP despite of non-uniform irradiance conditions.

4.1.2 Power Losses in Bypass Diodes

The one-MPP area on the right side of Fig. 4.1 is caused by the power losses in the forward biased bypass diodes connected in anti-parallel with the shaded PV cells. This phenomenon is illustrated in Figs. 4.8–4.9 in which U-I and P-I curves of the PV power generator are shown in conditions with a shading strength of 50% and system shadings of 77.8% and 96.3% (42 and 52 out of the total amount of 54 blocks of 18 series-connected PV cells were shaded, respectively). In case of the system shading of 77.8%, the power

of the non-shaded cells is enough to forward bias the bypass diodes to bypass the current around the shaded blocks, which causes two MPPs on the power curve of the generator. In case of the system shading of 96.3%, only two blocks of cells are non-shaded. Their power is in this case too low to forward bias the total of 52 bypass diodes in anti-parallel with the shaded cells, when the generator current is in the high current region $(1 - y)I_{\mathrm{SC}} < I \leq I_{\mathrm{SC}}$ and so only one MPP exists at low currents.

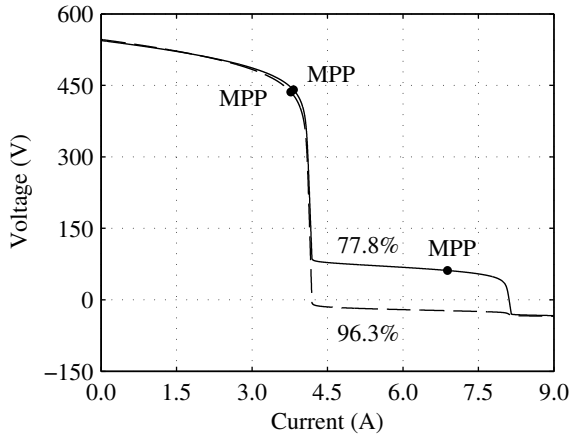

Fig. 4.8: *U-I* characteristics of the PV power generator under partial shading conditions with a shading strength of 50% and system shadings of 77.8% and 96.3%.

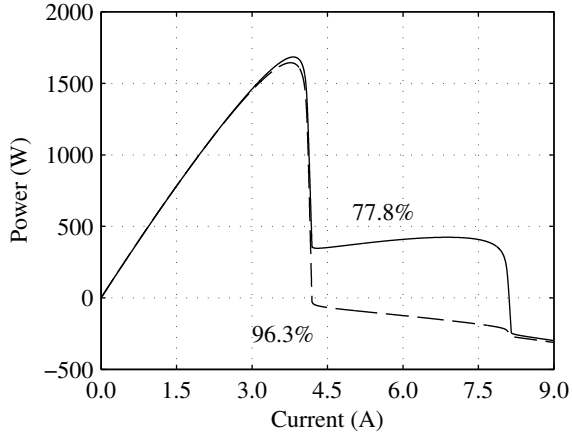

Fig. 4.9: *P-I* characteristics of the PV power generator under partial shading conditions with a shading strength of 50% and system shadings of 77.8% and 96.3%.

The phenomenon shown in Figs. 4.8–4.9 can also be explained analytically by using

the ideal PV cell model without the effects of parasitic resistances, but now with positive constant voltage for a conducting bypass diode U_{bd}. PV power generator voltage is now

$$U = \begin{cases} (1-x)N_{\mathrm{s}}U_{\mathrm{ns}} + xN_{\mathrm{s}}U_{\mathrm{s}}, & 0 \leq I \leq (1-y)I_{\mathrm{SC}} \\ (1-x)N_{\mathrm{s}}U_{\mathrm{ns}} - xN_{\mathrm{s}}U_{\mathrm{bd}}, & (1-y)I_{\mathrm{SC}} < I \leq I_{\mathrm{SC}}. \end{cases} \tag{4.7}$$

The number of MPPs when using the model in Eq. (4.7) is shown in Fig. 4.10 for bypass diode voltage of $U_{\mathrm{bd}} = 0.6$ V. The ideality factor A has been chosen so that $I_{\mathrm{MPP,high}}/I_{\mathrm{SC}}$ is the same under uniform conditions as in the model with which the results in Fig. 4.1 have been obtained. The horizontal solid/dashed line close to a shading strength of 10% represents the minimum value for which two MPPs exist. This means that $y_{\max}$ defined in Eq. (4.6) is just below this line.

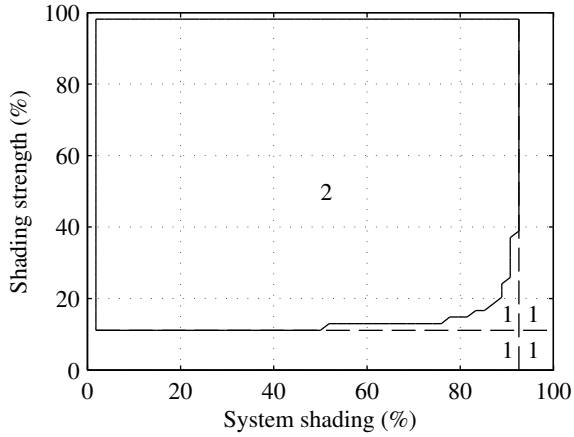

Fig. 4.10: Number of MPPs of the ideal PV power generator as a function of system shading and shading strength with a finite non-zero voltage $U_{\mathrm{bd}} = 0.6$ V for a conducting bypass diode.

The power derivative $\mathrm{d}P/\mathrm{d}I$ including the voltage of a conducting bypass diode U_{bd} in the current interval $(1-y)I_{\mathrm{SC}} < I \leq I_{\mathrm{SC}}$ can be solved as

$$\frac{\mathrm{d}P}{\mathrm{d}I} = (1-x)N_{\mathrm{s}}U_{\mathrm{ns}} - xN_{\mathrm{s}}U_{\mathrm{bd}} - (1-x)N_{\mathrm{s}}AU_{\mathrm{t,ns}}\frac{I}{I_{\mathrm{SC}} - I}, \qquad (1-y)I_{\mathrm{SC}} < I \leq I_{\mathrm{SC}} \tag{4.8}$$

The limit of system shading x_{lim} with only one MPP on the power curve can be solved when the power derivative $\mathrm{d}P/\mathrm{d}I$ approaches zero when I approaches $(1-y)I_{\mathrm{SC}}$. This

can be written as

$$\left.\frac{\mathrm{d}P}{\mathrm{d}I}\right|_{I=(1-y)I_{\mathrm{SC}}} = (1-x_{\mathrm{lim}})N_{\mathrm{s}}U_{\mathrm{MPP,ns}} - x_{\mathrm{lim}}N_{\mathrm{s}}U_{\mathrm{bd}} - (1-x_{\mathrm{lim}})N_{\mathrm{s}}AU_{\mathrm{t,ns}}\frac{(1-y)I_{\mathrm{SC}}}{I_{\mathrm{SC}}-(1-y)I_{SC}} = 0. \quad (4.9)$$

The limit of system shading x_{lim}, for which there is only one MPP, can be solved from Eq. (4.9) as

$$x_{\mathrm{lim}} = \frac{U_{\mathrm{MPP,ns}} + AU_{\mathrm{t,ns}}(1-1/y)}{U_{\mathrm{MPP,ns}} + U_{\mathrm{bd}} + AU_{\mathrm{t,ns}}(1-1/y)}. \quad (4.10)$$

Both the current through and the losses in bypass diodes are at maximum when the value of shading strength is at the maximum of 100% ($y = 1.0$) for certain operating conditions. The maximum value of x_{lim} corresponding the vertical dashed line in Fig. 4.10 can be obtained by inserting $y = 1.0$ into Eq. (4.10).

The maximum value of x_{lim} of the studied system is between the simulation steps of the system shading of 96.3% (vertical solid/dashed line in Fig. 4.10) and 98.1%. In these cases two or one block out of the total amount of 54 blocks of 18 series-connected PV cells are non-shaded, respectively. The maximum value of x_{lim} is determined by the magnitudes of U_{bd} and $U_{\mathrm{MPP,ns}}$, which are known system parameters. It can easily be seen that the value of x_{lim} depends on the voltage of a conducting bypass diode (U_{bd}) and the amount of series-connected PV cells ($U_{\mathrm{MPP,ns}}$) in a PV block with an anti-parallel-connected bypass diode.

The one-MPP area bounded by the dashed lines and the line between two and one-MPP areas in Fig. 4.10 is due to the effect of bypass diode losses to the MPP and the ratio $I_{\mathrm{MPP,high}}/I_{\mathrm{SC}}$. When operating at MPP at 7.3 A in Fig. 4.11, the bypass diodes in anti-parallel with the shaded cells bypass the current around the shaded cells. This will cause losses in bypass diodes which are proportional to the amount of conducting bypass diodes and the current through them. Therefore, the bypass diode losses shift the MPP to lower values of current compared to the MPP current of the non-shaded cells. This is because the power at the MPP in the high current region $(1-y)I_{\mathrm{SC}} < I \leq I_{\mathrm{SC}}$ is the sum of the power produced by the non-shaded cells and the power consumed by shaded cells having anti-parallel-connected bypass diodes. This can also be seen in Fig. 4.10 where the minimum value of shading strength, for which there exist two MPPs, increases for high values of system shading (i.e. for high amounts of conducting bypass diodes).

The change of $I_{\mathrm{MPP,high}}/I_{\mathrm{SC}}$ is illustrated in Figs. 4.11–4.12 for system shading and shading strength of 50%. As can be seen, the shaded cells with anti-parallel-connected bypass diodes consume power when they operate at currents higher than 4.1 A (i.e.

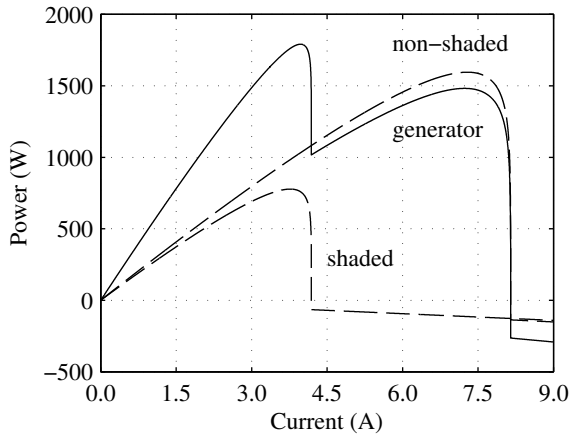

Fig. 4.11: *P-I* characteristics of the PV power generator and of the non-shaded and shaded cells for system shading and shading strength of 50%.

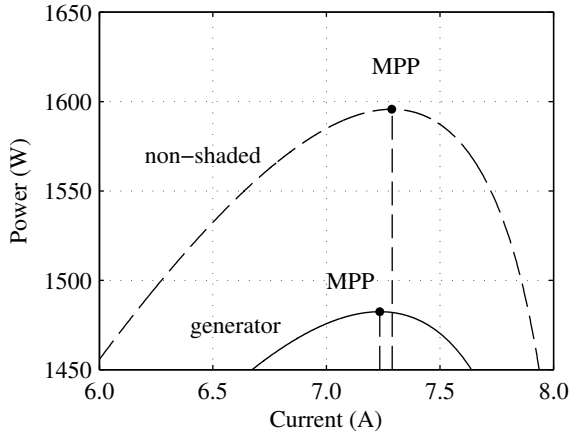

Fig. 4.12: An extended view of *P-I* characteristics of the PV power generator and of the non-shaded and shaded cells for system shading and shading strength of 50% at high currents.

$(1-y)I_{\mathrm{SC}}$) and the power consumed is directly proportional to the current through the bypass diodes in anti-parallel with shaded cells as shown in Fig. 4.9. If the voltage and power of the conducting bypass diodes were zero, the MPP would be at the same current as the MPP on the 'non-shaded' curve and the ratio of MPP current to SC current would be as defined in Eq. (4.5). The shift of the MPP to lower currents due to the power losses in bypass diodes can clearly be seen in Fig. 4.12, which is an extended view of Fig. 4.11 at high values of current.

The phenomenon can also be studied by using the ideal model for a PV power generator with constant bypass diode voltage U_{bd} by solving the ratio $I_{\mathrm{MPP,high}}/I_{\mathrm{SC}}$ as a function of system shading x from Eq. (4.9) at the MPP so that

$$\frac{I_{\mathrm{MPP,high}}}{I_{\mathrm{SC}}} = \frac{U_{\mathrm{MPP,ns}} - U_{\mathrm{bd}}x/(1-x)}{U_{\mathrm{MPP,ns}} + AU_{\mathrm{t,ns}} - U_{\mathrm{bd}}x/(1-x)} = 1 - \frac{AU_{\mathrm{t,ns}}}{U_{\mathrm{MPP,ns}} + AU_{\mathrm{t,ns}} - U_{\mathrm{bd}}x/(1-x)}. \quad (4.11)$$

It becomes clear from Eq. (4.11) that $I_{\mathrm{MPP,high}}/I_{\mathrm{SC}}$ also depends on the system shading x when the voltage of a conducting bypass diode $U_{\mathrm{bd}} > 0$ V. As can be seen, $I_{\mathrm{MPP,high}}/I_{\mathrm{SC}}$ decreases as the system shading x increases and, therefore, the distance between the line between the two and one-MPP areas and the horizontal dashed line on the bottom right corner in Fig. 4.10 increases. To further illustrate the shift of the MPP current due to the power losses in bypass diodes, the ratio $I_{\mathrm{MPP,high}}/I_{\mathrm{SC}}$ is shown in Fig. 4.13 as a function of system shading for a shading strength of 50%. As can be seen, $I_{\mathrm{MPP,high}}/I_{\mathrm{SC}}$ decreases as system shading increases. For low values of system shading the decrease is moderate, but when approaching x_{lim} the decreasing becomes faster and finally, when x_{lim} has been reached, the value of $I_{\mathrm{MPP,high}}/I_{\mathrm{SC}}$ collapses to zero. In Fig. 4.13, the last positive value of $I_{\mathrm{MPP,high}}/I_{\mathrm{SC}} = 0.62$ (62%) before the collapse occurs is when 50 out of 54 blocks of PV cells are shaded yielding a system shading of 92.6%. For system shadings higher than x_{lim}, $I_{\mathrm{MPP,high}}/I_{\mathrm{SC}} = 0$ in accordance with the one-MPP area on the right in Fig. 4.10.

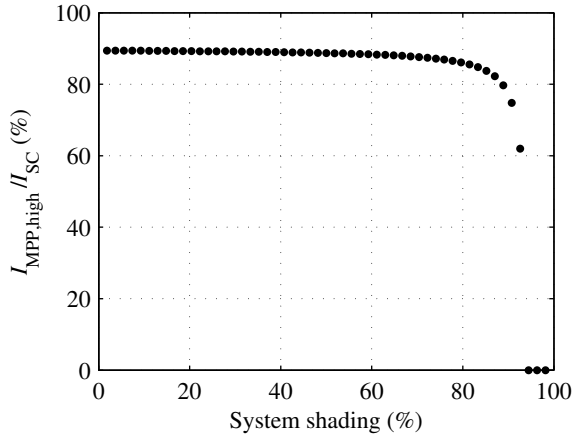

Fig. 4.13: The ratio of current at the MPP at high currents to SC current as a function of system shading for a shading strength of 50%.

4.1.3 Shunt Resistance

The one-MPP area on the top left corner of Fig. 4.1 is caused by the low value of the parasitic shunt resistance R_{sh}. The magnitude of the resistance defines the size of the area so that the smaller the R_{sh}, the larger the area. This phenomenon is illustrated in Figs. 4.14–4.15 in which U-I and P-I curves of the PV power generator are shown in conditions with a system shading of 11.1% and shading strengths of 74.1% and 90.7% corresponding to two and one-MPP areas, respectively. The effect of partial shading of the PV power generator can be seen both in the U-I and P-I curves in Figs. 4.14–4.15.

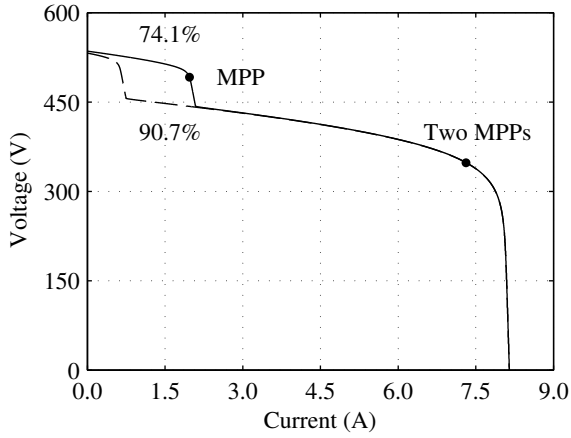

Fig. 4.14: U-I characteristics of the PV power generator under partial shading conditions with a system shading of 11.1% and shading strengths of 74.1% and 90.7%.

The phenomenon can be studied by using the ideal PV cell model in Eq. (4.1), but now with a finite value for parasitic shunt resistance R_{sh}. This time the losses in bypass diodes are neglected. Because R_{sh} is now included in the model of a PV cell, $I_{\mathrm{ph}} \neq I_{\mathrm{SC}}$ and the current of the generator is

$$I = I_{\mathrm{ph}} - I_{\mathrm{o}} \left[\exp\left(\frac{U}{A U_{\mathrm{t}}} \right) - 1 \right] - \frac{U}{R_{\mathrm{sh}}} \tag{4.12}$$

and the voltage of the generator is

$$U = \begin{cases} (1-x) N_{\mathrm{s}} A U_{\mathrm{t,ns}} \ln\left(\frac{I_{\mathrm{SC}} - I - U_{\mathrm{ns}}/R_{\mathrm{sh}}}{I_{\mathrm{o,ns}}} \right) \\ \qquad + x N_{\mathrm{s}} A U_{\mathrm{t,s}} \ln\left(\frac{(1-y) I_{\mathrm{SC}} - I - U_{\mathrm{s}}/R_{\mathrm{sh}}}{I_{\mathrm{o,s}}} \right), & 0 \leq I \leq (1-y) I_{\mathrm{SC}} \\ (1-x) N_{\mathrm{s}} A U_{\mathrm{t,ns}} \ln\left(\frac{I_{\mathrm{SC}} - I - U_{\mathrm{ns}}/R_{\mathrm{sh}}}{I_{\mathrm{o,ns}}} \right), & (1-y) I_{\mathrm{SC}} < I \leq I_{\mathrm{SC}}. \end{cases} \tag{4.13}$$

The number of MPPs including the parasitic shunt resistance of 63 Ω for a block of

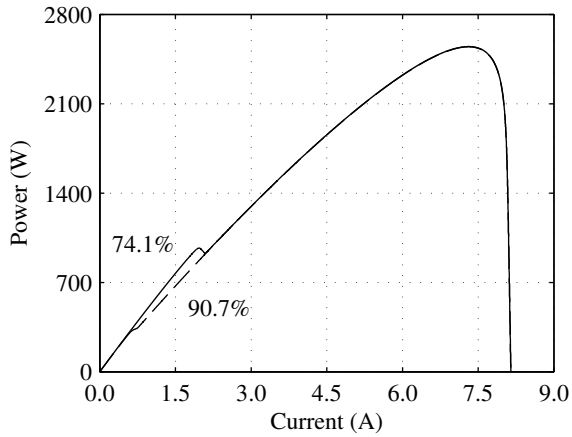

Fig. 4.15: *P-I* characteristics of the PV power generator under partial shading conditions with a system shading of 11.1% and shading strengths of 74.1% and 90.7%.

18 series-connected PV cells in the simulation model is shown in Fig. 4.16. The shunt resistance is the same as in the case of the model used to obtain results for the real PV power generator in Fig. 4.1. The parameters are chosen so that under uniform conditions the ratio $I_{\mathrm{MPP,high}}/I_{\mathrm{SC}}$ has the same value as in the case of Fig. 4.1. The comparison of Figs. 4.6 and 4.10 with Fig. 4.16 clearly demonstrates how shunt resistance R_{sh} causes the one-MPP area for conditions with low system shading and high shading strength.

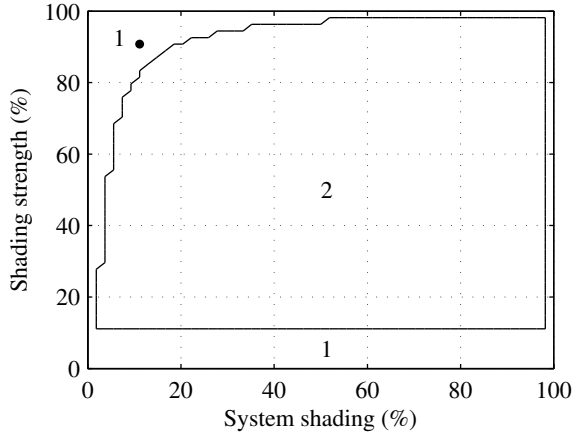

Fig. 4.16: Number of MPPs of the PV power generator according to the ideal model with $R_{\mathrm{sh}} = 63\ \Omega$. The black dot shows the conditions (system shading of 11.1% and shading strength of 90.7%) in which the *P-U* curves with different values of shunt resistances are shown in Fig. 4.17.

The effect of shunt resistance on the slope of the *P-U* curve can be seen from Fig. 4.17 in which an extended view of the *P-U* curve for a system shading of 11.1% and shading strength of 90.7% is shown. As can be seen, there is clearly an MPP for infinite shunt resistance in accordance with Figs. 4.6 and 4.10. The *P-U* characteristics have two MPPs and in this case the contour of the number of MPPs is as was shown in Fig. 4.6. For R_{sh} = 63 Ω there is clearly no MPP in the low current region and only one MPP exists in accordance with Figs. 4.1. For R_{sh} = 109 Ω, there is a point in which the derivative of power with respect to voltage is zero at $I = (1-y)I_{\mathrm{SC}}$, but no MPP exists, just a plateau on the power curve. In this case, the border between the one and two-MPP areas would almost intersect the dot in Fig. 4.16.

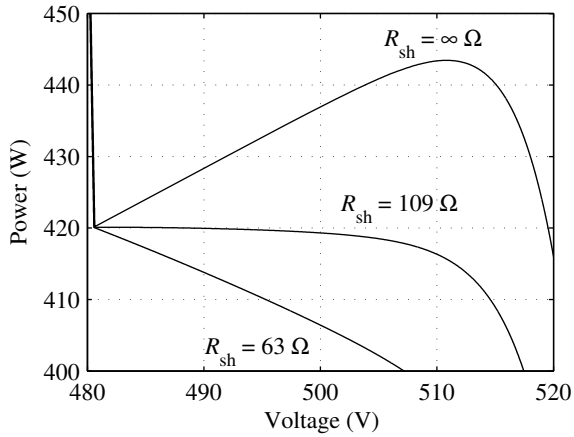

Fig. 4.17: Extended view of *P-U* characteristics of the PV power generator at low values of current (at voltages ≥ 480 V) with a system shading of 11.1% and shading strength of 90.7% (the black dot in Fig. 4.16) for infinite and two realistic values of shunt resistance.

The border of one and two-MPP areas takes place when the power derivative $\mathrm{d}P/\mathrm{d}I$ in the low current region $0 \leq I \leq (1-y)I_{\mathrm{SC}}$ is zero at $I = (1-y)I_{\mathrm{SC}}$. $\mathrm{d}P/\mathrm{d}I$ on that border can be written as

$$\left.\frac{\mathrm{d}P}{\mathrm{d}I}\right|_{I=(1-y)I_{\mathrm{SC}}} = U + (1-y)I_{\mathrm{SC}} \left.\frac{\mathrm{d}U}{\mathrm{d}I}\right|_{I=(1-y)I_{\mathrm{SC}}} = (1-x)N_{\mathrm{s}}U_{\mathrm{ns}}$$
$$+ xN_{\mathrm{s}}U_{\mathrm{s}} + (1-y)I_{\mathrm{SC}} \left((1-x)N_{\mathrm{s}} \left.\frac{\mathrm{d}U_{\mathrm{ns}}}{\mathrm{d}I}\right|_{I=(1-y)I_{\mathrm{SC}}} + xN_{\mathrm{s}} \left.\frac{\mathrm{d}U_{\mathrm{s}}}{\mathrm{d}I}\right|_{I=(1-y)I_{\mathrm{SC}}} \right) = 0. \tag{4.14}$$

The voltage derivates $\mathrm{d}U_{\mathrm{ns}}/\mathrm{d}I$ and $\mathrm{d}U_{\mathrm{s}}/\mathrm{d}I$ in Eq. (4.14) can be solved from Eq. (4.12).

At the border of one and two-MPP areas $I = (1-y)I_{\mathrm{SC}}$ and we obtain

$$\left.\frac{\mathrm{d}U_{\mathrm{ns}}}{\mathrm{d}I}\right|_{I=(1-y)I_{\mathrm{SC}}} = -\frac{AU_{\mathrm{t,ns}}R_{\mathrm{sh}}}{R_{\mathrm{sh}}yI_{\mathrm{SC}} - U_{\mathrm{ns}} + AU_{\mathrm{t,ns}}}. \tag{4.15}$$

A corresponding equation can also be derived for $\mathrm{d}U_{\mathrm{s}}/\mathrm{d}I$ at the border. However, at $I = (1-y)I_{\mathrm{SC}}$ the shaded cells operate in SC and the voltage of a shaded block of 18 series-connected PV cells is $U_{\mathrm{s}} = 0$ V. Therefore, the voltage derivative of shaded cells at $I = (1-y)I_{\mathrm{SC}}$ is simply $\mathrm{d}U_{\mathrm{s}}/\mathrm{d}I = -R_{\mathrm{sh}}$. By substituting these into Eq. (4.14), we finally obtain

$$\begin{aligned}\left.\frac{\mathrm{d}P}{\mathrm{d}I}\right|_{I=(1-y)I_{\mathrm{SC}}} &= (1-x)N_{\mathrm{s}}U_{\mathrm{ns}} \\ &+ (1-y)I_{\mathrm{SC}}\left[(1-x)N_{\mathrm{s}}\frac{-AU_{\mathrm{t,ns}}R_{\mathrm{sh}}}{R_{\mathrm{sh}}yI_{\mathrm{SC}} - U_{\mathrm{ns}} + AU_{\mathrm{t,ns}}} - xN_{\mathrm{s}}R_{\mathrm{sh}}\right] = 0.\end{aligned} \tag{4.16}$$

Shading strength y corresponding to the border of one and two-MPP areas increases with increasing system shading x at high shading strengths and low system shadings in accordance with earlier findings (Figs. 4.1 and 4.16). Furthermore, y increases with increasing shunt resistance R_{sh} in line with Fig. 4.17 (higher R_{sh} yields smaller one-MPP area). To further illustrate this, the contour graphs of one and two-MPP areas are shown in Fig. 4.18 as a function of system shading and shading strength for various shunt resistances. The contour of $R_{\mathrm{sh}} = 63\ \Omega$ corresponds to a typical value of R_{sh} in case of an industrial PV module in accordance with Fig. 4.1. It becomes clear from Fig. 4.18 that the one-MPP area in the top left corner decreases with increasing shunt resistance. The increase of R_{sh} increases the fill factor of PV cells and, consequently, the overall energy yield available from the PV cell. This means that ideal PV cells have an infinite shunt resistance and, accordingly, at least two MPPs under partial shading conditions of high shading strength and low system shading. This will, on the other hand, complicate MPPT if only a few cells of the generator are shaded. In this case a two-MPP condition is undesirable because in case of low system shading and high shading strength, the MPP at high currents is always the global MPP which means that partial shading condition like this causes another MPP at low currents which is always a local MPP (Mäki et al., 2012).

The value of shading strength y_{lim} for which there exists only one MPP at high currents and a plateau on the power curve at $I = (1-y)I_{\mathrm{SC}}$ can be solved from Eq. (4.16) as a function of system shading and shunt resistance. The exact solution is not easily understandable, but by neglecting the terms with thermal voltage of non-shaded cells $U_{\mathrm{t,ns}}$, a more readable approximation can be obtained. This is a reasonable assumption for practical values of shunt resistance R_{sh}. Consequently, the value of limit for which

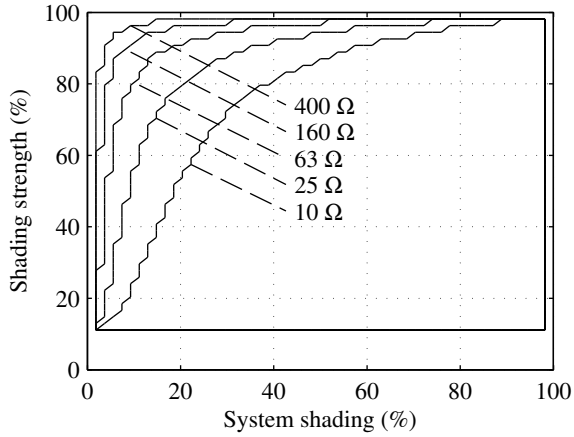

Fig. 4.18: Contour graphs of one and two-MPP areas as a function of system shading and shading strength according to the ideal model for five different shunt resistances R_{sh} from 10 to 400 Ω.

there is only one MPP y_{lim} can be approximated as

$$y_{\mathrm{lim}} \approx 1 - \frac{(1-x)}{x} \frac{U_{\mathrm{ns}}}{R_{\mathrm{sh}} I_{\mathrm{SC}}}. \tag{4.17}$$

Neglecting the terms with $U_{\mathrm{t,ns}}$ causes the accuracy of the approximation to decrease a bit for very low values of x ($< 5\%$). The approximation shows clearly how y_{lim} increases with increasing x and finally approaches the upper value one in accordance with Figs. 4.1, 4.10 and 4.18. The effect of shunt resistance on the one-MPP area can also be clearly seen from Eq. (4.17). y_{lim} increases with increasing shunt resistance and, thereby, the one-MPP area decreases. If the value of shunt resistance is high, which is typical for high quality PV cells, the value of y_{lim} is close to one also at low values of x (e.g. for $R_{\mathrm{sh}} = 400$ Ω in Fig. 4.18).

The shunt resistance in one-diode model is often assumed to be constant in all operating conditions, e.g. in (Villalva et al., 2009a). However, the PV cell impedance measurements by Kumar et al. (2009) and Mäki et al. (2010) indicate that the magnitude of the shunt resistance increases as the irradiance decreases. Soto et al. (2006) state that the value of shunt resistance is inversely proportional to the irradiance and propose, based on literature and empirical study, that $R_{\mathrm{sh}} = R_{\mathrm{sh,STC}} G_{\mathrm{STC}}/G$, where $R_{\mathrm{sh,STC}}$ is the shunt resistance in STC, $G_{\mathrm{sh,STC}}$ the irradiance in STC and G the irradiance of the PV cells. In this case, the one-MPP area caused by the low value of shunt resistance would shrink noticeably and the contour graph of the number of MPPs would look identical to Fig. 4.6.

It was confirmed by measurements by the author of this thesis that the phenomenon is present in practical generators which means that it is unlikely that the equation presented by Soto et al. (2006) holds for all PV power generators in all operating conditions. The measured *P-U* curve of a PV power generator composed of six series-connected NAPS NP190GKg PV modules operating under partial shading conditions with a shading strength of 91.5% and with only one block of 18 series-connected PV cells protected by an anti-parallel-connected bypass diode shaded (system shading of 5.6%) is shown in Fig. 4.19. Measurement was done at 13:08:23 on 4 December 2012. The same measurement setup was used as in the measurements for the verification of the simulation model in Chapter 3 (shown in Appendix D). Only six modules were used because the capacitor used in the measurements to vary the operating point from SC to OC was unable withstand more than 200 V. As can be seen, there is only one MPP at a voltage of 159 V. The value of shunt resistance is so low that the derivative of power with respect to voltage at the voltage range from 180 V to 200 V is negative and does not contain a local MPP.

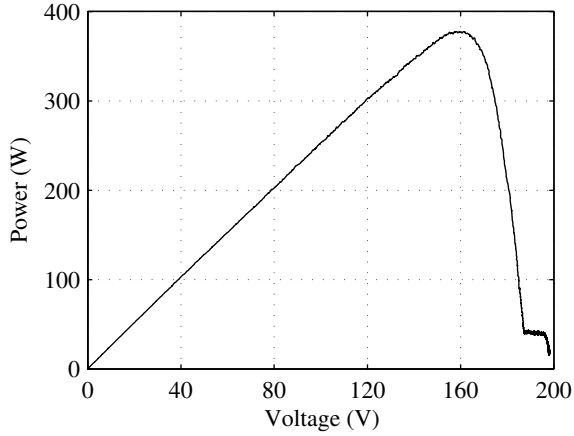

Fig. 4.19: Measured *P-U* characteristic of six series-connected PV modules operating under partial shading conditions with a system shading of 5.6% and shading strength of 91.5% at 13:08:23 on 4 December 2012. Only one MPP exists at a voltage of 159 V.

4.2 Characteristics of Maximum Power Points

As was shown in the previous sections, partial shading conditions typically causes multiple MPPs to the *P–U* curve of a PV power generator. In addition to number of MPPs, partial shading conditions affect the MPP voltages and currents. Especially the voltage and current of the global MPP are of interest when the purpose is to extract the maximum available power from the generator under all operating conditions. Depending on the

partial shading conditions, the global MPP can be at almost any voltage from zero to OC voltage. In this section, the prevailing behavior of MPPs under partial shading conditions are studied by using the systematic approach introduced in Chapter 3.

4.2.1 Voltage of the Global MPP

The conventional assumption that the MPP voltage is about 80% of the OC voltage for PV modules composed of silicon PV cells is correct only in cases of uniform operating conditions. For example, in partial shading conditions with a shading strength of 85% and system shading of 20%, the global MPP is at a voltage of less than 60% of the OC voltage as is shown in Fig. 4.20.

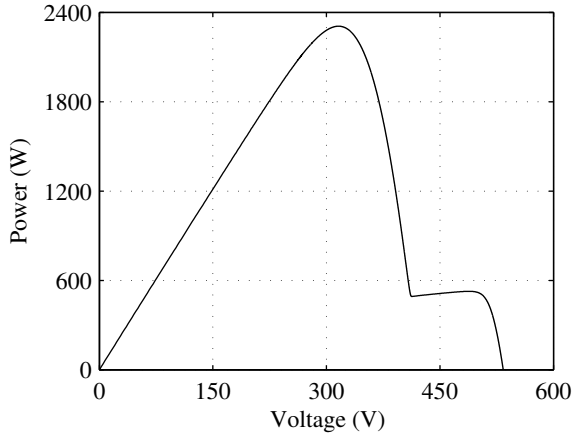

Fig. 4.20: *P-U* curve of the PV power generator under partial shading conditions with a shading strength of 85% and system shading of 20%.

The effect of partial shading on the voltage of the global MPP is illustrated with a contour graph in Fig. 4.21 as a function of system shading and shading strength obtained by using the systematic approach. As can be seen, the voltage of the global MPP can be at voltages lower than 100 V, which is lower than 20% of the OC voltage. At shading conditions below the diagonal from the origin to the top right corner in Fig. 4.21, the voltage of the global MPP stays over 400 V being around 75 to 85% of the OC voltage ranging from 400 V to over 450 V. In this area the global MPP is at high voltages (or low currents) and conventional MPPT methods which assume that the MPP voltage is around 80% of the OC voltage are able to function properly. MPP at high voltages and low voltages are defined the same way as MPP at low currents and high currents, respectively, in Section 4.1.

It should also be noticed that there is also an upper limit for the voltage of the global

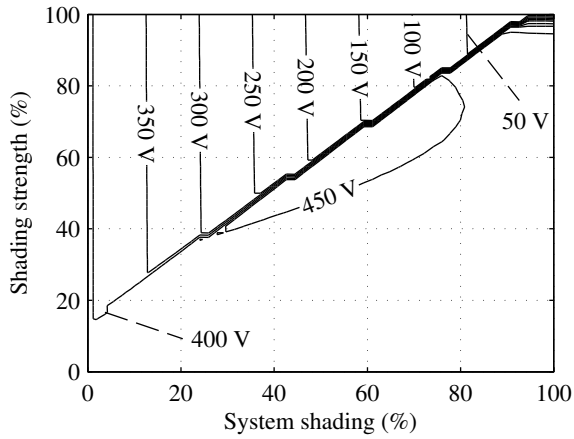

Fig. 4.21: Voltage of the global MPP as a function of system shading and shading strength.

MPP and it is naturally less than the OC voltage of the generator. This will be discussed more later on in this chapter when it is shown that if the voltage of an MPP is too high it cannot be the global MPP if it is assumed that there are two irradiance values at maximum affecting the generator. In the area above the diagonal in Fig. 4.21, global MPP voltage decreases strongly with increasing system shading. In this area the MPP at low voltages is the global MPP. If shading with a shading strength of over 20% covers the PV power generator gradually, the voltage of the global MPP decreases with increasing system shading. This can cause problems for connecting the PV power generator to the electrical grid, because of the wide voltage range required from the MPPT device.

Further problems for the MPPT will occur if the diagonal in Fig. 4.21 is crossed. For example, in the case of a shading strength of 50% and system shading of 50%, the voltage of the global MPP is over 450 V. If the shading strength increases to 70%, the voltage of the global MPP drops below 200 V. The *P-U* characteristics of the above mentioned conditions are shown in Fig. 4.22. There are two MPPs almost at the same voltages in both operating conditions presented in Fig. 4.22. In the case of a shading strength of 50%, the global MPP is at high voltages. When the shading strength increases to 70%, the MPP at lower voltages becomes the global MPP. Conventional MPPT methods will easily fail to track the global MPP in these kinds of cases because they are unable to recognize the other MPP.

4.2.2 Differentiation Between Local and Global MPPs

MPPs under partial shading conditions can be classified into MPPs at low and high voltages (high and low currents) based on the operating point of individual shaded and

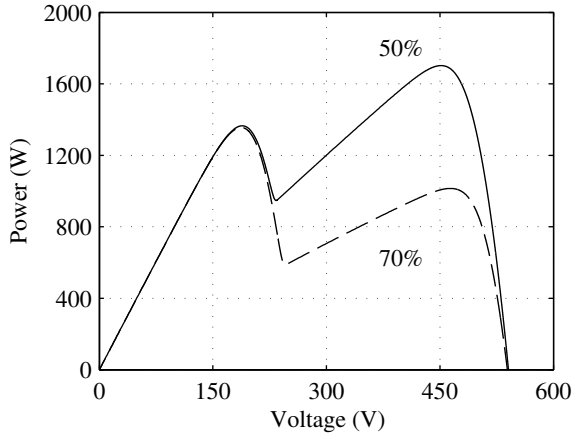

Fig. 4.22: *P-U* characteristics of the PV power generator with a system shading of 50% and shading strengths of 50% and 70%.

non-shaded PV cells as was already discussed in Section 4.1. If the PV power generator operates at an MPP at low voltages (high currents), non-shaded cells operate near to their MPPs while the bypass diodes protecting the shaded cells bypass the current exceeding the SC current of the shaded cells. This means that the voltage of the block of shaded cells and the bypass diode is negative having the magnitude of the threshold voltage of a forward biased bypass diode. Therefore, the MPP voltage of the generator is slightly lower than the MPP voltage of non-shaded cells. If, on the other hand, the generator is operating at an MPP at high voltages (low currents), shaded cells operate near to their MPPs while the non-shaded cells have the voltage defined by the current of the MPP at high voltages (low currents). The voltage of individual non-shaded cells is then between the MPP and OC voltages.

The prevailing behavior of MPP currents and voltages of the PV power generator operating under partial shading condition has been demonstrated with results of specific simulated shading conditions. *I-U* and *P-U* curves of the PV power generator operating under partial shading conditions with shaded cells receiving half of the irradiance received by the non-shaded cells (shading strength of 50%) and with one-third, two-thirds and all of the PV cells in the generator shaded (system shadings of 33.3%, 66.7% and 100%) are shown in Figs. 4.23 and 4.24. In the case of a system shading of 100%, every PV cell is shaded and, therefore, there is only one MPP on the electrical characteristics of the generator at 437 V. In the cases of partial shading conditions with system shadings of 66.7% and 33.3% there are MPPs at low voltages of 117 V and 261 V and at high voltages of 446 V and 459 V, respectively. The global MPP is at low voltages only in the case of a system shading of 33.3%. In other conditions, the global MPP is at high

voltages as can be seen in Fig. 4.24.

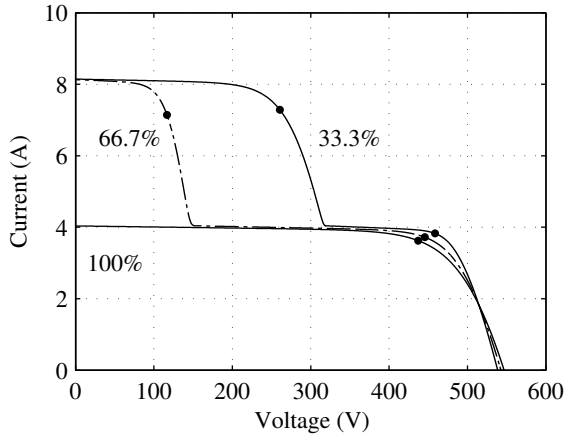

Fig. 4.23: *I-U* curves with MPPs (dots on the curves) of the PV power generator under partial shading conditions with shading strength of 50% and system shadings of 33.3%, 66.7% and 100%.

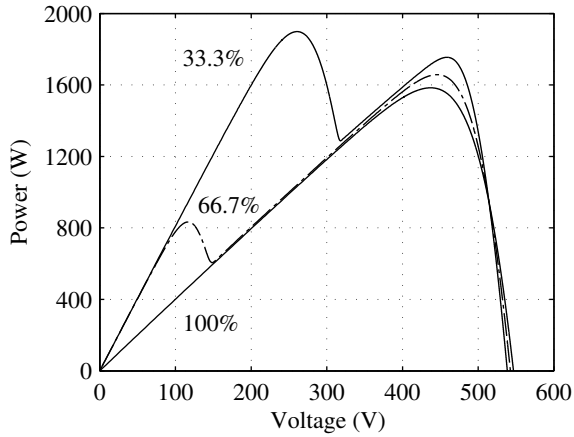

Fig. 4.24: *P-U* curves with MPPs of the PV power generator under partial shading conditions with shading strength of 50% and system shadings of 33.3%, 66.7% and 100%.

It can further be seen in Fig. 4.24 that the voltage of the MPPs at low voltages changes strongly as a function of system shading. This is due to the fact that the MPP voltage of an MPP at low voltages comprises of the sum of the MPP voltages of the non-shaded cells and threshold voltages of conducting bypass diodes. Therefore, MPP voltage at low voltages is inversely proportional to the system shading because the amount of non-shaded cells decreases with increasing system shading. It is also important to notice that

the MPP current of MPPs at low voltages stays almost constant. On the other hand, the MPP voltage at high voltages changes only slightly as a function of system shading. The small increase of the MPP voltage at high voltages with decreasing system shading is due to increasing portion of non-shaded cells in the PV power generator which are forced to operate at higher voltages than their own MPP voltage. The voltage of a non-shaded cell is between the MPP and OC voltages of the cell depending on the MPP current at high voltages and, therefore, the shading strength.

Another prevailing perspective on the behavior of MPP currents and voltages of the PV power generator operating under partial shading conditions can be obtained by simulations with a fixed system shading and varying shading strength. *I-U* and *P-U* curves of the PV power generator operating under partial shading conditions with a system shading of 50% and shading strengths of 33.3%, 66.7% and 100% are shown in Figs. 4.25 and 4.26. In the case of a shading strength of 100% there is only one MPP at 186 V. In the cases of shading strengths of 66.7% and 33.3% there are MPPs at low voltages of 188 V and 190 V and at high voltages of 462 V and 437 V, respectively. The global MPP is now at high voltages only in the case of a shading strength of 33.3%. In the other two cases, the global MPP is at low voltages.

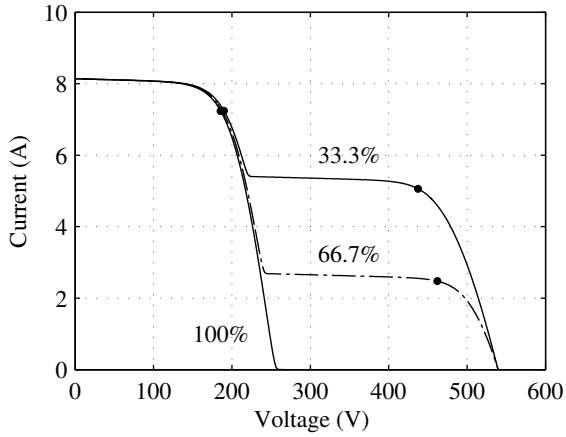

Fig. 4.25: *I-U* curves with MPPs (dots on the curves) of the PV power generator under partial shading conditions with a system shading of 50% and shading strengths of 33.3%, 66.7% and 100%.

It can further be seen in Figs. 4.25 and 4.26 that the voltage of the MPP at low voltages remains almost the same despite the change in shading strength. This is due to the fact that the change in shading strength affects only the voltages of the conducting bypass diodes. The magnitudes of currents and voltages of the bypass diodes increase only slightly with increasing shading strength and, therefore, the change of voltage of the

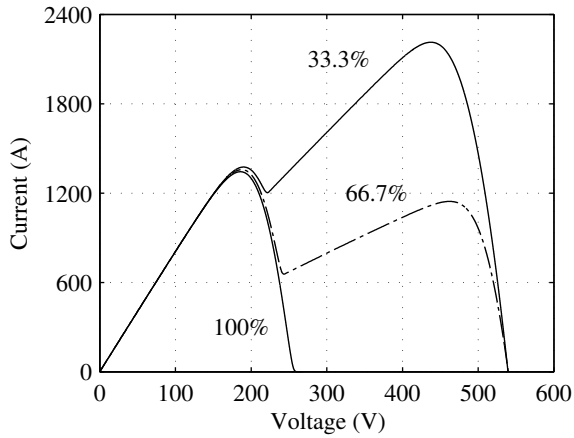

Fig. 4.26: *P-U* curves of the PV power generator under partial shading conditions with a system shading of 50% and shading strengths of 33.3%, 66.7% and 100%.

MPP at low voltages is also minimal (MPPs at 186 V to 190 V). On the other hand, the change in the MPP voltage of the MPPs at high voltages as a function of shading strength is more significant. The change in MPP voltage happens due to the same phenomenon as for the MPPs at high voltages in Fig. 4.24. This time the amount of shaded cells remains the same as the system shading is kept constant, but as the MPP current at high voltages decreases with increasing shading strength, the voltage of the non-shaded cells increases towards their OC voltage.

The behavior of MPP currents and voltages of the PV power generator was demonstrated with selected shading conditions in Figs. 4.23–4.26. As the next step it will be shown that the demonstrated prevailing behavior of MPP currents and voltages is a predominant property of the PV power generator composed of series-connected PV modules operating under partial shading conditions.

I-U and *P-U* curves of the PV power generator operating under partial shading conditions have been simulated with 55 steps both for shaded cells (system shading) and irradiances for the shaded cells (shading strength) with a total amount of 3025 different operating conditions. All the MPP current and voltage pairs of the MPPs under these operating conditions are presented in Fig. 4.27. As can be seen, there are clearly two distinctive regions in which the MPPs lie representing the MPPs at low and high voltages as classified before. Low voltage MPPs are close to the current of 7.3 A corresponding to the MPP current of the non-shaded modules receiving an irradiance of 1000 W/m^2. High voltage MPPs are between 400 and 500 V with MPP current varying from 0 to 7.3 A.

Extended views of both low and high voltage ranges of Fig. 4.27 are shown in Figs. 4.28

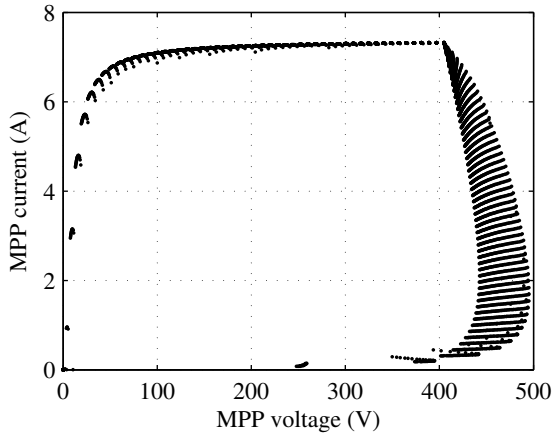

Fig. 4.27: MPP current and voltage pairs of the PV power generator operating under 3025 different partial shading conditions.

and 4.29 in which local and global MPPs are marked with black and red dots, respectively. The MPPs under uniform conditions are marked with red circles around the leftmost red dots in Fig. 4.29. These points correspond to the curve with temperature-rise coefficient $K_\mathrm{t} = 0.033$ Km^2/W in Fig. 3.1 in Section 3.1.

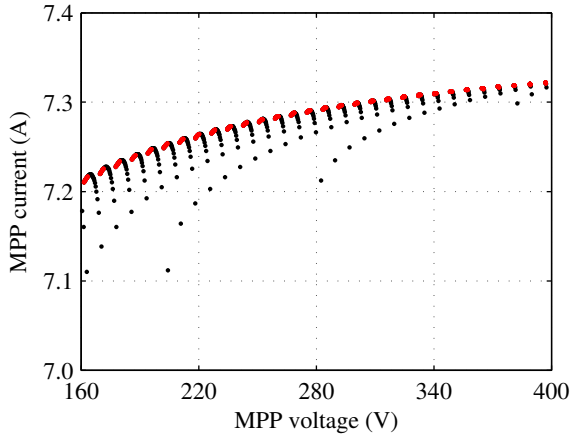

Fig. 4.28: MPP current and voltage pairs of the PV power generator at low voltages under partial shading conditions. Local and global MPPs are presented with black and red dots, respectively.

As can be seen in Fig. 4.28, the global MPPs are at higher currents than the local MPPs when the PV power generator is operating at an MPP at low voltages. The global MPP current changes only slightly with varying MPP voltages, which is a noteworthy

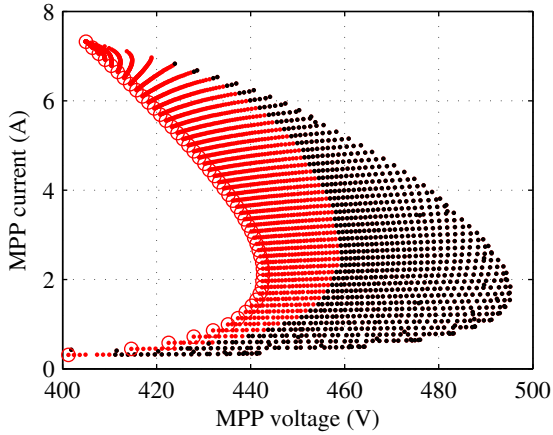

Fig. 4.29: MPP current and voltage pairs of the PV power generator at high voltages under partial shading conditions. Local and global MPPs are presented with black and red dots, respectively, and red circles represent MPPs under uniform conditions.

feature of the PV power generator. Furthermore, differences between global and local MPPs are very small and they are hard to separate from each other according to either current or voltage in contrast to the MPPs at high voltages in Fig. 4.29, which can clearly be divided into local and global MPPs based on the MPP voltage.

The MPPs at high voltages in Fig. 4.29 are grouped in rows having nearly the same MPP current with varying MPP voltage. For example, in the case of an MPP current of 2.0 A, the MPP voltage varies from 442 to 495 V. For all of the MPPs in each of these rows the shading strength is constant, but system shading varies. This corresponds to a realistic condition for PV power generators, when some shading due to an obstacle gradually increases. The voltage of the MPP at high voltages gradually decreases with increasing system shading, but the MPP current stays almost constant corresponding to the irradiance under shading. It can also be clearly seen in Fig. 4.29 that an MPP cannot be the global MPP if it has a voltage higher than the voltage at the border between the red and black dots.

The phenomenon shown in Fig. 4.29 can also be seen in Fig. 4.23 in the case of MPPs at high voltages. All the MPPs at high voltages in Fig. 4.23 are part of a single row of MPPs in Fig. 4.29 with almost the same MPP current (from 3.62 A to 3.96 A). The MPP for system shading of 100%, representing uniform conditions, is one of the red dots with a red circle at 3.62 A and 437 V in Fig. 4.29. The global MPP voltage for a system shading of 66.7% is a red dot at 3.72 A and 446 V. The local MPP for a system shading of 33.3% is a black dot at 3.83 A and 459 V.

It is reasonable to assume that during a typical shading event of a PV power generator

shading strength is more or less constant but system shading can vary from 0 to 100% (Armstrong and Hurley, 2010). Accordingly, the voltage difference between the MPPs at high voltages under partial shading and uniform conditions (fully shaded) increases with decreasing system shading. In conditions with high system shading, the MPP at high voltages is the global one (red dots in Fig. 4.29). With decreasing system shading the voltage difference increases and, finally, MPPs at high voltages become local MPPs (black dots in Fig. 4.29).

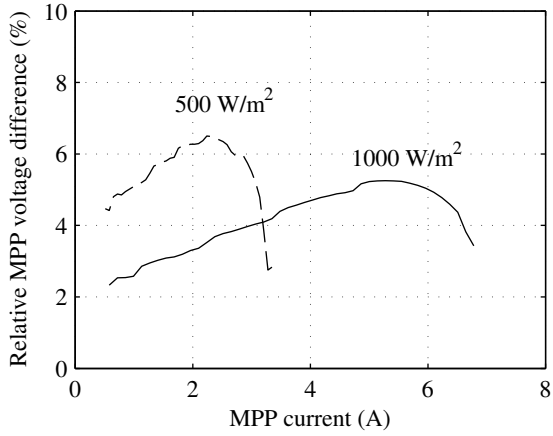

Fig. 4.30: The relative MPP voltage difference between the local MPP with highest value of system shading (border of local and global MPPs in Fig. 4.29) and the MPP under uniform conditions is presented as a function of MPP current. In addition to irradiance of 1000 W/m^2 for non-shaded cells, a corresponding curve of 500 W/m^2 for non-shaded cells is also shown.

The leftmost local MPPs (black dots) in Fig. 4.29 represent MPPs under such operating conditions that the powers of the local MPPs at low and high voltages are nearly the same. The voltage difference between these MPPs compared to the voltage of the MPPs under uniform conditions is shown in Fig. 4.30. The relative MPP voltage difference is the ratio of the voltage difference to the MPP voltage under uniform conditions. In Fig. 4.30, irradiances of the non-shaded cells are 1000 W/m^2 yielding MPP current of 7.32 A at maximum and 500 W/m^2 yielding MPP current of 3.62 A at maximum.

If the relative voltage difference between an MPP under partial shading conditions at high voltages and the MPP under uniform conditions is smaller than the voltage difference limits shown in Fig. 4.30 for a certain MPP current, the PV power generator is operating at the global MPP. If the voltage difference is higher, the generator is operating at a local MPP and the global MPP is at low voltages.

The relative voltage differences in Fig. 4.30 are typically below 6% irrespective of the irradiance for non-shaded cells (500 or 1000 W/m^2). Furthermore, local MPPs have the

same power when the voltage of the local MPP at high voltages is such that it corresponds to the voltage difference limit in Fig. 4.30. Therefore, based on Fig. 4.30 it looks feasible that the voltage difference limit could be used as an indicator whether the MPP at high voltages is the global MPP or that there is an MPP with more power at low voltages.

The power difference between the MPPs based on the systematic approach is shown as a contour graph in Fig. 4.31. As can be seen, the power difference of the MPPs is small in the area of the diagonal on which the powers of the MPPs are almost the same. This means that operation at the relative voltage difference limit in Fig. 4.30 corresponds to the operation close to the diagonal of Fig. 4.31. Therefore, despite the fact that the voltage difference limit in Fig. 4.30 is not constant as a function of MPP current (and basically shading strength), the power losses due to operating at a local MPP instead of the global one are small when operating in the area of the diagonal of Fig. 4.31.

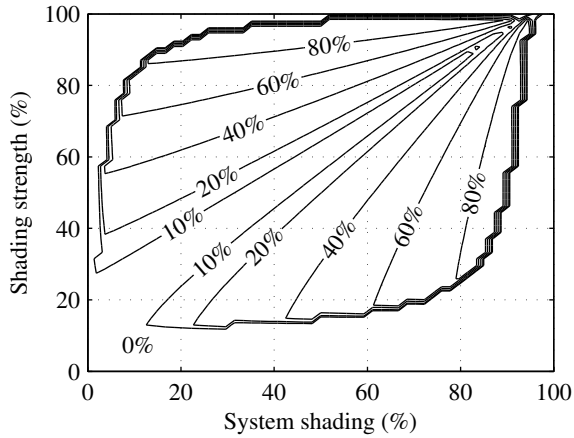

Fig. 4.31: The relative power difference of two MPPs as a function of system shading and shading strength compared to the power of global MPP. In the case of only one MPP, the difference is set to zero.

As was shown in Fig. 4.28, it is difficult to differentiate between the local and global MPPs in case of an MPP at low voltages based on the voltage or the current at the MPP. However, in practice, shading caused by a static object such as a building causes high values of shading strength. In the case of a shading like this only the diffuse part of the irradiance is received by the shaded modules which is approximately 20% of the global irradiance corresponding to shading strength of 80% (Armstrong and Hurley, 2010; Oozeki et al., 2005). In case of a shading strength of 80%, the MPP at low voltages is the global MPP if the relative MPP voltage difference between the MPP under uniform conditions and the voltage of an MPP at low voltages is lower than 80%. This can be seen in Fig. 4.32 where the relative MPP voltage difference between an MPP under uniform

conditions and an MPP at low voltages with the same value of MPP current is presented as a function of shading strength. The limit in Fig. 4.28 is calculated in such conditions that the powers at both of the local MPPs are approximately the same which means that the relative MPP voltage difference in the figure is calculated similarly as the limit for the MPP at high voltages in Fig. 4.29 but now for the MPPs at low voltages.

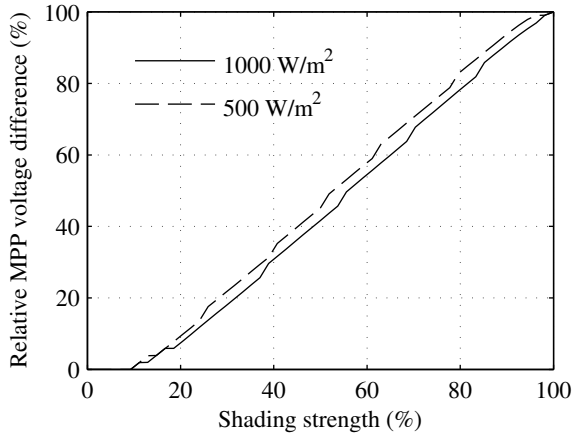

Fig. 4.32: The relative MPP voltage difference between an MPP under uniform conditions and a local MPP at low voltages with the same MPP current in such conditions that the powers at both MPPs are the same as a function of shading strength. In addition to irradiance of 1000 W/m^2 for non-shaded cells a corresponding curve of 500 W/m^2 for non-shaded cells is also shown.

If the information presented above was to be used as a part of an MPPT algorithm, limits for the relative voltage difference could be defined based on Figs. 4.30 and 4.32. By defining the voltage difference limits separately, they can be chosen so that the performance of the method is optimized. For example, the relative voltage difference limit in case of an MPP at high voltages $U_{\mathrm{lim,high}}$ can be chosen to be of the order of the MPP voltage difference limits shown in Fig. 4.30. This way the differentiation method recognizes that there exists another MPP at lower voltages only if it is probable that the MPP at high voltages is not the global one.

In the case of an MPP at low voltages, a voltage difference limit $U_{\mathrm{lim,low}}$ can be chosen so that under conditions with very low system shading the method does not recognize another MPP on the power curve, because the present MPP is most probably the global MPP. $U_{\mathrm{lim,low}}$ can also be chosen by considering that the shading strength is typically of the order of 80 to 85% (slightly higher during mornings and evenings) based on Fig. 4.32. Then, if the operating point is at an MPP at low voltages, system shading must be large enough (voltage difference big enough) for having another MPP at high voltages with higher power. It is, however, also possible to estimate the value of shading strength quite

accurately by measuring global and diffuse irradiances and, therefore, to improve the method in case of operating at the MPP at low voltages without the need to assume any specific value for the shading strength.

5 EFFECT OF GENERATOR CONFIGURATION ON MISMATCH LOSSES UNDER PARTIAL SHADING CONDITIONS

The first section of this chapter presents the results of the systematic study of the effects of partial shading conditions on mismatch losses in PV power generators with different configurations. Different configurations are based on different inverter concepts used to interface PV power generators to the electrical grid. The results, however, apply to stand-alone systems as well. The contents of the first section is based on the results presented in (Mäki and Valkealahti, 2011, 2012b).

In the second section, the effect of partial shading conditions due to clouds on mismatch losses are discussed. The analysis of actual measured data recorded with the data acquisition system of TUT Solar Photovoltaic Power Station Research Plant will be presented. The contents of the last section is based on the results presented in (Mäki and Valkealahti, 2012a).

5.1 Mismatch Losses in Different Generator Configurations

Mismatch losses of PV power generators with different configurations (shown in Fig. 3.4 in Section 3.3) have been calculated by comparing the power of the global MPP to the sum of the maximum powers of the individual blocks of 18 series-connected cells with an anti-parallel-connected bypass diode. The mismatch losses are power losses due to the fact that every block of PV cells does not operate in its own MPP although the whole PV power generator operates in its global MPP. Mismatch losses are a characteristic property of each generator configuration. The mismatch losses of different generators under partial shading conditions are shown in Figs. 5.1–5.3 as a function of system shading and shading strength as contour graphs.

Mismatch losses of the Long string generator are highest near the diagonal from origin to top right corner of Fig. 5.1, where the powers at the two local MPPs, when both of them exist, are equal. The power at the MPP at low voltages decreases as system shading increases and the power of the MPP at high voltages decreases as shading strength increases. On the diagonal of Fig. 5.1 the powers of the MPPs are equal, which leads to high mismatch losses, because both the system shading and shading strength

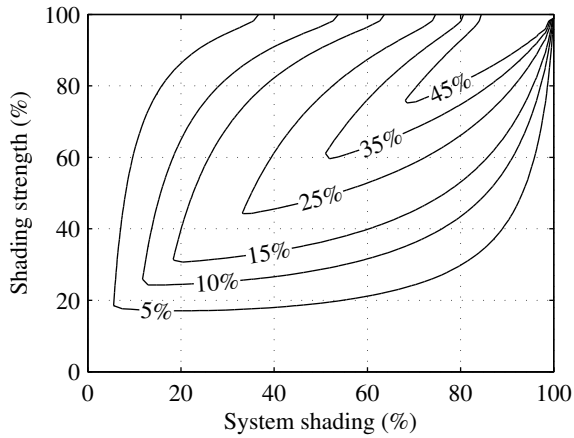

Fig. 5.1: Mismatch losses of Long string PV power generator as a function of system shading and shading strength.

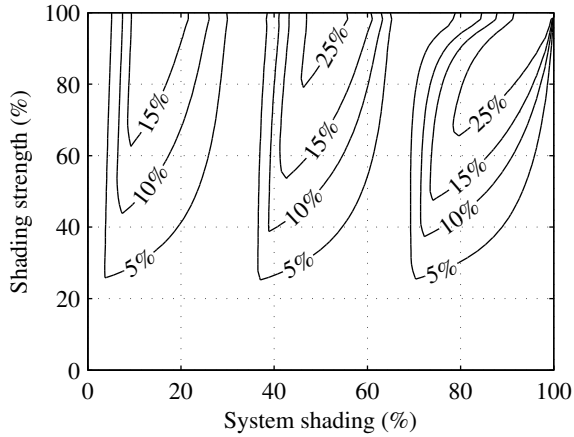

Fig. 5.2: Mismatch losses of Parallel strings PV power generator as a function of system shading and shading strength.

are equally high. For Parallel strings and Multi-string generators, three different partial shading conditions lead to two local MPPs with equal powers as can been seen in Figs. 5.2 and 5.3, because of three parallel operating strings. The mismatch losses are zero for the Multi-string generator and almost zero for the Parallel strings generator when every string is either completely non-shaded or completely shaded. These conditions can be seen in Figs. 5.2 and 5.3 for system shadings of 33.3% or 66.7%.

Mismatch losses in case of the Long string generator can be considerable if both the system shading and shading strength are very high as can be seen in the top right corner

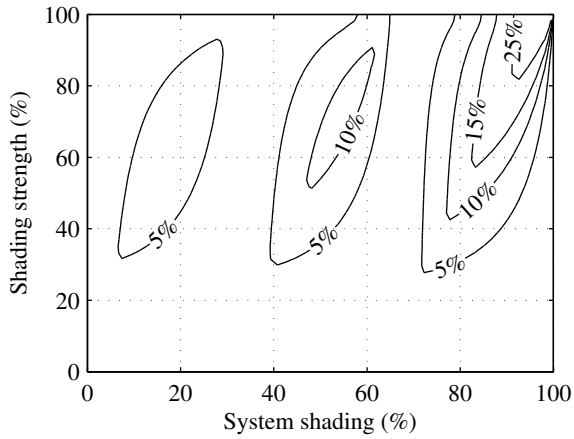

Fig. 5.3: Mismatch losses of Multi-string PV power generator as a function of system shading and shading strength.

of Fig. 5.1. In general, mismatch losses are lower for the Parallel strings and Multi-string generators than for the Long string generator and are the lowest for the Multi-string generator. In certain partial shading conditions the mismatch losses in the Long string generator are considerable, while they are almost zero for the other two generators as can be seen, for example, for system shadings of 33.3% and 66.7% in Figs. 5.1–5.3.

When a PV power generator operates under partial shading conditions, the direct part is blocked and only the diffuse part of the irradiance is received by the shaded modules. On a clear sky day, the diffuse part of the irradiance is typically about 15 to 20% of the global irradiance (Armstrong and Hurley, 2010; Oozeki et al., 2005). The mismatch losses of the different PV power generators under partial shading conditions with a shading strength of 85% are illustrated in Fig. 5.4 as a function of system shading. The curves in the figure are cross cuttings from Figs. 5.1–5.3.

As shown in Fig. 5.4, the mismatch losses of the Multi-string generator on a clear sky day are never higher than for the Long string or Parallel strings generators. Mismatch losses for Parallel strings are mostly lower than for the Long string generator. Mismatch losses for Parallel strings are higher than for Long string predominantly in case when shading strength is higher than 50% and system shading is low as can be seen by comparing mismatch losses in Figs. 5.1 and 5.2. This can most clearly be seen for the shading strength of 85% in Fig. 5.4 for system shadings below 26% (first peak of the Parallel strings curve) and around 48% (second peak of the Parallel strings curve). For a system shading of 11%, the mismatch losses for Parallel strings are 21% whereas the mismatch losses for the Long string and Multi-string generators are only 3%. For a system shading of 48%, the mismatch losses for Parallel strings are 27% whereas the

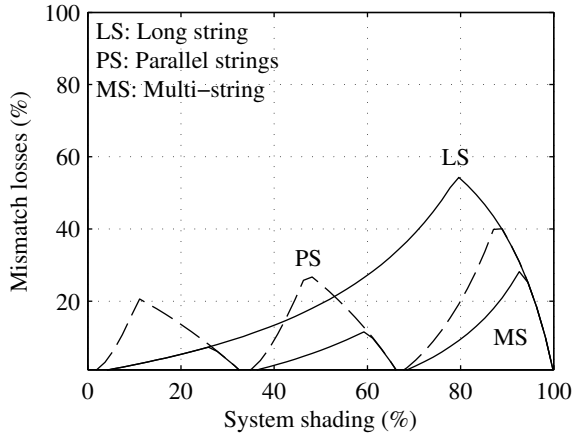

Fig. 5.4: Mismatch losses of the PV power generators under partial shading conditions as a function of system shading for a shading strength of 85%.

mismatch losses for the Long string and Multi-string generators are only 18% and 6%, respectively.

The *P-U* curve of the Parallel strings generator and individual *P-U* curves of the three parallel-connected strings are shown in Figs. 5.5 and 5.6 for a shading strength of 85% and system shadings of 11% and 48%, respectively. As can be seen in Fig. 5.5 in the case of system shading of 11%, two strings are without shading and String 1 operates under partial shading conditions. The global MPP of the generator is at 140 V, where String 1 has a power of 125 W and both Strings 2 and 3 have power of 818 W. In this case, total mismatch losses are 457 W (20.6% of the maximum available power). The losses are distributed so that the losses in Strings 2 and 3 are almost zero (< 1 W) and basically the mismatch losses happen in String 1 which operates under partial shading conditions. The losses in the shaded modules of String 1 are 8 W because they are not operating exactly at their MPP at a voltage of 160 V. The losses in the non-shaded modules of String 1 are 448 W. This is because the generator is operating at a voltage of 140 V and the non-shaded modules produce only 111 W although the maximum available power from them would be 559 W (36 W more than at the MPP at 90 V in String 1 because of the losses in the bypass diodes of shaded modules).

In the case of a system shading of 48% in Fig. 5.6, String 1 is completely shaded, String 2 is under partial shading conditions, and String 3 is without shading. The MPP voltages of Strings 1 and 3 are close to the global MPP voltage of the Parallel strings generator, but the voltage of the global MPP of String 2 is close to 73 V with power of almost 300 W higher than at the local MPP at high voltages. The situation is the same as for String 1 in Fig. 5.5. The mismatch losses of the Parallel strings generator are now

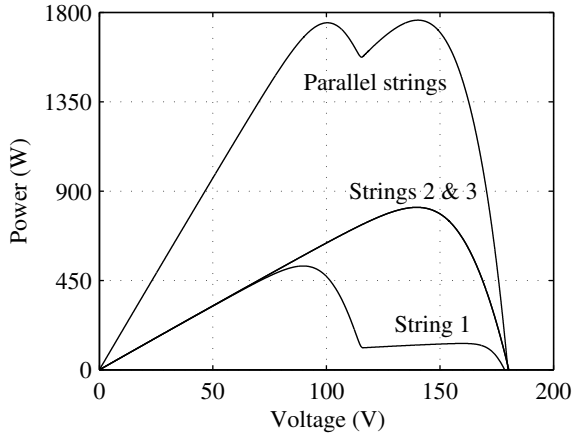

Fig. 5.5: *P-U* curve of the Parallel strings generator and individual curves of parallel-connected Strings 1, 2 and 3 under partial shading conditions with a shading strength of 85% and system shading of 11%.

as high as 27% because the maximum available power of the generator has decreased due to increased overall shading.

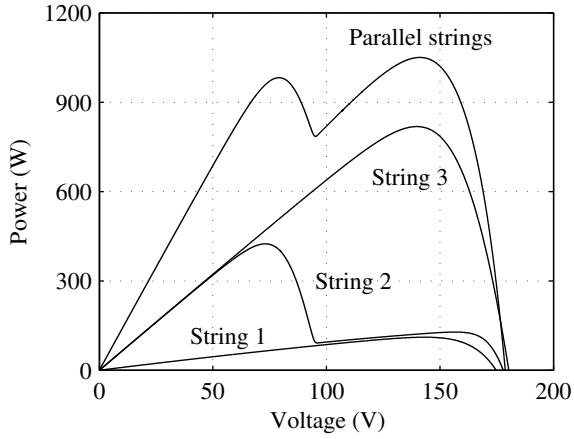

Fig. 5.6: *P-U* curve of the Parallel strings generator and individual curves of parallel-connected Strings 1, 2 and 3 under partial shading conditions with a shading strength of 85% and system shading of 48%.

The reason for high mismatch losses of the Parallel strings generator at system shadings below 60% is that all the strings of the generator have the same voltage and, thereby, the local MPPs of the string under partial shading determines the MPP voltages of the whole generator. On the contrary, if the parallel strings are allowed to operate at their

own MPPs according to the Multi-string generator configuration, mismatch losses are smallest for all shading conditions. When system shading increases to over 50%, the Long string generator has the highest mismatch losses, the Parallel string generator the second highest and the Multi-string generator the lowest losses.

5.1.1 Practical Shading Scenarios

In order to illustrate the significance of the PV power generator configuration on the mismatch energy losses under partial shading conditions, the operation of the PV power generators (Long string, Parallel strings and Multi-string) was also studied in three practical partial shading scenarios.

The amount of shaded PV cells in the generator (system shading) in the case of three partial shading scenarios is shown in Fig. 5.7 as a function of time for the period of one day. It should be noticed that system shading is a relevant parameter only in the daytime, because at nighttime the PV modules receive no radiation. In all of the three scenarios, the non-shaded PV cells receive the global irradiance and shaded cells the diffuse irradiance. The global and diffuse irradiances are shown in Fig. 5.8 during the simulated day. The ambient temperature was chosen to be 20 °C during the whole day and the temperatures of the PV modules were calculated based on the ambient temperature, irradiance and temperature-rise coefficient presented in Eq. (3.5).

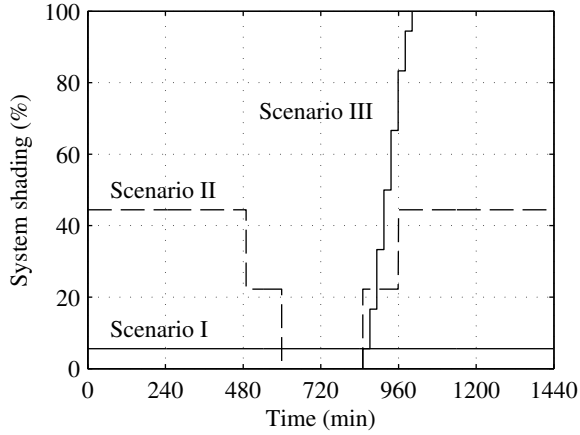

Fig. 5.7: System shading of the PV power generators in different partial shading scenarios during the simulated day.

In Scenario I, there is one PV module in the PV power generators shaded the entire day (three sets of 18 series-connected PV cells with a bypass diode connected in parallel corresponding to a system shading of 5.6%). In practice, shading conditions like this

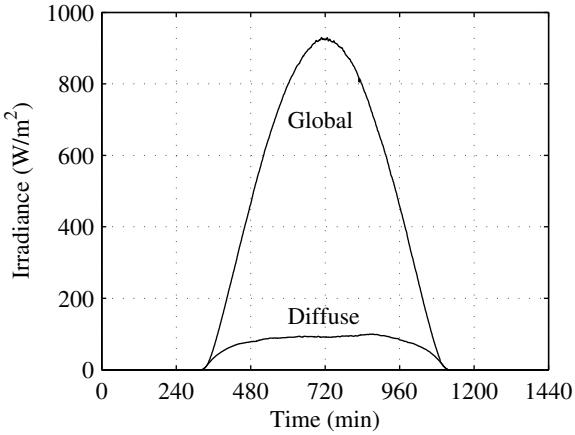

Fig. 5.8: Global and diffuse irradiances during the simulated day.

could be caused for example by a small tree, a chimney, an air conditioning device or some other relatively small object or objects located near the PV power generator.

In Scenario II, the PV power generators are assumed to be built using three consecutive rows of PV modules, each composed of six PV modules. In the morning and evening, the first module row shades a part of the second row and the second row shades a part of the third row. In the morning after sunrise and in the evening before sunset the shading is more severe and two-thirds of the PV cells are shaded in the second and third rows (two sets of 18 series-connected PV cells protected by a bypass diode in each shaded module). Approaching noon, the shading becomes less severe and only one-third of the PV cells are shaded in the second and third rows (one set of 18 series-connected PV cells protected by a bypass diode in each shaded module). Around noon the solar altitude, which is the angle between the sun and horizontal, is assumed to be so high that there is no mutual shading between the PV module rows.

In Scenario III, the generators are built in the same way as in Scenario II with three consecutive rows of PV modules, but in this scenario there is no mutual shading between the module rows. In Scenario III, the shading is caused for example by a large object such as a tall building in built environment that starts to shade the PV power generator gradually in the afternoon and finally shades the generator entirely for the rest of the day.

The mismatch energy losses during the day in the partial shading scenarios are shown in Table 5.1. Multi-string generator has the smallest mismatch energy losses between 1.15% and 3.61% in all scenarios in accordance with earlier findings in the previous section and in (Mäki and Valkealahti, 2012b). It is somewhat of a surprise that the Long string generator has only slightly larger mismatch losses than the Multi-string generator. The

explanation for this and the specious contradiction between Fig. 5.4 and Table 5.1 is that in the figure there are mismatch power losses under the respective shading conditions, but the values in Table 5.1 are mismatch energy losses during one day. The available total energy yield decreases with increasing system shading. This means that absolute energy losses of Parallel strings generator at system shadings below 26%, for example, are much higher than absolute energy losses of the Long string generator at high system shadings around 80% in Fig 5.4.

Table 5.1: Mismatch energy losses of PV power generators during one day in case of three partial shading scenarios.

Generator	Scenario		
	I	II	III
Multi-string	1.15%	3.61%	1.48%
Long string	1.15%	3.68%	1.62%
Parallel strings	6.35%	8.27%	3.27%

In Scenario I, the system shading was 5.6% during the whole day corresponding to a small shade of, for example, a tree or a chimney. As would be deduced from Fig. 5.4, the mismatch losses in the energy yield are the same for Multi-string and Long string generators. For Parallel strings generator the mismatch losses are higher than for the other two generators because the parallel-connected strings have the same operating voltage and so there are high losses in the shaded strings as was shown in Fig. 5.5. In Scenario I, the energy yield of the Parallel strings generator will be over 5% lower than for the other generator configurations.

In Scenario II, the system shading is 44% early in the morning and late in the afternoon and decreases towards noon as shown in Fig. 5.7. This scenario corresponds to a quite realistic case where consecutive PV module strings shade each other when the Sun is close to the horizon. It can be seen in Table 5.1 that losses in Scenario II in all generator configurations are much higher than in the other two scenarios. This means that the layout of the PV power generator should be carefully designed to avoid mismatch losses due to mutual shading of the PV modules rows as was also noticed by Quaschning and Hanitsch (1998). Losses in the Multi-string and Long string generators in Scenario II are almost the same at around 3.6%, which is in accordance with Fig. 5.4. Losses in the Parallel strings generator are over two times higher (8.27%), which is due to high absolute mismatch losses at low system shading values shown in Fig. 5.4.

In scenario III, the system shading increases in the afternoon gradually within 2.5 hours from 0% to 100% corresponding to a practical case where the generator is shaded by a large object such as a building. Mismatch losses for Multi-string and Long string generators are of the same order of magnitude, close to 1.5%. This result could be

misleadingly interpreted to be in contradiction with Fig. 5.4. However, at high system shading values, the irradiance received by the generators is only a fraction of the clear sky irradiance with a system shading of 0%. Therefore, the large fictitious difference in mismatch losses between the three generator configurations at high system shading values in Fig. 5.4 has a small effect on absolute energy losses in this scenario. Losses in the Parallel strings generator are over two times higher (3.27%), which is again due to high mismatch losses at low system shading values shown in Fig. 5.4.

Parallel strings generator has clearly the highest mismatch losses in all scenarios. In Scenario I the losses are almost six times higher than for the other two generators having a value of 6.35%. In Scenarios II and III, the Parallel strings generator has at least twice as high mismatch losses than the other generator configurations. The losses are 8.27% and 3.27%, respectively. Parallel strings generator has substantial mismatch losses in all the studied scenarios indicating that great caution is needed when using this configuration in PV power generators.

5.2 Mismatch Losses due to Partial Shading Caused by Clouds

In this section, the mismatch losses caused by non-uniform operating conditions due to clouds in five PV power generators with different configurations are studied. Different configurations were introduced in Section 3.4. The analysis is based on actual measured irradiances and PV module temperatures during a time period of 180 days. The data was divided into three different sets of data: dark, uniform and non-uniform conditions. Dark conditions, during which no irradiance reached the sensors, constituted 23.3% of the whole 180-day time period. Uniform conditions were present 69.7% and non-uniform conditions the remaining 7.0% of the time.

5.2.1 Effect of Shading due to Clouds on Irradiance

When cloud is covering up the area where PV modules have been installed, it typically covers one module at a time until every module is shaded in certain time interval depending on the size of the area and the speed of the cloud. An example of the effect of shading due to a cloud is shown in Fig. 5.9 in which the irradiances of six photodiodes sensors are shown from 17:14:13 to 17:14:28 on 3 June 2012. At the beginning in the figure, the cloud is covering the whole area of the PV power generator. Then after one second, the shade caused by the cloud starts to move away from the area. There is a period of around three seconds during which the radiation first gradual increase, then a second period with a steep increase and finally again a period with gradual increase. After 12 seconds, the whole area is completely non-shaded. Blue curve in Fig. 5.9 represents the measurement of the first non-shaded photodiode sensor (marked as S9 in the layout in the Appendix E). Green curve represents the photodiode sensor 4.52 m away

from the reference sensor (S10), black curve the sensor 11.85 m from the reference sensor (S11) and so on. Other distances between the sensors are given in the caption of Fig. 5.9. The maximum irradiance difference in Fig. 5.9 of 158 W/m^2 occurs between sensors with distance of 40.47 m (blue and magenta lines, S9 and S14) and is marked in Fig. 5.9 with dots. The cloud causes instantaneous partial shading conditions for the PV power generator during a period of some 10 seconds, which, in turn, causes mismatch losses due to non-uniform irradiance conditions.

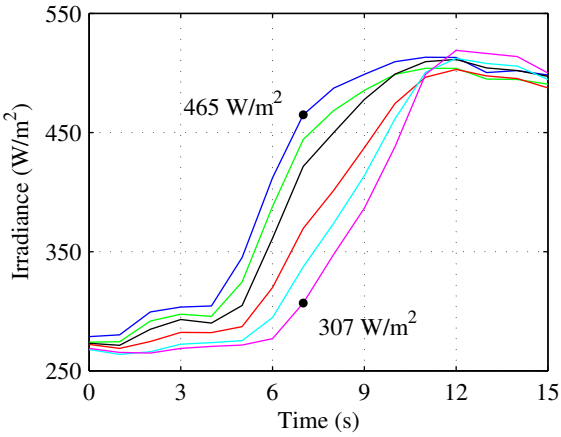

Fig. 5.9: Irradiance measurements of the six photodiode sensors from 17:14:13 to 17:14:28 on 3 June 2012 when a moving cloud is leaving the area of the PV power generator. Blue curve corresponds to the irradiance measured by the reference sensor. Distances of other sensors from the reference sensor are 4.52 m (green), 11.85 m (black), 22.36 m (red), 29.97 m (cyan) and 40.47 m (magenta).

The reason for irregular distances between the photodiode sensors is that the sensors were installed to the ends of rows of adjacent PV modules. The structures on the roof imposed certain requirements for the layout of the system and, therefore, prevent regular distances between sensors. It should also be noticed that the sensors were installed to study the operation of the whole PV power plant composed of several PV module strings, and not for this specific study. The measurements in Fig. 5.9 are from the photodiode sensors (S9–S14) attached to PV modules in an east-west orientated PV module string (String 2) visible in the Appendix E.

The dynamic nature of the effect of clouds on irradiance can also be seen in Fig. 5.10, where cumulative distributions of instantaneous irradiance differences between the measurements of photodiode sensors during the 180-day period are shown for several distances between the sensors. One of the six sensors was chosen as a reference sensor (S9 in Appendix E) respect to which the measurements of other sensors were compared. As can be seen in Fig. 5.10, measured irradiance differences are all quite small for sensors close

to each other. In case of sensors with distances of 4.52 m and 40.47 m (green and magenta curves in Fig. 5.9) from the reference sensor S9, 90% of all irradiance differences are smaller than 30 W/m^2 and 207 W/m^2, respectively. The amount of high values of irradiance differences clearly increases with increasing distance between the sensors.

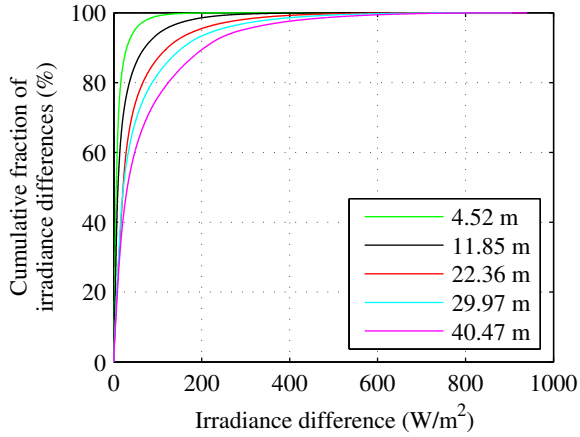

Fig. 5.10: Cumulative distributions of instantaneous irradiance differences for several distances between the photodiode sensors during non-uniform irradiance conditions caused by moving clouds.

The operation of PV power generators and the amount of mismatch losses under partial shading conditions is highly affected by shading strength, i.e. the attenuation of irradiance caused by the shading object and not so much by the absolute values of the irradiance as was discussed in Chapter 4. In line with that, the shading strength has been defined in this chapter as the ratio of the absolute value of the irradiance difference to the higher value of irradiance of the two photodiode sensors. This means that the shading strength is independent of which one of the sensors measures the higher value. The cumulative distributions of shading strengths are shown in Fig. 5.11. As can be seen, the amount of high shading strengths increases when the distance between two sensors increases. In this case for sensors with distances of 4.52 m and 40.47 m (green and magenta curves in Fig. 5.11), 90% of all shading strengths are smaller than 6.6% and 40.7%, respectively.

5.2.2 Mismatch Losses in PV Power Generators due to Clouds

The dynamic effect of clouds on irradiance shown in Figs. 5.9–5.11 obviously also affects the operation of PV power generators. These non-uniform conditions cause mismatch losses in PV power generators composed of interconnected PV modules. In order to illustrate the effect of moving clouds on the irradiance conditions of a PV power generator

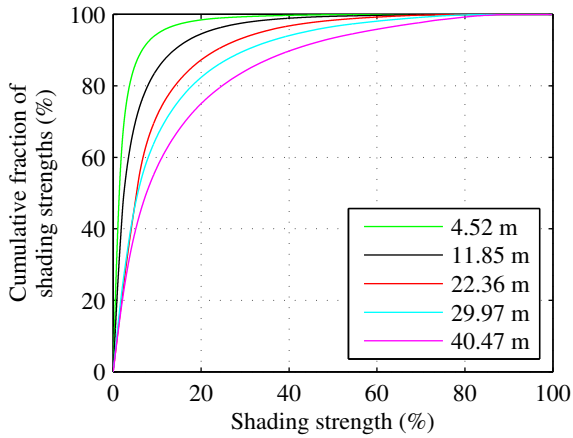

Fig. 5.11: Cumulative distributions of instantaneous shading strengths for several distances between the photodiode sensors during non-uniform irradiance conditions caused by moving clouds. Shading strength is the absolute value of the ratio of irradiance difference to the higher value of irradiance of the two sensors.

(Figs. 5.10–5.11) and consequently on mismatch losses, let us consider a case of two series-connected PV modules which are located at the same places as the photodiode sensors. The total amount of mismatch losses in this PV power generator are shown in Fig. 5.12 as a function of distance between the modules during non-uniform irradiance conditions caused by moving clouds during the whole 180-day period. As can be seen, the mismatch losses increase almost linearly as a function of distance between the modules. The linear increase of mismatch losses as a function of distance is a plausible result because the speed of a cloud can be assumed to be constant during a shading event of a PV power generator. Accordingly, the time of partial shading due to moving clouds increase with increasing distance between the modules.

The results presented in Fig. 5.12 suggest that the mismatch losses in PV power generators increase as the physical diameter of the generator increases. Therefore, PV modules feeding a load or an interfacing device (such as an inverter) should be located as close to each other as possible and configurations with long strings and adjacent or consecutive series-connected PV modules should be avoided.

The mismatch energy losses of the studied PV power generators with different configurations during the 180-day period are shown in Table 5.2. In addition to mismatch losses during non-uniform conditions caused by clouds, the mismatch losses during uniform conditions and the total losses during non-uniform and uniform conditions are also presented. Mismatch losses during non-uniform conditions are calculated by comparing the maximum available energy from the PV power generator during non-uniform condi-

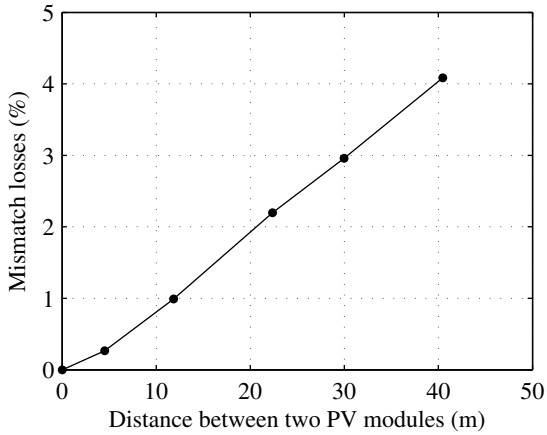

Fig. 5.12: Mismatch losses in a PV power generator composed of two series-connected PV modules as a function of distance between the modules during non-uniform conditions caused by moving clouds.

tions to the maximum energy that could be extracted during non-uniform conditions if all the PV cells were operating at their own MPPs all the time (i.e. no mismatch losses). The losses during uniform conditions and total mismatch losses are also calculated similarly. This is the reason why total mismatch losses are not simply a sum of losses during non-uniform and uniform conditions. As can be seen, the mismatch losses increase as the length and amount of series-connected PV modules increases. Losses in case of long series connection are clearly the largest. It should also be noticed that the parallel connections of strings cause more mismatch losses than multi-string configurations.

Table 5.2: Mismatch losses in different PV power generator configurations.

Generator	Mismatch losses		
	Non-uniform	Uniform	Total
Short multi-strings	0.82%	0.22%	0.33%
Short parallel strings	1.09%	0.35%	0.49%
Long multi-strings	1.43%	0.33%	0.44%
Long parallel strings	1.76%	0.49%	0.61%
Long string	3.79%	0.47%	1.08%

Mismatch losses in non-uniform operation conditions are bigger than in uniform conditions for all generator configurations as expected. Losses increase considerably with increasing length of series connections in non-uniform conditions. Parallel strings generators have slightly larger losses than multi-string configurations. Losses in Long string configuration are considerably high, close to 4%. This demonstrates that the configura-

tion of a PV power generator has a major impact on the amount of harvested electrical energy when building PV power generators in locations where half-cloudy climatic conditions are typical.

Mismatch losses during uniform conditions are clearly higher for parallel-connected strings than for multi-string configurations with the same number of modules. Actually, the losses during uniform conditions were larger for Parallel short than for Multi-string long generator and similarly also for Parallel long generator compared to the losses in Long string generator. This increase in losses is due to different temperatures between the PV modules under uniform irradiance conditions because the uniform conditions were defined so that they were present always when irradiance of none of the photodiode sensors was changing. This means that although irradiance conditions were uniform, there could have been differences in the temperatures of the PV modules. Temperature has a larger effect on the OC voltage of the PV modules than on the SC current and, therefore, also on MPP voltage. This causes higher losses for parallel-connected than for series-connected PV modules in case of uniform irradiance conditions. The reason for this is that the common voltage in parallel connection forces individual modules to operate further away from their own MPPs than in case of series-connected PV modules. This phenomenon could further be studied by classifying the data also based on the PV module temperature conditions (non-uniform or uniform temperatures). In this thesis, however, the focus is on the losses caused by the moving clouds on irradiances of the PV modules.

Due to the higher losses during uniform conditions in the case of parallel-connected strings, the total mismatch losses are lowest for generators with multi-string configurations. The total mismatch losses are still clearly highest for the Long string generator.

Under uniform irradiance conditions, which in practice exist in the most feasible areas for PV power generators, mismatch losses are below 0.5% for all generator configurations. In these kinds of conditions mismatch losses due to clouds are not a major concern. However, in areas with frequent cloud coverage, mismatch losses can be considerable for a generator composed of a long string of series-connected PV modules. In southern Finland these losses were shown to be close to 4%. This should be taken carefully into account when designing PV power systems.

6 CONCLUSIONS AND RECOMMENDATIONS FOR FUTURE WORK

This chapter presents the summary of the thesis. The most important findings and scientific contributions are summarized. Also some recommendations for the topics of further research work will be presented.

6.1 Main Conclusions of the Thesis

This thesis studied the effect of partial shading conditions on silicon-based PV power generators by using a systematic and comprehensive approach developed by the author of the thesis. Different phenomena were studied by using Matlab Simulink simulation model based on the well-known one-diode model of the operation of PV cells. The operation of the simulation model was experimentally verified by the author of the thesis. The simulation model was shown to be sufficiently accurate for the objectives of the thesis. Also a vast amount of measured irradiance and PV module temperature data was used in the analyses in this thesis.

Partial shading conditions have been recognized to have a major effect of the operation of PV power generators. Typically there are multiple MPPs on the electrical characteristics of PV power generators when operating under partial shading conditions. It was, however, shown that there are certain conditions where there is only one MPP despite the partial shading conditions. Three different reasons for this were found and analyzed. It was found that reasons for having one or more MPPs originated directly from the physical properties of PV modules: The ratio of MPP current to SC current, power losses in bypass diodes and the value of parasitic shunt resistance of PV cells.

The characteristics of MPPs were also studied by using the developed systematic approach. It was found that it is possible to differentiate between local and global MPPs based on the MPP at which the system operates without losing energy when scanning the whole or part of the *P-U* curve of the PV power generator. This finding can be used to improve existing MPPT algorithms or even to develop completely new methods to track the global MPP.

PV power generators can be built using different generator configurations. Typically different configurations are based on the interfacing device connected between the PV

power generator and the electrical grid such as the central inverter, string inverter or multi-string inverter. Mismatch losses in PV power generators with different configurations under partial shading conditions in were also studied by using the systematic approach. Mismatch losses are losses due to non-uniform conditions under which all the PV cells in the PV power generator are not operating at their own MPP although the generator would operate at its own MPP. It was noticed that the configuration which is based on the multi-string inverter concept had the lowest mismatch losses and that long series connections of PV modules should be avoided when building PV power generators.

The mismatch losses were also studied by using three practical shading scenarios. Based on this case study, multi-string configuration has least mismatch losses but the amount of losses of long series string and parallel-connected strings differed from the results based on the systematic study. It was shown that the layout of the PV power generator can have a major effect of the mismatch losses if the consecutive PV module rows cause mutual shading. The layout and configuration should be carefully designed when building the PV power generators.

Partial shading conditions due to buildings and clouds have different kinds of effects on the operation of PV power generators. While static objects such as buildings cause shadows whose edges are sharp so that the irradiance changes rapidly, the irradiance changes more gradually on the edge of a shade caused by a cloud. The effect of partial shading conditions due to clouds on mismatch losses was also studied in the thesis by using measured irradiances and PV module temperature as input for the simulation models. It was found that the longer the strings of series-connected PV modules, the more there are mismatch losses during shading events caused by clouds.

6.2 Future Research Topics

This thesis presents a systematic and comprehensive study on the effects of partial shading conditions on PV power generators. The number of MPPs as well as the MPP voltages and currents were investigated. Interesting topics for further research work arising from this thesis include:

1. The systematic approach developed and presented in Chapter 3 utilized only one value for non-shaded and shaded PV cells. As a next step, the number of different values of irradiances could be increased. This would need a new approach in order to preserve the systematic perspective. By increasing the number of different values of irradiances, new information about the operation of PV power generators could be achieved. This would be a very interesting and challenging topic for further research work.

2. The basic unit of the simulation model used to obtain the results presented in the thesis was 18 series-connected PV cells with an anti-parallel-connected bypass diode. In

further research, a cell-based model with an additional term for reverse characteristics of PV cells could be developed and used. The same systematic method could be used and the results could be compared to see if more accurate model will give much different results related to power losses and location of MPPs if only one or few cells are shaded of the 18 series-connected cells with an anti-parallel bypass diode. It would be interesting to see if new phenomena arise which are not visible by using the simulation model in this thesis such as hot-spot phenomenon related issues.

3. The results in this thesis were obtained by using systematical simulation studies. In further work, it would be interesting to verify the findings by using the vast amount of measurement data recorded by the data acquisition system of TUT Solar Photovoltaic Power Station Research Plant. By analyzing mismatch losses and characteristics of MPPs, it would be possible to recognize the most important practical partial shading conditions and operating conditions in general. This would be a very interesting continuation of the research work presented in this thesis.

4. The method to differentiate between local and global MPPs presented in Chapter 4 could be implemented into an existing MPPT algorithm or even develop a new algorithm. The implementation and testing of this algorithm is a very interesting task on the way of developing the optimal MPPT algorithm. It has to be taken into account that the algorithm based on the differentiation of local and global MPPs will require extensive computational capability from the microprocessor. In addition to that the sensitivity of the parameters to the changes in the MPP voltages and currents due to, for example, aging should be investigated carefully.

5. In this thesis, one of the major topics was the operation of electrically different configurations of PV power generators under partial shading conditions. There are also another configuration in addition to ones in this thesis such as Total Cross Tied and Bridge Linked configuration (Wang and Hsu, 2011a) which should be studied in future. As a further work, the effect of the physical layout of the generator should also be studied. PV power generators are often built by using series-connected, adjacent PV modules. It would be interesting to compare the operation of a PV power generator composed of adjacent PV modules to the operation of a generator with modules installed on a physically square-like area. The square-like shape for the generator should be beneficial under partial shading caused by clouds because the maximum diameter of the generator is shorter compared to generator with adjacent PV modules. This way the differences between the irradiances of the PV modules can be made smaller. This should cause less mismatch losses and affect less the voltage of the global MPP. In addition, the effect of mounting positions and orientation of a single module could be taken into account when comparing the operation of physically different generators.

REFERENCES

Abbott, D. (2010). Keeping the energy debate clean: how do we supply the world's energy needs?, *Proceedings of the IEEE* **98**(1): 42–66. DOI: 10.1109/JPROC.2009.2035162.

Abella, M. A. and Chenlo, F. (2004). Choosing the right inverter for grid-connected pv systems, *Renewable Energy World* **7**(2): 132–146.

Acciari, G., Graci, D. and Scala, A. L. (2011). Higher pv module efficiency by a no-val cbs bypass, *IEEE Transactions on Power Electronics* **26**(5): 1333–1336. DOI: 10.1109/TPEL.2010.2095469.

Ahmed, N. A. and Miyatake, M. (2008). A novel maximum power point tracking for photovoltaic applications under partially shaded insolation conditions, *Electric Power Systems Research* **78**(5): 777–784. DOI: 10.1016/j.epsr.2007.05.026.

Al-Rawi, N. A., Al-Kaisi, M. M. and Asfer, D. J. (1994). Reliability of photovoltaic modules ii. interconnection and bypass diodes effects, *Solar Energy Materials and Solar Cells* **4**(4): 469–480. DOI: 10.1016/0927-0248(94)90189-9.

Alonso-García, M. C. and Ruiz, J. M. (2006). Analysis and modelling the reverse characteristic of photovoltaic cells, *Solar Energy Materials and Solar Cells* **90**(7-8): 1105–1120. DOI: 10.1016/j.solmat.2005.06.006.

Alonso-García, M. C., Ruiz, J. M. and Chenlo, F. (2006). Experimental study of mismatch and shading effects in the I-V characteristic of a photovoltaic module, *Solar Energy Materials and Solar Cells* **90**(3): 329–340. DOI: 10.1016/j.solmat.2005.04.022.

Alonso-García, M. C., Ruiz, J. M. and Herrmann, W. (2006). Computer simulation of shading effects in photovoltaic arrays, *Renewable Energy* **31**(12): 1986–1993. DOI: 10.1016/j.renene.2005.09.030.

Alonso, R., Ibanez, P., Martínez, V., Román, E. and Sanz, A. (2009). An innovative perturb, observe and check algorithm for partially shaded pv systems, *13th European Conference on Power Electronics and Applications*, pp. 1–8.

Araújo, S. V., Zacharias, P. and Mallwitz, R. (2010). Highly efficient single-phase transformerless inverters for grid-connected photovoltaic systems, *IEEE Transactions on Industrial Electronics* **57**(9): 3118–3128. DOI: 10.1109/TIE.2009.2037654.

Armstrong, S. and Hurley, W. G. (2010). A new methodology to optimise solar energy extraction under cloudy conditions, *Renewable Energy* **35**(4): 780–787. DOI: 10.1016/j.renene.2009.10.018.

ASTM International (2008). Astm g173-03 standard tables for reference solar spectral irradiances: Direct normal and hemispherical on 37° tilted surface. American Society for Testing and Materials (ASTM), URL: http://rredc.nrel.gov/solar/spectra/am1.5/. Accessed 18.4.2013.

Barroso, L. A., Rudnick, H., Sensfuss, F. and Linares, P. (2010). The green effect, *IEEE Power and Energy Magazine* **8**(5): 22–35. DOI: 10.1109/MPE.2010.937595.

Bishop, J. W. (1988). Computer simulation of the effects of electrical mismatches in photovoltaic cell interconnection circuits, *Solar Cells* **25**(1): 73–89. DOI: 10.1016/0379-6787(88)90059-2.

Bishop, J. W. (1989). Microplasma breakdown and hot-spots in silicon solar cells, *Solar Cells* **26**(4): 335–349. DOI: 10.1016/0379-6787(89)90093-8.

Bose, B. K. (2010). Global warming: energy, environmental pollution, and the impact of power electronics, *IEEE Industrial Electronics Magazine* **4**(1): 6–17. DOI: 10.1109/MIE.2010.935860.

Brano, V. L., Orioli, A., Ciulla, G. and Gangi, A. D. (2010). An improved five-parameter model for photovoltaic modules, *Solar Energy Materials and Solar Cells* **94**(8): 1358–1370. DOI: 10.1016/j.solmat.2010.04.003.

Bucciarelli, L. L. (1979). Power loss in photovoltaic arrays due to mismatch in cell characteristics, *Solar Energy* **23**(4): 277–288. DOI: 10.1016/0038-092X(79)90121-X.

Bull, S. R. (2001). Renewable energy today and tomorrow, *Proceedings of the IEEE* **89**(8): 1216–1226. DOI: 10.1109/5.940290.

Carrasco, J. M., Franquelo, L. G., Bialasiewicz, J. T., Galván, E., Guisado, R. C. P., Ángeles Martín Prats, M., León, J. I. and Moreno-Alfonso, N. (2006). Power-electronic systems for the grid integration of renewable energy sources: a survey, *IEEE Transactions on Industrial Electronics* **53**(4): 1002–1016. DOI: 10.1109/TIE.2006.878356.

Chamberlin, C. E., Lehman, P., Zoellick, J. and Pauletto, G. (1995). Effect of mismatch losses in photovoltaic arrays, *Solar Energy* **54**(3): 165–171. DOI: 10.1016/0038-092X(94)00120-3.

Chapin, D. M., Fuller, C. S. and Pearson, G. L. (1954). A new silicon p–n junction photocell for converting solar radiation into electrical power, *Journal of Applied Physics* **25**(5): 676–677. DOI: 10.1063/1.1721711.

Ding, J. and Radhakrishnan, R. (2008). A new method to determine the optimum load of a real solar cell using the lambert w-function, *Solar Energy Materials and Solar Cells* **92**(12): 1566–1569. DOI: 10.1016/j.solmat.2008.07.004.

Drif, M., Pérez, P. J., Aguilera, J. and Aguilar, J. D. (2008). A new estimation method of irradiance on a partially shaded pv generator in grid-connected photovoltaic systems, *Renewable Energy* **33**(9): 2048–2056. DOI: 10.1016/j.renene.2007.12.010.

Dunlop, J. (2005). *Photovoltaic Systems*, American Technical Publishers. ISBN 978-0-8269-1287-9.

Eltawil, M. A. and Zhao, Z. (2010). Grid-connected photovoltaic power systems: technical and potential problems – a review, *Renewable and Sustainable Energy Reviews* **14**(1): 112–129. DOI: 10.1016/j.rser.2009.07.015.

Esram, T. and Chapman, P. L. (2007). Comparison of photovoltaic array maximum power point tracking techniques, *IEEE Transactions on Energy Conversion* **22**(2): 439–449. DOI: 10.1109/TEC.2006.874230.

European Commission (2012). The EU climate and energy package. URL: http://ec.europa.eu/clima/policies/package/index_en.htm. Accessed 26.4.2013.

Femia, N., Petrone, G., Spagnuolo, G. and Vitelli, M. (2005). Optimization of perturb and observe maximum power point tracking method, *IEEE Transactions on Power Electronics* **20**(4): 963–973. DOI: 10.1109/TPEL.2005.850975.

Galiana, B., Algora, C. and Rey-Stolle, I. (2008). Explanation for the dark i-v curve of iii-v concentrator solar cells, *Progress in Photovoltaics: Research and Applications* **16**(4): 331–338. DOI: 10.1002/pip.805.

Gao, L., Dougal, R. A., Liu, S. and Iotova, A. P. (2009). Parallel-connected solar pv system to address partial and rapidly fluctuating shadow conditions, *IEEE Transactions on Industrial Electronics* **56**(5): 1548–1556. DOI: 10.1109/TIE.2008.2011296.

García, M., Maruri, J. M., Marroyo, L., Lorenzo, E. and Pérez, M. (2008). Partial shadowing, mppt performance and inverter configurations: observations at tracking pv plants, *Progress in Photovoltaics: Research and Applications* **16**(6): 529–536. DOI: 10.1002/pip.833.

Ghani, F., Duke, M. and Carson, J. (2013). Numerical calculation of series and shunt resistance of a photovoltaic cell using the lambert W-function: experimental evaluation, *Solar Energy* **87**: 246–253. DOI: 10.1016/j.solener.2012.11.002.

Giesler, B., Haselhuhn, R., Komarek, T., Krüll, Y., Öchsner, P., Nisar, S. A. and Zehner, M. (2012). Influence of limitation of the mpp-range from pv inverters, *27th European Photovoltaic Solar Energy Conference and Exhibition*, Frankfurt, Germany, pp. 3770–3774. DOI: 10.4229/27thEUPVSEC2012-5CO.6.4.

Giraud, F. and Salameh, Z. M. (1999). Analysis of the effects of a passing cloud on a grid-interactive photovoltaic system with battery storage using neural networks, *IEEE Transactions on Energy Conversion* **14**(4): 1572–1577. DOI: 10.1109/60.815107.

Gow, J. A. and Manning, C. D. (1999). Development of a photovoltaic array model for use in power-electronics simulation study, *IEE Proceedings - Electric Power Applications* **146**(2): 193–200. DOI: 10.1049/ip-epa:19990116.

Gow, J. A. and Manning, C. D. (2000). Photovoltaic converter system suitable for use in small scale stand-alone or grid connected applications, *IEE Proceedings - Electric Power Applications* **147**(6): 535–543. DOI: 10.1049/ip-epa:20000789.

Green, M. A. and Emery, K. (1993). Solar cell efficiency tables, *Progress in Photovoltaics: Research and Applications* **1**(1): 25–29. DOI: 10.1002/pip.4670010104.

Green, M. A., Emery, K., Hishikawa, Y., Warta, W. and Dunlop, E. D. (2013). Solar cell efficiency tables (version 41), *Progress in Photovoltaics: Research and Applications* **21**(1): 1–11. DOI: 10.1002/pip.2352.

Guyemard, C. A. (2004). The sun's total and spectral irradiance for solar energy applications and solar radiation models, *Solar Energy* **76**(4): 423–453. DOI: 10.1016/j.solener.2003.08.039.

Häberlin, H. (2012). *Photovoltaics system design and practice*, John Wiley & Sons, Chichester, West Sussex, United Kingdom. ISBN 978-1-119-99285.

Hussein, K. H., Muta, I., Hoshino, T. and Osakada, M. (1995). Maximum photovoltaic power tracking: an algorithm for rapidly changing atmospheric conditions, *IEE Proceedings - Generation, Transmission and Distribution* **142**(1): 59–64. DOI: 10.1049/ip-gtd:19951577.

Iannone, F., Noviello, G. and Sarno, A. (1998). Monte carlo techniques to analyse the electrical mismatch losses in large-scale photovoltaic generators, *Solar Energy* **62**(2): 85–92. DOI: 10.1016/S0038-092X(97)00085-6.

International Energy Agency (2012). Key world energy statistics. OECD/International Energy Agency (IEA), URL: http://www.iea.org/publications/freepublications/publication/kwes.pdf, Accessed: 15.4.2013.

Jäger-Waldau, A. (2007). Photovoltaics and renewable energies in europe, *Renewable and Sustainable Energy Reviews* **11**(7): 1414–1437. DOI: 10.1016/j.rser.2005.11.001.

Jewell, W. and Ramakumar, R. (1987). The effects of moving clouds on electric utilities with dispersed photovoltaic generation, *IEEE Transactions on Energy Conversion* **2**(4): 570–576. DOI: 10.1109/TEC.1987.4765894.

Jewell, W. and Unruh, T. D. (1990). Limits on cloud-induced fluctuation in photovoltaic generation, *IEEE Transactions on Energy Conversion* **5**(1): 8–14. DOI: 10.1109/60.50805.

Karatepe, E., Boztepe, M. and Çolak, M. (2007). Development of a suitable model for characterizing photovoltaic arrays with shaded solar cells, *Solar Energy* **81**(8): 977–992. DOI: 10.1016/j.solener.2006.12.001.

Karatepe, E., Hiyama, T., Boztepe, M. and Çolak, M. (2008). Voltage based power compensation system for photovoltaic generation system under partially shaded insolation conditions, *Energy Conversion and Management* **49**(8): 2307–2316. DOI: 10.1016/j.enconman.2008.01.012.

Kaushika, N. D. and Gautam, N. K. (2003). Energy yield simulations of interconnected solar pv arrays, *IEEE Transactions on Energy Conversion* **18**(1): 127–134. DOI: 10.1109/TEC.2002.805204.

Kaushika, N. D. and Rai, A. K. (2007). An investigation of mismatch losses in solar photovoltaic cell networks, *Energy* **32**(5): 755–759. DOI: 10.1016/j.energy.2006.06.017.

Kawamura, H., Naka, K., Yonekura, N., Yamanaka, S., Kawamura, H., Ohno, H. and Naito, K. (2003). Simulation of i-v characteristics of a pv module with shaded pv cells, *Solar Energy Materials and Solar Cells* **75**(3-4): 613–621. DOI: 10.1016/S0927-0248(02)00134-4.

Kazmi, S., Goto, H., Ichinokura, O. and Guo, H.-J. (2009). An improved and very efficient mppt controller for pv systems subjected to rapidly varying atmospheric conditions and partial shading, *Australasian Universities Power Engineering Conference 2009*, pp. 1–6.

Kern, E. C., Gulachenski, E. M. and Kern, G. A. (1989). Cloud effects on distributed photovoltaic generation: slow transients at the gardner, massachusetts photovoltaic experiment, *IEEE Transactions on Energy Conversion* **4**(2): 184–190. DOI: 10.1109/60.17910.

Kjaer, S. B., Pederson, J. K. and Blaabjerg, F. (2005). A review of single-phase grid-connected inverters for photovoltaic modules, *IEEE Transactions on Industry Applications* **41**(5): 1292–1306. DOI: 10.1109/TIA.2005.853371.

Kobayashi, K., Takano, I. and Sawada, Y. (2006). A study of a two stage maximum power point tracking control of a photovoltaic system under partially shaded insolation condition, *Solar Energy Materials and Solar Cells* **90**(18-19): 2975–2988. DOI: 10.1016/j.solmat.2006.06.050.

Kovach, A. and Schmid, J. (1996). Determination of energy output losses due to shading of building-integrated photovoltaic arrays using a raytracing technique, *Solar Energy* **57**(2): 117–124. DOI: 10.1016/S0038-092X(96)00066-7.

Kroposki, B., Margolis, R. and Ton, D. (2009). Harnessing the sun, *IEEE Power and Energy Magazine* **7**(3): 22–33. DOI: 10.1109/MPE.2009.932305.

Kumar, S., Singh, P. K. and Chilana, G. S. (2009). Study of silicon solar cell at different intensities of illumination and wavelengths using impedance spectroscopy, *Solar Energy Materials and Solar Cells* **93**(10): 1881–1884. DOI: 10.1016/j.solmat.2009.07.002.

Lashway, C. (1988). Photovoltaic system testing techniques and results, *IEEE Transactions on Energy Conversion* **3**(3): 503–506. DOI: 10.1109/60.8058.

Liu, S. and Dougal, R. A. (2002). Dynamic multiphysics model for solar array, *IEEE Transactions on Energy Conversion* **17**(2): 285–294. DOI: 10.1109/TEC.2002.1009482.

Lopez-Lapeña, O. and Penella, M. T. (2012). Low-power focv mppt controller with automatic adjustment of the sample&hold, *Electronic Letters* **48**(20): 1301–1303. DOI: 10.1049/el.2012.1345.

Luque, A. and Hegedus, S. (2003). *Handbook of Photovoltaic Science and Engineering*, John Wiley & Sons, Chichester, West Sussex, England. ISBN 0-471-49196-9.

Martínez-Moreno, F., Muñoz, J. and Lorenzo, E. (2010). Experimental model to estimate shading losses on pv arrays, *Solar Energy Materials and Solar Cells* **94**(12): 2298–2303. DOI: 10.1016/j.solmat.2010.07.029.

Messenger, R. A. and Ventre, J. (2010). *Photovoltaic systems engineering*, 3 edn, CRC Press, Boca Raton, Florida. ISBN 978-1-4398-0292-2.

Miyatake, M., Veerachary, M., Toriumi, F., Fujii, N. and Ko, H. (2011). Maximum power point tracking of multiple photovoltaic arrays: a pso approach, *IEEE Transactions on Aerospace and Electronic Systems* **47**(1): 367–380. DOI: 10.1109/TAES.2011.5705681.

Mäki, A. and Valkealahti, S. (2011). Operation of long series-connected silicon-based photovoltaic module string and parallel-connected short strings under partial shading conditions, *26th European Photovoltaic Solar Energy Conference and Exhibition*, Hamburg, Germany, pp. 4227–4232. DOI: 10.4229/26thEUPVSEC2011-5BV.2.10.

Mäki, A. and Valkealahti, S. (2012a). Mismatch losses in photovoltaic power generators due to partial shading caused by moving clouds, *27th European Photovoltaic Solar Energy Conference and Exhibition*, Frankfurt, Germany, pp. 3911–3915. DOI: 10.4229/27thEUPVSEC2012-5AV.1.6.

Mäki, A. and Valkealahti, S. (2012b). Power losses in long string and parallel-connected short strings of series-connected silicon-based photovoltaic modules due to partial chading conditions, *IEEE Transactions on Energy Conversion* **27**(1): 173–183. DOI: 10.1109/TEC.2011.2175928.

Mäki, A. and Valkealahti, S. (2013a). Effect of photovoltaic generator components on the number of mpps under partial shading conditions, *IEEE Transactions on Energy Conversion* . DOI: 10.1109/TEC.2013.2274280.

Mäki, A. and Valkealahti, S. (2013b). Differentiation of multiple maximum power points of partially shaded photovoltaic power generators, *Renewable Energy* . in review.

Mäki, A., Valkealahti, S. and Leppäaho, J. (2012). Operation of series-connected silicon-based photovoltaic modules under partial shading conditions, *Progress in Photovoltaics: Research and Applications* **20**(3): 298–309. DOI: 10.1002/pip.1138.

Mäki, A., Valkealahti, S. and Suntio, T. (2010). Dynamic terminal characteristics of a photovoltaic generator, *14th International Power Electronics and Motion Control Conference*, Ohrid, Macedonia, pp. T12–76–T12–80. DOI: 10.1109/EPEPEMC.2010.5606786.

Muñoz, J., Lorenzo, E., Martínez-Moreno, F., Marroyo, L. and García, M. (2008). An investigation into hot-spots in two large grid-connected pv plants, *Progress in Photovoltaics: Research and Applications* **16**(8): 693–701. DOI: 10.1002/pip.844.

Nema, R. K., Nema, S. and Agnihotri, G. (2009). Computer simulation based study of photovoltaic cells/modules and their experimental verification, *International Journal of Recent Trends in Engineering* **1**(3): 151–156.

Newton, J. D. (1987). *Uncommon friends: life with Thomas Edison, Henry Ford, Harvey Firestone, Alexis Carrel & Charles Lindbergh*, Harcourt, INC., San Diego, New York, London. ISBN 0-15-692620-2.

Nguyen, D. and Lehman, B. (2008). An adaptive solar photovoltaic array using model-based reconfiguration algorithm, *IEEE Transactions on Industrial Electronics* **55**(7): 2644–2654. DOI: 10.1109/TIE.2008.924169.

Nguyen, T. L. and Low, K.-S. (2010). A global maximum power point tracking scheme employing direct search algorithm for photovoltaic systems, *IEEE Transactions on Industrial Electronics* **57**(10): 3456–3467. DOI: 10.1109/TIE.2009.2039450.

Nobelprize.org (2013a). The nobel prize in physics 1921. URL: http://www.nobelprize.org/nobel_prizes/physics/laureates/1921/. Accessed 19.4.2013.

Nobelprize.org (2013b). The nobel prize in physics 1956. URL: http://www.nobelprize.org/nobel_prizes/physics/laureates/1956/. Accessed 6.8.2013.

Noguchi, T., Togashi, S. and Nakamoto, R. (2002). Short-current pulse-based maximum-power-point tracking method for multiple photovoltaic-and-converter module system, *IEEE Transactions on Industrial Electronics* **49**(1): 217–223. DOI: 10.1109/41.982265.

Nousiainen, L., Puukko, J., Mäki, A., Messo, T., Huusari, J., Jokipii, J., Viinamäki, J., Torres Lobera, D., Valkealahti, S. and Suntio, T. (2013). Photovoltaic generator as an input source for power electronic converters, *IEEE Transactions on Power Electronics* **28**(6): 3028–3038. DOI: 10.1109/TPEL.2012.2209899.

NREL (2013). Best research-cell efficiencies. URL: http://www.nrel.gov/ncpv/images/efficiency_chart.jpg, Accessed: 16.4.2013.

Oozeki, T., Otani, K. and Kurokawa, K. (2005). Accuracy of estimated shading loss ratio by means of the sv method - an extraction algorithm of maximum pattern, *31st IEEE Photovoltaic Specialists Conference*, Lake buena Vista, Florida, pp. 1804–1807. DOI: 10.1109/PVSC.2005.1488502.

Paraskevadaki, E. V. and Papathanassiou, S. A. (2011). Evaluation of mpp voltage and power of mc-si pv modules in partial shading conditions, *IEEE Transactions on Energy Conversion* **26**(3): 923–932. DOI: 10.1109/TEC.2011.2126021.

Patel, H. and Agarwal, V. (2008). Matlab-based modeling to study the effects of partial shading on pv array characteristics, *IEEE Transactions on Energy Conversion* **23**(1): 302–310. DOI: 10.1109/TEC.2007.914308.

Petrone, G., Spagnuolo, G. and Vitelli, M. (2007). Analytical model of mismatched photovoltaic fields by means of lambert w-function, *Solar Energy Materials and Solar Cells* **91**(18): 1652–1657. DOI: 10.1016/j.solmat.2007.05.021.

Pirinen, P., Simola, H., Aalto, J., Kaukoranta, J.-P., Karlsson, P. and Ruuhela, R. (2012). Tilastoja suomen ilmastosta 1981-2010, *Technical report*, Finnish Meteorological Institute. ISBN 978-951-697-766-2.

Quaschning, V. and Hanitsch, R. (1996). Numerical simulation of current-voltage characteristics of photovoltaic systems with shaded solar cells, *Solar Energy* **56**(6): 513–520. DOI: 10.1016/0038-092X(96)00006-0.

Quaschning, V. and Hanitsch, R. (1998). Increased energy yield of 50% at flat roof and field installations with optimized module structures, *2nd World Conference and Exhibition on Photovoltaic Solar Energy Conversion*, Vienna, Austria, pp. 1993–1996.

Ramabadran, R. and Mathur, B. (2009b). Matlab based modelling and performance study of series connected spva under partial shaded conditions, *Journal of Sustainable Development* **2**(3): 85–94.

Razykov, T. M., Ferekides, C. S., Morel, D., Stefanakos, E., Ullal, H. S. and Upadhyaya, H. M. (2011). Solar photovoltaic electricity: Current status and future prospects, *Solar Energy* **85**(8): 1580–1608. DOI: 10.1016/j.solener.2010.12.002.

Reinoso, C. R. S., Milone, D. H. and Buitrago, R. H. (2010). Efficiency study of different photovoltaic plant connection schemes under dynamic shading, *International Journal of Hydrogen Energy* **35**(11): 5838–5843. DOI: 10.1016/j.ijhydene.2009.12.130.

Reinoso, C. R. S., Milone, D. H. and Buitrago, R. H. (2013). Simulation of photovoltaic centrals with dynamic shading, *Applied Energy* **103**: 278–289. DOI: 10.1016/j.apenergy.2012.09.040.

Renewable Energy Policy Network for the 21st Century (2008). Renewables 2007 global status report. URL: http://www.ren21.net/pdf/RE2007_Global_Status_Report.pdf. Accessed 26.4.2013.

Roche, D., Outhred, H. and Kaye, R. J. (1995). Analysis and control of mismatch power loss in photovoltaic arrays, *Progress in Photovoltaics: Research and Applications* **3**(2): 115–127. DOI: 10.1002/pip.4670030201.

Rogner, H.-H. (2012). World energy demand and supply. URL: http://www.iaea.org/nuclearenergy/nuclearknowledge/schools/NEM-school/2012/AbuDhabi/PDFs/day1/04_Rogner_World_Energy_D%26S.pdf, Accessed: 15.4.2013.

Rubio, F., Martínez, M. and Banda, P. (2010). Concentrator photovoltaic field installations, *in* L. Fraas and L. Partain (eds), *Solar cells and their applications*, Wiley & Sons, Hoboken, New Jersey, USA, chapter 17, pp. 377–394. ISBN 978-0-470-44633-1.

Saetre, T. O., Midtgårg, O.-M. and Yordanov, G. H. (2011). A new analytical solar cell i-v curve model, *Renewable Energy* **36**(8): 2171–2176. DOI: 10.1016/j.renene.2011.01.012.

Saha, H., Bhattacharya, G. and Mukherjee, D. (1988). Mismatch losses in series combinations of silicon solar cell modules, *Solar Cells* **25**(2): 143–153. DOI: 10.1016/0379-6787(88)90018-X.

Salas, V., Olías, E., Barrado, A. and Lázaro, A. (2006). Review of the maximum power point tracking algorithms for stand-alone photovoltaic systems, *Solar Energy Materials and Solar Cells* **90**(11): 1555–1578. DOI: 10.1016/j.solmat.2005.10.023.

Sandrolini, L., Artioli, M. and Reggiani, U. (2010). Numerical method for the extraction of photovoltaic module double-diode model parameters through cluster analysis, *Applied Energy* **87**(2): 442–451. DOI: 10.1016/j.apenergy.2009.07.022.

Shockley, W. (1949). The theory of p–n junctions in semiconductors and p–n junction transistors, *Bell System Tech* **28**(3): 435–489.

Shockley, W. and Queisser, H. J. (1961). Detailed balance limit of efficiency of p–n junction solar cells, *Journal of Applied Physics* **32**(3): 510–519. DOI: 10.1063/1.1736034.

Shockley, W., Sparks, M. and Teal, G. K. (1951). p–n junction transistors, *Physical Review* **83**(1): 151–164.

Silvestre, S., Boronat, A. and Chouder, A. (2009). Study of bypass diodes configuration on pv modules, *Applied Energy* **86**(9): 1632–1640. DOI: 10.1016/j.apenergy.2009.01.020.

Silvestre, S. and Chouder, A. (2008). Effects of shadowing on photovoltaic module performance, *Progress in Photovoltaics: Research and Applications* **16**(2): 141–149. DOI: 10.1002/pip.780.

Soto, W. D., Klein, S. A. and Beckman, W. A. (2006). Improvement and validation of a model for photovoltaic array performance, *Solar Energy* **80**(1): 78–88. DOI: 10.1016/j.solener.2005.06.010.

Spertino, F. and Akilimali, J. S. (2009). Are manufacturing I–V mismatch and reverse currents key factors in large photovoltaic arrays?, *IEEE Transactions on Industrial Electronics* **56**(11): 4520–4531. DOI: 10.1109/TIE.2009.2025712.

Teodorescu, R., Liserre, M. and Rodríquez, P. (2011). *Grid converters for photovoltaic and wind power systems*, Wiley & Sons, Chichester, West Sussex, United Kingdom. ISBN 978-0-470-05751-3.

Tiedje, T., Yablonovitch, E., Cody, G. D. and Brooks, B. G. (1984). Limiting efficiency of silicon solar cells, *IEEE Transactions on Electron Devices* **31**: 711–716. DOI: 10.1109/T-ED.1984.21594.

Ubisse, A. and Sebitosi, A. (2009). A new topology to mitigate the effect of shading for small photovoltaic installations in rural sub-saharan africa, *Energy Conversion and Management* **50**(7): 1797–1801. DOI: 10.1016/j.enconman.2009.03.016.

Uchida, D., Otani, K. and Kurokawa, K. (2001). Evaluation of effective shading factor by fitting a clear-day pattern obtained from hourly maximum irradiance data, *Solar Energy Materials and Solar Cells* **67**(1-4): 519–528. DOI: 10.1016/S0927-0248(00)00321-4.

Valkealahti, S. (2011). Forecasting the future of renewables, *in* J. Blanco and H. Kheradmand (eds), *Climate change – sosioeconomic effects*, InTech, Rijeka, Croatia, chapter 22, pp. 425–440. ISBN 978-953-307-411-5, DOI: 10.5772/1511.

Villalva, M. G., Gazoli, J. R. and Filho, E. R. (2009a). Comprehensive approach to modeling and simulation of photovoltaic arrays, *IEEE Transactions on Power Electronics* **24**(5): 1198–1208. DOI: 10.1109/TPEL.2009.2013862.

Vorster, F. J. and van Dyk, E. E. (2005). Current-voltage characteristics of high-concentration, photovoltaic arrays, *Progress in Photovoltaics: Research and Applications* **13**(1): 55–66. DOI: 10.1002/pip.563.

Wang, Y.-J. and Hsu, P.-C. (2011a). An investigation on partial shading of pv modules with different connection configurations of pv cells, *Energy* **36**(5): 3069–3078. DOI: 10.1016/j.energy.2011.02.052.

Wang, Y.-J. and Hsu, P.-C. (2011b). Modelling of solar cells and modules using piecewise linear parallel branches, *IET Renewable Power Generation* **5**(3): 215–222. DOI: 10.1049/iet-rpg.2010.0134.

Wenham, S. R., Green, M. A., Watt, M. E. and Corkish, R. (2007). *Applied Photovoltaics*, second edn, Earthscan.

Wiese, A., Kaltschmitt, M. and Lee, W. Y. (2009). Renewable power generation - a status report, *Renewable Energy Focus* **10**(4): 64–69. DOI: 10.1016/S1755-0084(09)70157-7.

Wiese, A., Kleineidam, P., Schallenberg, K., Ulrich, A. J. and Kaltschmitt, M. (2010). Renewable power generation - a status report, *Renewable Energy Focus* **11**(4): 32–39,42–45. DOI: 10.1016/S1755-0084(10)70090-9.

Woyte, A., Nijs, J. and Belmans, R. (2003). Partial shadowing of photovoltaic arrays with different system configurations: literature review and field test results, *Solar Energy* **74**(3): 217–233. DOI: 10.1016/S0038-092X(03)00155-5.

Xiao, W., Ozog, N. and Dunford, W. G. (2007a). Topology study of photovoltaic interface for maximum power point tracking, *IEEE Transactions on Industrial Electronics* **54**(3): 1696–1704. DOI: 10.1109/TIE.2007.894732.

APPENDIX A. METHOD TO OBTAIN PARASITIC RESISTANCES FOR ONE-DIODE MODEL

This appendix presents the code for a Matlab m-file that can be used to obtain the values of parasitic resistances for one-diode model of a PV cell/module to fit it with the values of SC current, OC voltage and current and voltage at MPP measured and presented by the manufacturer of the cell/module in STC.

```
################################################################################

% Anssi Mäki
% Tampere University of Technology
% Department of Electrical Engineering
% 2012
% Filename: One_diode_model_parameters.m

% Graphical method to obtain the parasitic resistances for one-diode model

clear
clc

Isc=input('Short-circuit current (A) ? '); % (A)
Impp=input('Current at MPP (A)? '); % (A)
Uoc=input('Open-circuit voltage (V)? '); % (V)
Umpp=input('Voltage at MPP (V)? '); % (V)
A=input('Ideality factor (use 1.3 if unknown)? '); % ()
Ns=input('Number of series-connected cells? '); % ()

k=1.3806503e-23; % Boltzmann constant (m^2 kg / s^2)
q=1.60217646e-19; % Elementary charge (C)
Ut=298.15*Ns*k/q; % Thermal voltage (V)


Io=Isc/(exp(Uoc/(Ut*A))-1); % Saturation current to match at open-circuit

maxres = 2; % Maximum value of series resistance

ppo = 100000; % Number of values for series resistance

Rs=transpose(0:maxres/ppo:maxres);
MPP=(Umpp+Rs.*Impp)/(Ut*A); % Inside exponential at MPP
OC = Uoc/(Ut*A); % Inside exponential at OC
```

```
Rsh1=-(Umpp+Impp*Rs-Isc*Rs-((exp(MPP)-1).*(Uoc-Isc*Rs)) ...
./(exp(Uoc/(A*Ut))-1))./(Impp-Isc+(Isc*(exp(MPP)-1)) ...
./(exp(Uoc/(A*Ut))-1));
Rsh2=(A*Umpp*Ut + Umpp*Uoc*exp(MPP) - A*Umpp*Ut*exp(OC) ...
- Impp.*Rs*Uoc.*exp(MPP) - Isc.*Rs*Umpp.*exp(MPP) ...
+ Impp*Isc.*((Rs).^2).*exp(MPP) - A*Impp.*Rs*Ut ...
+ A*Impp.*Rs*Ut*exp(OC))./(A*Impp*Ut + Isc*Umpp.*exp(MPP) ...
- A*Impp*Ut*exp(OC) - Impp*Isc.*Rs.*exp(MPP));

for j=1:ppo-1
    if Rsh2(j,1)>=0 && Rsh1(j,1)>=0
        if abs(Rsh2(j,1)-Rsh2(j+1,1))<1000 && abs(Rsh1(j,1)-Rsh1(j+1,1))<1000
            if Rsh2(j,1)-Rsh1(j,1)>=0 && Rsh2(j+1,1)-Rsh1(j+1,1)<0
                kk1=(Rsh1(j+1,1)-Rsh1(j,1))/(Rs(j+1,1)-Rs(j,1));
                kk2=(Rsh2(j+1,1)-Rsh2(j,1))/(Rs(j+1,1)-Rs(j,1));
                Rseries=Rs(j,1)+(Rsh2(j,1)-Rsh1(j,1))/(kk1-kk2)
                Rshunt=kk1*(Rseries-Rs(j,1))+Rsh1(j,1)

            else if Rsh2(j,1)-Rsh1(j,1)<=0 && Rsh2(j+1,1)-Rsh1(j+1,1)>0
                kk1=(Rsh1(j+1,1)-Rsh1(j,1))/(Rs(j+1,1)-Rs(j,1));
                kk2=(Rsh2(j+1,1)-Rsh2(j,1))/(Rs(j+1,1)-Rs(j,1));
                Rseries=Rs(j,1)+(Rsh2(j,1)-Rsh1(j,1))/(kk1-kk2)
                Rshunt=kk1*(Rseries-Rs(j,1))+Rsh1(j,1)

                end
            end
        end
    end
end

plot(Rs,Rsh1,'b.',Rs,Rsh2,'r.')
legend('MPP','Der. @ MPP')
axis([0 maxres 0 1000])
xlabel('Series resistance (\Omega)')
ylabel('Shunt resistance (\Omega)')
grid

clear OC kk1 kk2 MPP Rs Rsh1 Rsh2 i j

%%%%%%%%%%%%%%%%%%%%%%%%%%%%%%%%%%%%%%%%%%%%%%%%%%%%%%%%%%%%%%%%%%%%%%%%%%%%%%%
```

APPENDIX B. MATLAB SIMULINK MODEL OF A PV MODULE

This appendix presents Matlab Simulink model of a PV module.

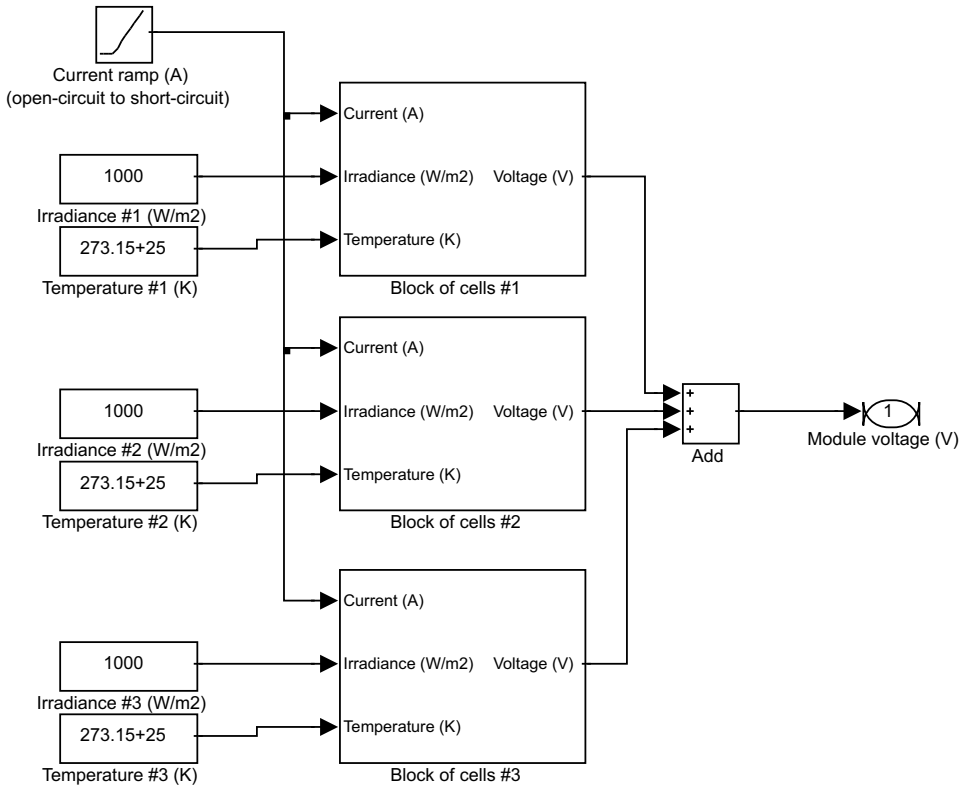

Fig. B.1: Matlab Simulink model of a PV module composed of three blocks of series-connected PV cells protected by an anti-parallel-connected bypass diode.

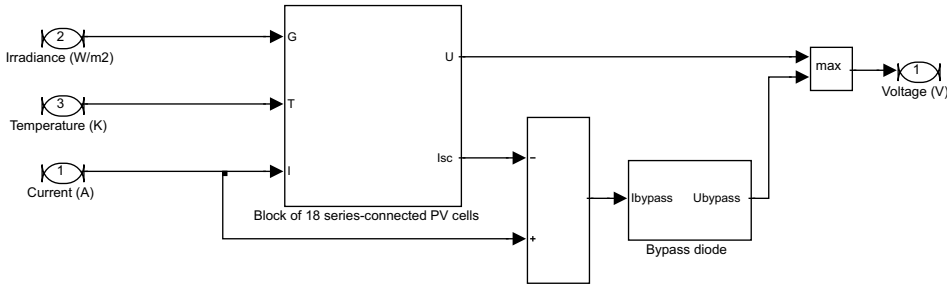

Fig. B.2: Matlab Simulink submodel of series-connected PV cells (in this case 18) with an anti-parallel-connected bypass diode.

APPENDIX C. TECHNICAL DESCRIPTION OF NAPS NP190GKG PV MODULE

This appendix presents the technical description of NAPS NP190GKg PV module. This PV module composed of 54 series-connected polycrystalline silicon PV cells is designed to be used in grid-connected PV systems.

Technical Description

Photovoltaic Module NP190GKg
Product Code: 13189

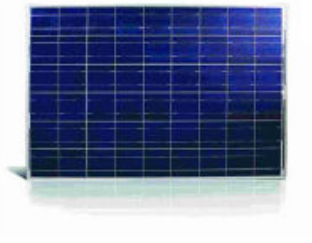

54 polycrystalline Si solar cells
Main application: grid PV systems

Module Electrical Performance under Standard Test Conditions
Refers to standard test conditions of 1000 Wm $^{-2}$ solar irradiance, 25°C cell temperature, Air Mass 1.5.
Note: Maximum power point is subject to +5W/-0W variation. All other values are typical and for guidance only.
Maximum Power Point: 190 Watts, 7.33 Amps at 25.9 Volts.
Short Circuit: 8.02 Amps. Open circuit: 33.1 Volts.

Dimensions and Weight *all dimensions +/- 2mm, weight approximately +/-0.3kg*
Length: 1475mm. Width: 986mm. Thickness at edge: 35mm. Weight: 19.5kg

Construction
Top cover material: low iron tempered glass 4mm
Encapsulant (lamination material): EVA
3 factory-fitted bypass diodes
2 x 1m cables 4 sq mm
Rear cover material: PVDF-PET-PVDF
Frame: anodised aluminium
1 junction box type S1410-2

Fig. C.1: Electrical characteristics of a NAPS NP190GKg PV module in STC.

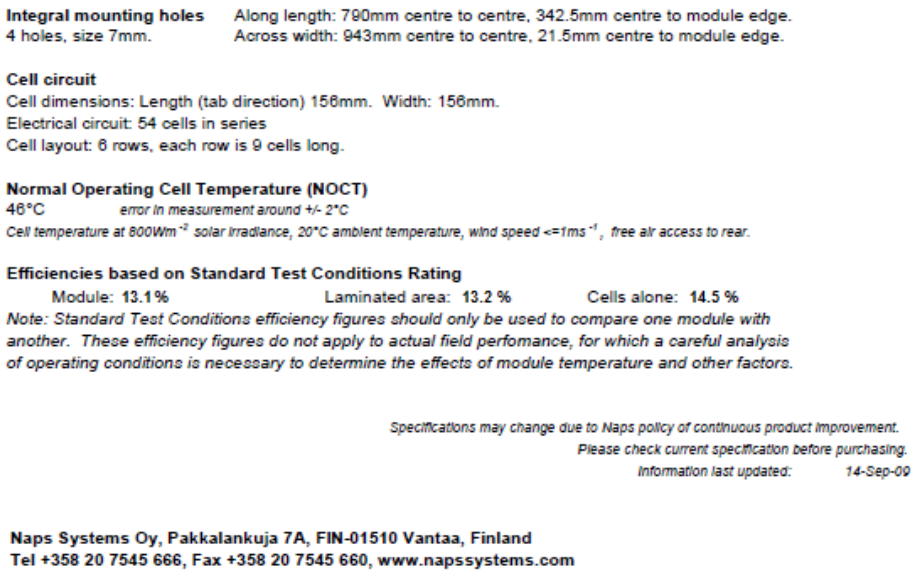

Integral mounting holes
4 holes, size 7mm.

Along length: 790mm centre to centre, 342.5mm centre to module edge.
Across width: 943mm centre to centre, 21.5mm centre to module edge.

Cell circuit
Cell dimensions: Length (tab direction) 156mm. Width: 156mm.
Electrical circuit: 54 cells in series
Cell layout: 6 rows, each row is 9 cells long.

Normal Operating Cell Temperature (NOCT)
46°C *error in measurement around +/- 2°C*
Cell temperature at 800Wm^{-2} solar irradiance, 20°C ambient temperature, wind speed <=1ms^{-1}, free air access to rear.

Efficiencies based on Standard Test Conditions Rating
Module: **13.1 %** Laminated area: **13.2 %** Cells alone: **14.5 %**
Note: Standard Test Conditions efficiency figures should only be used to compare one module with another. These efficiency figures do not apply to actual field perfomance, for which a careful analysis of operating conditions is necessary to determine the effects of module temperature and other factors.

Specifications may change due to Naps policy of continuous product improvement.
Please check current specification before purchasing.
Information last updated: 14-Sep-09

Naps Systems Oy, Pakkalankuja 7A, FIN-01510 Vantaa, Finland
Tel +358 20 7545 666, Fax +358 20 7545 660, www.napssystems.com

Fig. C.2: Electrical characteristics of a NAPS NP190GKg PV module in NOCT.

APPENDIX D. MEASUREMENT SETUP FOR PV MODULE ELECTRICAL CHARACTERISTICS

This appendix presents the laboratory setup for measuring the electrical characteristics of PV modules.

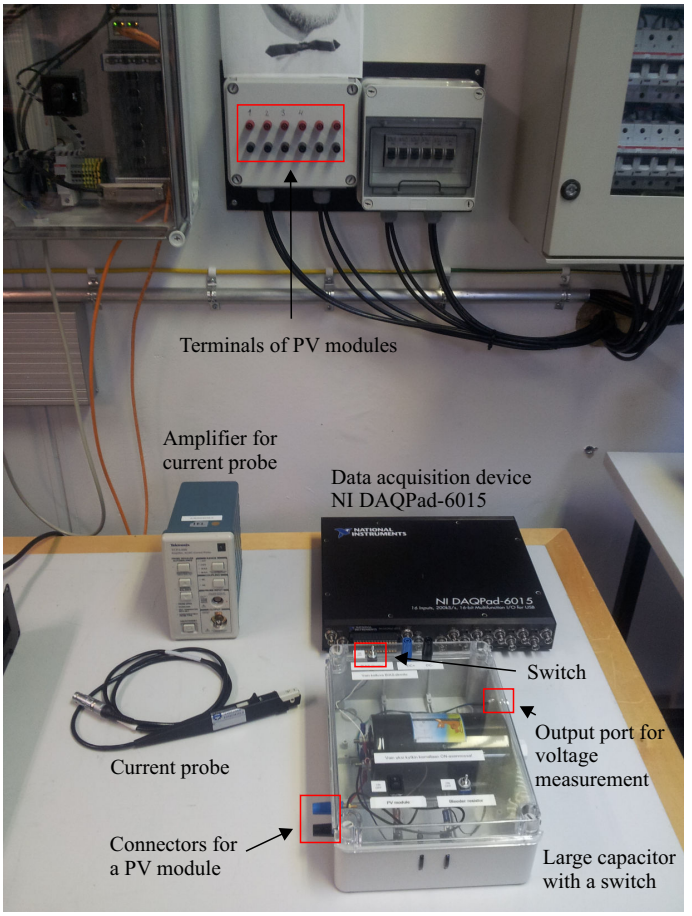

Fig. D.1: Setup and devices for measurement of PV module *I-U* curves.

APPENDIX E. LAYOUT OF TUT SOLAR PHOTOVOLTAIC POWER STATION RESEARCH PLANT

This appendix presents the layout of the TUT Solar Photovoltaic Power Station Research Plant. Kipp & Zonen SP Lite2 photodiodes, which are attached to the frame of the PV modules and have the same tilt angle as the module, are marked with dots. PT100 sensors measuring the temperatures of PV module backplates are marked with triangles.

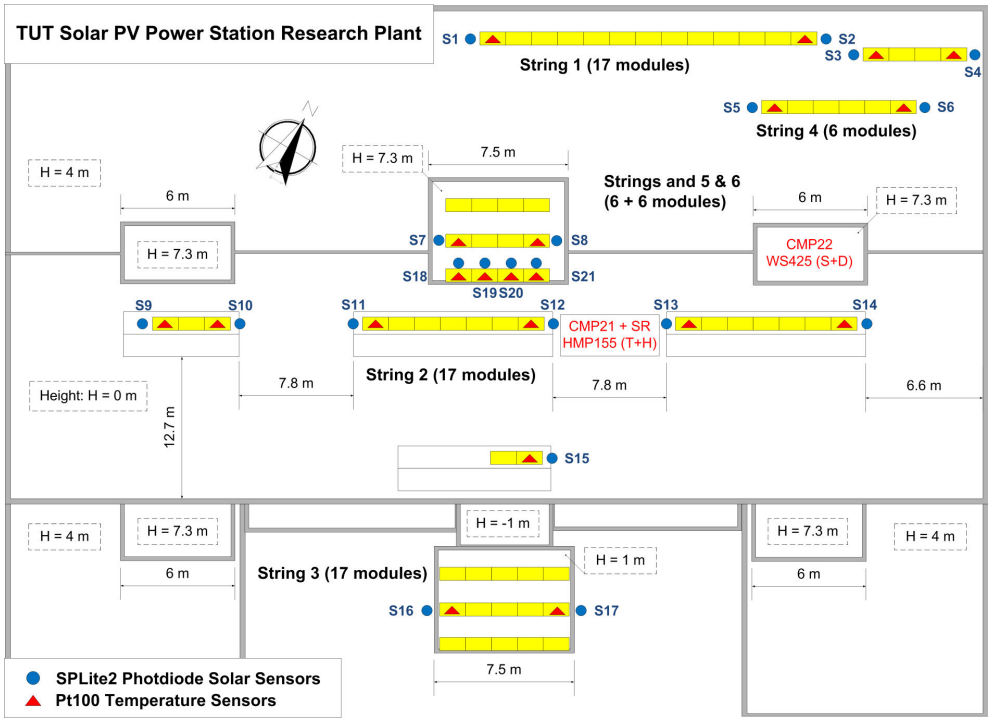

Fig. E.1: Layout of TUT Solar Photovoltaic Power Station Research Plant. SP Lite2 sensors are marked with blue dots and PT100 sensors with red triangles.

Tampereen teknillinen yliopisto
PL 527
33101 Tampere

Tampere University of Technology
P.O.B. 527
FI-33101 Tampere, Finland

ISBN 978-952-15-3137-8
ISSN 1459-2045